博士論文（要約）

A Novel Function of a Transmembrane Protein Yip1A

in the Unfolded Protein Response

(小胞体ストレス応答における膜貫通タンパク質 Yip1A の新規機能)

田口　由起

Contents

List of abbreviations

ATF4: activating transcription factor-4

ATF6: activating transcription factor-6

ATG: autophagy-related

B. abortus: *Brucella abortus*

BCV: Brucella-containing vacuole

Bip: immunoglobulin binding protein

*B. melitensi*s: *Brucella melitensi*s

BSA: bovine serum albumin

Brucella spp.: *Brucella* species

B. suis: *Brucella suis*

CFU: colony forming unit

COPII: coat protein complex II

CstA: conserved Sec24A-targeted protein A

DMEM: Dulbecco's Modified Eagle's Medium

Dot: defect in organelle trafficking

eIF2α: eukaryotic translation-initiation factor 2α

EM: electron microscopy

ER: endoplasmic reticulum

ERES: ER exit sites

ERGIC: ER-Golgi intermediate compartment

ERK: extracellular signal-regulated kinase

ERSE: ER stress response element

FCS: fetal calf serum

GAP: GTPase activating protein

GAPDH: glyceraldehyde-3-phosphate dehydrogenase

GDF: GDI displacement factor

GDI: guanine nucleotide dissociation inhibitor

GEF: guanine nucleotide exchange factor

GFP: green fluorescent protein

HRP: horseradish peroxidase

Icm: intracellular multiplication

IP: immunoprecipitation

IRE1: inositol-requiring enzyme 1

JNK: c-Jun NH_2-terminal kinase

kDa: kilodalton

Lamp2: lysosome-associated membrane protein 2

LC3: microtubule-associated protein 1 light chain 3

LCV: *Legionella*-containing vacuole

LidA: lowered viability in the presence of dotA

L. pneumophila: Legionella pneumophila

MOI: multiplicity of infection

NF-κB: nuclear factor kappa light chain enhancer of activated B cells

PAGE: polyacrylamide gel electrophoresis

PBS: phosphate-buffered saline

PERK: protein kinase RNA (PKR)-like ER kinase

p.i.: post infection

pIRE1: phosphorylated IRE

pPERK: phosphorylated PERK

RicA: Rab2 interacting conserved protein A

S1P: site-1 protease

S2P: site-2 protease

siRNA: small interfering RNA

SLO: streptolysin O

T4SS: type IV secretion system

TBS: Tris-buffered saline

TcpB: TIR domain containing-protein B

Tm: tunicamycin

TRAF2: tumor-necrosis factor receptor associated factor 2

UPR: unfolded protein response

XBP1: X box-binding protein 1

Yip1A: Ypt-interacting protein 1A

YIPF5: Ypt1p-interacting protein 1 domain family, member 5

1. Introduction

1.1 Unfolded protein response

The endoplasmic reticulum (ER) is an essential organelle that functions in protein synthesis, folding and secretion, lipid and sterol synthesis, and calcium homeostasis (Baumann and Walz, 2001). Properly folded proteins are transported from the ER to their target organelles, whereas misfolded or unfolded proteins are retained and degraded. When misfolded or unfolded proteins accumulate in the ER, ER stress is induced. To restore homeostasis in the ER, cells trigger intracellular signaling pathway called unfolded protein response (UPR) (Liu and Kaufman, 2003). The UPR alleviates the ER stress by reducing global protein synthesis, by increasing the folding capacity of the ER, and by removing misfolded or unfolded proteins from the ER.

In mammalian cells, the UPR is composed of three pathways that are initiated by distinct ER sensors: inositol-requiring enzyme 1 (IRE1), protein kinase RNA (PKR)-like ER kinase (PERK), and activating transcription factor-6 (ATF6) (Liu and Kaufman, 2003, Schröder and Kaufman, 2005, Ron and Walter, 2007) (Figure 1). These sensors are usually held in an inactive state by the ER chaperone immunoglobulin binding protein (Bip). Under conditions of ER stress, Bip is released from the ER sensors, which allows activation of the UPR. Activation of each sensor produces an active transcription factor, which in turn induces the transcription of downstream target genes to restore ER homeostasis. IRE1 oligomerizes upon release of Bip, which drives trans-autophosphorylation (Korennykh et al., 2009). Activated IRE1 removes a short

intron from X box-binding protein 1 (XBP1) mRNA, which results in the production of an active transcription factor, spliced-XBP1 protein (Cox and Walter, 1996, Yoshida et al., 2001). Spliced-XBP1 activates the transcription of genes encoding proteins that are involved in ER biogenesis (Sriburi et al., 2007) and ER quality control (Yoshida et al., 2001, Hetz, 2012). PERK homodimerizes and undergoes trans-autophosphorylation in response to ER stress. The activation of the PERK pathway transiently inhibits protein synthesis. Activated PERK phosphorylates eukaryotic translation-initiation factor 2α (eIF2α), which suppresses global mRNA translation, but activates translation of activating transcription factor-4 (ATF4) (Harding et al., 1999). ATF4 is a transcription factor that translocates to the nucleus and activates UPR target genes (Harding et al., 2000). Activated ATF6 transits from the ER to the Golgi, where it is cleaved proteolytically by site-1 protease (S1P) and site-2 protease (S2P) (Haze et al., 1999, Ye et al., 2000). The cleaved-ATF6 translocates to the nucleus and induces genes that contain the ER stress response element (ERSE) (Yoshida et al., 1998). Recently, the UPR has been reported to induce autophagy (Ogata et al., 2006, Yorimitsu et al., 2006, Hoyer-Hansen, 2007, Suh et al., 2012, Shinohara et al, 2013). During the UPR, transcription of autophagy-related genes is upregulated and autophagosome formation is facilitated to remove protein aggregates and damaged organelles (Kouroku et al., 2007, Hoyer-Hansen, 2007). Although the UPR mediated a pro-survival response, when the UPR fails to restore ER homeostasis, apoptotic cell death is induced to eliminate the stressed cells (Walter and Ron, 2011).

The UPR has been implicated in the pathogenesis of several viral and bacterial

infections, such as those of influenza A virus (Hassan et al., 2012), hepatitis C virus (Tardif et al., 2004), Japanese encephalitis virus (Su et al., 2002), Dengue virus (Pena and Harris, 2011), West Nile virus (Medigeshi et al., 2007), *Mycobacterium tuberculosis* (Seimon et al, 2010), and group A *Streptococcus* (Baruch et al., 2014). These pathogens modulate individual pathways of the UPR in distinct ways to establish more favorable environment for their replication in host cells. For example, West Nile virus activates chaperone production and membrane biogenesis by the UPR for their benefit. Hepatitis C virus has been demonstrated to activate all three UPR signaling pathways followed by the induction of autophagy (Shinohara et al., 2013). However, the precise role of the UPR in the intracellular life of pathogens, and the mechanism by which pathogens modulates the UPR remain to be elucidated.

1.2 Autophagy

Autophagy is a cellular catabolic process that is highly conserved among organisms. Cytoplasmic contents are sequestered into double-membrane vesicles known as autophagosomes, which then fuse with the endosomal-lysosomal system to generate autolysosomes. The sequestered contents are degraded by lysosomal proteases and released into the cytoplasm. Autophagy is induced to maintain cellular homeostasis in response to stresses such as nutrient starvation, pathogenic protein aggregation, and invading pathogens. To date, a number of autophagy-related (ATG) genes have been identified (Mizushima et al., 2011). Autophagy consists of four steps: nucleation, elongation, maturation, and degradation (Dreux and Chisar, 2010, Lamb et al., 2013)

(Figure 2). First, the isolation membrane, which is a cup-shaped structure of a double membrane cisterna, is formed to initiate autophagy. The P150-VPS34-Beclin1 complex involves in this nucleation step. During elongation step, the Atg5-Atg12-Atg16L complex and the microtubule-associated protein 1 light chain 3 (LC3)-Atg4 complex are recruited to the isolation membrane. Cytosolic LC3 is conjugated to phosphatidyl ethanolamine and inserted into isolation membranes. The ATG proteins dissociate from the membrane before the closure of the autophagosome, but LC3 remains on the inner surface of the autophagosome and therefore serves as a marker for autophagosome formation. Eventually, autophagosomes mature into autolysosomes by fusing with endocytic compartments including late endosomes and lysosomes. The inner membrane and contents of autophagosome are degraded by lysosomal proteases.

Various organelles including the ER (Simonsen and Stenmark, 2008, Axe et al., 2008, Hayashi-Nishino et al., 2009, Yla-Anttila et al., 2009), the ER-Golgi intermediate compartment (ERGIC) (Ge et al., 2013), the Golgi (van der Vaart et al., 2010, Ohashi and Munro, 2010), mitochondria (Hailey et al., 2010), the plasma membrane (Ravikumar et al., 2010) and recycling endosomes (Longatti et al., 2012) have been implicated to supply membrane source for autophagosomes. In mammalian cells, the most plausible origin of the isolation membrane under nutrient starvation is a subdomain of the ER, and other organelles contribute to supply membrane for elongation of the isolation membrane (Lamb et al., 2013). Several studies have demonstrated that ER exit sites (ERES) and the ERGIC play important roles in autophagy (Zoppino et al., 2010, Ge et al., 2013, Graef et al., 2013). Functional ERES

and coat protein complex II (COPII) vesicle trafficking from the ER to the ERGIC are required for autophagosome formation, and the membranes enriched in ERGIC markers enhance LC3-II lipidation. ERES are subdomains of the ER where dynamic membrane fission events occur, and closely associated with the ERGIC. Thus autophagy is interconnected with the secretory pathway.

Autophagy can function as a host defense system against viral and bacterial infections to eliminate those pathogens, while certain viruses and bacteria such as hepatitis C virus (Dreux and Chisari, 2011, Shinohara et al., 2013), Japanese encephalitis virus (Jin et al., 2013), Dengue virus (Khakpoor et al., 2009, Panyasrivanit et al., 2009), poliovirus (Jackson et al., 2005), *Staphylococcus aureus* (Schnaith et al., 2007), *Coxiella burnetii* (Gutierrez et al., 2005, Romano et al., 2007), *Legionella pneumophila* (*L. pneumophila*) (Amer and Swanson, 2005), *Brucella abortus* (*B. abortus*) (Pizarro-Cerdá et al., 1998a, 1998b), *Brucella melitensi*s (*B. melitensi*s) (Guo et al., 2012) have evolved strategies to subvert the autophagy machinery for their intracellular survival. For instance, hepatitis C virus exploits UPR-autophagy pathways to generate the membrane structures that are required for its replication and progeny production (Dreux et al., 2011, Shinohara et al., 2013). Some bacterial pathogens such as *Brucella* species (*Brucella* spp.) and *L. pneumophila* exploit autophagy to establish their safe replication niche. These bacteria are sequestered into autophagosomes, but prevent autophagosome fusion with lysosomes, which results in replicative bacterium-containing vacuoles.

1.3 Brucella spp.

1.3.1 Intracellular trafficking of *Brucella* spp.

Brucella spp. is a gram-negative facultative pathogen that infect many mammalian species, including cows, goats, sheep, dogs and pigs, as well as humans (Pappa et al., 2005). The pathogens cause a zoonotic disease known as brucellosis, which is characterized by abortion and sterility in animals, and debilitating disorders in humans. *B. abortus*, *B. melitensis*, and *Brucella suis* (*B. suis*) are most pathogenic species for human, and the pathogen can be transmitted through contacts with infected animals or ingestion of contaminated food products. Infection with *Brucella* spp. results in a significant economic and health burden due to its high infectivity, chronic nature, and difficulties in vaccine production. Better understanding of the host-pathogen interplay that supports *Brucella* replication is essential for the development of effective treatments for brucellosis.

Brucella spp. can replicate in both phagocytic and non-phagocytic cells. After being internalized within host cells, it resides in a membrane-bound compartment, the *Brucella*-containing vacuole (BCV). BCVs undergo a series of interactions with vesicular trafficking pathways in host cells (Figure 3). They transiently interact with early and late endosomes (Comerci et al., 2001, Celli et al., 2003), and then lysosomes in a limited way (Starr et al., 2008). Following the interaction with the endocytic compartments, BCVs are targeted to the ER, where they interact with ERES (Celli et al., 2003). The interaction leads to fusogenic events between the BCVs and ER membranes, generating ER-derived replicative BCVs (Pizarro-Cerda et al., 1998a, 1998b, Celli et al.,

2005, Star et al., 2008). Celli et al. (2005) suggested that functional ERES and specific interaction with COPII compartments at ERES are required for the biogenesis of replicative BCVs. However, the mechanisms by which the bacteria are sequestered into such vacuoles and obtain a continuous membrane supply for their replication remain unknown.

1.3.2 *Brucella* effectors and host factors

Intracellular *Brucella* spp. secrete effector molecules into the host cytoplasm or onto the BCV membrane through a unique secretion system, and modulate intracellular trafficking to establish a safe replication niche. The VirB type IV secretion system (T4SS) is known to be required for fusion of BCVs with ER membranes (Comerci et al., 2001, Celli et al., 2003). A VirB mutant strain of *Brucella* spp. cannot interact with the ER and fails to survive and replicate.

To date, several *Brucella* effectors have been reported. For example, VceA and VceC are translocated into the host cytoplasm (de Jong et al., 2008), and VceC triggers a host inflammatory response by inducing UPR-dependent NF-κB signaling (de Jong et al., 2013). RicA (Rab2 interacting conserved protein A) interacts with host Rab2, and affects the trafficking of BCVs (de Barsy et al., 2011). CstA (conserved Sec24A-targeted protein A) interacts with Sec24A (de Barsy et al., 2012), whereas BspA, BspB, and BspF are targeted to the compartments of the secretory pathway (Myeni et al., 2013). TcpB (TIR domain containing-protein B) induces the upregulation of UPR target genes and structural reorganization of the ER (Smith et al., 2013). The

molecular functions of these effectors in *Brucella* replication need to be further characterized.

Host factors that are involved in the ER-Golgi vesicular transport pathways, such as Sar1 (Celli et al., 2005), Rab2, and glyceraldehyde-3-phosphate dehydrogenase (GAPDH) (Fugier et al., 2009) have been shown to be required for intracellular replication of *B. abortus*. The bacteria exploit Sar1 at ERES for BCVs to fuse with the ER (Celli et al., 2005). GAPDH and Rab2 are recruited onto BCV membranes, which indicates that BCVs intercept retrograde trafficking and interact with the ERGIC (Fugier et al., 2009). Recently, several studies have suggested that *Brucella* infection might also induce the UPR (Qin et al., 2008, de Jong et al., 2013, Smith et al., 2013). Qin et al. (2008) demonstrated that *Brucella* replication is suppressed following the knockdown of IRE1 in insect cells and murine embryonic fibroblasts. De Jong et al. (2013) suggested that *B. abortus* infection activated the IRE1 pathway, whereas Smith et al. (2013) showed that all three UPR pathways were induced in infection of murine macrophages with *B. melitensis*. Therefore, the mechanistic link between the UPR and *Brucella* infection remains controversial. The precise role of the UPR in the intracellular life of *Brucella* spp., the host factors involved in replication processes, and the mechanism by which *Brucella* modulates the UPR remain to be elucidated.

1.4 Yip1A and COPII vesicle biogenesis at ERES

Human Yip1A (Ypt-interacting protein 1A, also known as Ypt1p-interacting protein 1 domain family, member 5 (YIPF5)) is a 257 amino acids multi-pass transmembrane

protein belonging to the Yip1 family (Figure 4A and 4B). The Yip1 family proteins are highly conserved throughout the evolution and share several features (Yang et al., 1998, Tang et al, 2001, Calero et al., 2002, Shakoori et al., 2003). First, they have similar membrane topology with the hydrophilic N-terminus facing the cytoplasm and the hydrophobic C-terminus embedded in membranes. Second, Yip1 family proteins have an ability to interact with prenylated Rab proteins (Calero et al., 2003). Third, members of Yip1 family associate with each other (Yang et al., 1998, Ito et al., 2001, Calero et al., 2002), suggesting that they have potential to form a higher-order complex.

Rab proteins are small GTPases that function in vesicle formation, budding, transport, tethering, docking, and membrane fusion, and control vesicle trafficking (Stenmark, 2009). Rab proteins cycle between two forms (Figure 5). The GDP-bound form of Rab binds a guanine nucleotide dissociation inhibitor (GDI) in the cytoplasm. A GDI displacement factor (GDF) dissociates GDI from Rab, which leads to insertion of the Rab into the membrane via a prenyl group. The prenylated Rab is activated by a guanine nucleotide exchange factor (GEF) to the GTP-bound form. The GTP-bound Rab interacts with distinct effectors that mediate vesicle trafficking. Finally, a GTPase activating protein (GAP) catalyzes the hydrolysis of GTP to GDP, and the GDP-bound Rab is released from the membrane into the cytoplasm.

The yeast homolog Yip1p is first identified as an interacting protein with Rab GTPases Ypt1p and Ypt31p, the yeast homologs of Rab1 and Rab11 using a yeast two-hybrid system (Yang et al., 1998). Yip1p is essential for yeast cell viability and functions in ER-to-Golgi membrane transport. Although Yip1p has been shown to

interact with several Rab proteins (Calero et al., 2003, Chen et al., 2004), Yip1A has not been reported to interact with Rab proteins, suggesting that it may function independent of Rab proteins or indirectly interact with them. Yip1A is localized to ERES and the Golgi (Tang et al., 2001), and to the ERGIC (Yoshida et al., 2008, Kano et al., 2009). The distinct localization of Yip1A indicates that they might have specific function with binding partners where they are compartmentalized. Yip1A has been implicated in several trafficking steps between the ER and the Golgi, including COPII vesicle budding at ERES (Tang et al., 2001), vesicle tethering to the Golgi membrane (Jin et al., 2005), and COPI-independent retrograde vesicle transport (Kano et al., 2009). Yip1A has also been implicated in the maintenance of ER morphology (Dykstra et al., 2010).

The COPII vesicles are assembled at ERES (Lee et al., 2004, Lee and Miller, 2007) (Figure 6). First, the small GTPase Sar1 is recruited on the ER membrane through the membrane bound GEF Sec12 that converts the GDP-bound form of Sar1 into GTP-bound form. Activated Sar1 induces membrane bending, and leads to recruitment of the inner coat components Sec23-Sec24 by directly binding Sec23 (Bi et al., 2002). Sec24 binds cargo proteins and concentrates them (Miller et al., 2002), thus forming a 'pre-budding complex'. Then the outer coat components Sec13-Sec31 polymerize to collect pre-budding complexes and shape the vesicles. Finally, a transport vesicle buds from the ER and traffic to the ERGIC. Yip1A was shown to bind to the Sec23/Sec24 complex of COPII and antibodies against Yip1A inhibited the COPII vesicle budding from ERES (Tang et al., 2001). Dykstra et al. (2010) reported that the knockdown of Yip1A slowed the COPII-mediated protein export from the ER. However, others

demonstrated that Yip1A-knockdown did not affect anterograde transport (Yoshida et al., 2008, Kano et al., 2009). These studies raise the possibility that Yip1A might be involved in the biogenesis of the COPII vesicles at ERES that are not destined for the secretory pathway.

1.5 The purpose of this study

In recent years, multiple links between cellular signaling pathways of host cells and intracellular pathogens have been revealed. Better understanding of the host-pathogen interplay that supports the survival of pathogens is essential for the development of effective treatments. While the UPR and autophagy allows cells to adapt detrimental physiological or pathological conditions and to restore cellular homeostasis, certain pathogens exploit these host machineries for their intracellular growth.

Brucella species replicate within host cells in the form of ER-derived vacuoles. The mechanisms by which the bacteria are sequestered into such vacuoles and obtain a continuous membrane supply for their replication remain to be elucidated. In the present study, I investigated a potential role of the UPR and autophagy in intracellular life of *B. abortus*, and unveiled a novel function of Yip1A in the activation of the IRE1 pathway of the UPR and the subsequent formation of autophagosome-like vacuoles.（未発表の共同研究内容が含まれるので未掲載）On the basis of these findings, I proposed a model for intracellular *Brucella* replication that exploits the host UPR and autophagy machineries, both of which are critical for *B. abortus* to establish a safe replication niche. Yip1A is indispensable for these processes.

2. Materials and Methods

2.1 Cell Culture

HeLa cells were cultured at 37°C in a 5% CO_2 atmosphere in Dulbecco's Modified Eagle's Medium (DMEM; Nissui) supplemented with 10% fetal calf serum (FCS) and penicillin/streptomycin (Gibco). For transfection, HeLa cells were seeded in 35-mm culture dishes. For confocal microscopy, cells were plated onto coverslips in 35-mm culture dishes. For infection, cells were inoculated into DMEM supplemented with 10% FCS (DMEM-10%FCS) in 6-well tissue culture plates 24 hr before infection. To induce the UPR, HeLa cells were treated with 5 µg/ml tunicamycin (Sigma) in DMEM and incubated at 37°C in a 5% CO_2 atmosphere.

2.2 Antibodies

The primary antibodies used were: mouse monoclonal anti-ERGIC53 (Alexis), rabbit monoclonal anti-GM130 (Abcam), rabbit polyclonal anti-Rab1 (Santa Cruz), mouse monoclonal anti-Rab2 (Abcam), rabbit polyclonal anti-Sec23 (Abcam), rabbit polyclonal anti-Sec24A (Proteintech), rabbit polyclonal anti-Sec24B (Sigma), rabbit polyclonal anti-Sec24C (Sigma), rabbit polyclonal anti-Sec24D (Sigma), mouse monoclonal anti-Sec31A (BD Biosciences), goat polyclonal anti-Sec61α (Abcam), mouse monoclonal anti-HSP47 (Enzo Life Sciences), rat monoclonal anti-HA (Roche), mouse monoclonal anti-GAPDH (Millipore), rabbit polyclonal anti-IRE1 (phospho S724; Abcam), rabbit polyclonal anti-IRE1 (Abcam), rabbit monoclonal

anti-phospho-PERK (Thr980; Cell Signaling Technology), rabbit polyclonal anti-ATF6 (Abcam), rabbit polyclonal anti-XBP1 (Abcam), rabbit polyclonal anti-Sar1 (Abcam), mouse monoclonal anti-lysosome-associated membrane protein 2 (Lamp2) (developed by J. T. August and J. E. K. Hildreth, obtained from the Developmental Studies Hybridoma Bank, created by the NICHD of the NIH, and maintained at The University of Iowa), rabbit polyclonal LC3 (Cell Signaling Technology), rabbit polyclonal anti-green fluorescent protein (GFP) (MBL), mouse monoclonal anti-β-tubulin (Sigma), rabbit polyclonal anti-Myc-tag (Cell Signaling Technology) and mouse monoclonal anti-calnexin (BD Biosciences) antibodies. The rabbit polyclonal anti-Yip1A antibody was raised as described in Kano et al. (2009). The guinea pig polyclonal anti-Yip1A antibody was generated by MBL (Medical and Biological Laboratories) against the Yip1A peptide MMQPQQPYTGQIYQPTQC. The polyclonal anti-*Brucella abortus* antibody was purified from rabbit serum immunized with formalin-inactivated whole cells of *B*. *abortus* 544. The secondary antibodies used for immunofluorescence were: Alexa Fluor® 488 Goat Anti-Rabbit IgG (H+L) (Life Technologies), Alexa Fluor® 488 Goat Anti-Mouse IgG (H+L) (Life Technologies), Alexa Fluor® 488 Goat Anti-rat IgG (H+L) (Life Technologies), Cy3-conjugated Goat Anti-Rabbit IgG (Chemicon), Cy3-conjugated Goat Anti-Mouse IgG (Chemicon), Alexa Fluor® 647 Goat Anti-mouse IgG (H+L) (Life Technologies), and Alexa Fluor® 647 Goat Anti-Guinea Pig IgG (H+L) (Life Technologies) antibodies. The secondary antibodies used for western blotting were: Horse Radish Peroxidase (HRP)-conjugated Goat Anti-Mouse IgG (Promega), HRP-conjugated Anti-Goat IgG (Santa Cruz), and HRP-conjugated

Goat Anti-Rabbit IgG (Cell Signaling) antibodies. Normal rabbit IgG was purchased from Santa Cruz.

2.3 Plasmids

Plasmids pEGFP-C1 and pCMV-Myc were purchased from Clontech. Plasmid pEU-E01-His-TEV-MCS-N1 was from CellFree Sciences Co., Ltd.

2.4 siRNA

Small interfering RNA (siRNA) against human Yip1A (ID 127564), siRNA against human IRE1 (s200430) and negative control siRNA (Silencer® Negative Control 1 siRNA) were obtained from Ambion.

2.5 Bacterial Strains

Brucella abortus strain 544 was obtained from the National Institute of Animal Health, Ibaraki, Japan and cultured on trypticase soy agar with 5% sheep blood (Nippon Becton Dickinson) at 37°C in a 10% CO_2 atmosphere.

2.6 Transfections

FuGENE® HD Transfection Reagent (Roche) was used for plasmid transfection, and Lipofectamine™ 2000 Transfection Reagent (Invitrogen) was used for siRNA transfection.

2.7 SDS-PAGE and Western Blotting

HeLa cells were scraped into RIPA buffer (50 mM Tris, pH 7.4, 150 mM NaCl, 1% NP 40, 0.25% sodium deoxycholate, 1 mM EDTA) that contained protease inhibitor cocktail (Roche) and passed 30 times through a 27-gauge needle. The cell lysates were mixed with 2× SDS sample buffer and boiled for 5 min. Proteins were separated on a 5–20% SDS polyacrylamide gel, and transferred onto PVDF membrane (Millipore). The membrane was blocked for 1 hr at room temperature with Tris-buffered saline (TBS) that contained 0.1% Tween 20 (TBST) and 5% BSA, and then incubated with the respective primary antibody in blocking buffer overnight at 4°C. After washing three times with TBST, the membrane was incubated with the respective secondary antibody in blocking buffer for 1 hr at room temperature. After washing three times with TBST, protein bands were detected using the ECL Western Blotting Detection Kit (Amersham) and a LAS-4000 mini imaging system (FUJIFILM). The intensity of the bands was quantified using the MultiGauge software (FUJIFILM).

2.8 Immunofluorescence Microscopy

HeLa cells were washed twice with phosphate-buffered saline (PBS), fixed and permeabilized with methanol-acetone (1:1, v/v) for 6.5 min at 4°C, and then washed three times with PBS. The cells were blocked for 30 min in PBS that contained 3% bovine serum albumin (BSA) and incubated with the respective primary antibody in blocking buffer for 2 hr at room temperature. After washing three times with PBS, the cells were incubated with the respective secondary antibody in blocking buffer for 1 hr

at room temperature. After washing three times with PBS, the coverslips were mounted in SlowFade Gold antifade reagent (Invitrogen) and examined under oil immersion on a Zeiss LSM 510 laser scanning confocal microscope.

2.9 Immunoprecipitation

HeLa cells were scraped into ice-cold lysis buffer (50 mM Tris, pH 8.0, 150 mM NaCl, 1% NP 40, 0.1% SDS, 0.5% sodium deoxycholate) that contained protease inhibitor cocktail and passed 15 times through a 27-gauge needle. The cells were incubated for 30 min at 4°C with rotation and centrifuged for 20 min at 15,000 rpm. The supernatant was immunoprecipated with rabbit anti-IRE1 (phospho S724) antibody or normal rabbit IgG for 3 hr at 4°C followed by Protein G Sepharose 4 Fast Flow (GE Healthcare) overnight at 4°C. After centrifugation at 13,000 rpm for 5 s, the precipitates were washed three times with lysis buffer and then boiled in 2× SDS sample buffer for 5 min. The immunoprecipitates were separated by SDS-PAGE and immunoblotted with rabbit anti-Yip1A antibody.

2.10 Native PAGE

HeLa cells were scraped into 50mM TBS that contained 1% Triton X-100 and protease inhibitor cocktail, and passed 30 times through a 27-gauge needle. The cell lysates were mixed with 2× Native PAGE loading buffer (Cosmo Bio). The same amounts of protein were loaded in each lane of a 5%~20% native gel. The electrophoresis ran at 10mA for 2.5hr at 4°C, and then the gel was subjected to western

blot analysis with a pIRE1 antibody.

2.11 Infections

HeLa cells were infected with log-phase cultures of *B. abortus* at a multiplicity of infection (MOI) of 400. The culture plates were centrifuged at 1,000 × g for 10 min at 20°C and then incubated for 1 hr at 37°C in a 5% CO_2 atmosphere. After washing twice with DMEM-10%FCS, the cells were incubated for 1 hr in DMEM-10%FCS supplemented with 50 μg/ml gentamicin to kill extracellular bacteria. Thereafter, the culture medium was replaced by DMEM-10%FCS supplemented with 10 μg/ml gentamicin.

2.12 Determination of colony forming unit

To evaluate intracellular *Brucella* growth, infected cells were washed three times with PBS and lysed with 0.5 ml of 0.1% Triton X-100 in PBS. Serial dilutions of the lysates were plated onto Thayer-Martin Agar (Nippon Becton Dickinson) and incubated for 3 days at 37°C in a 5% CO_2 atmosphere before colony forming units (CFUs) were counted.

2.13 Electron Microscopy

The ultrastructure of HeLa cells infected with *B. abortus* was examined by transmission electron microscopy. Infected HeLa cells were prefixed with 2.5%

glutaraldehyde and 2% paraformaldehyde in 0.1 M phosphate buffer, pH 7.4 for 2 hr at room temperature, post-fixed in 1% osmium tetroxide, and embedded in Epon. Ultrathin sections were stained with uranyl acetate and lead citrate, and then observed under a transmission electron microscope (H-7650, Hitachi Ltd.) at 80 kV.

2.14 RNA isolation and RT-PCR

Total RNA was purified from *Brucella*-infected HeLa cells using an RNeasy Mini Kit (Qiagen) and reverse-transcribed with the use of a ReverTra Ace® qPCR RT Kit (TOYOBO Co. Ltd.). One-step PCR was carried out using Fast SYBR® Green Master Mix (Applied Biosystems) and a StepOnePlus™ Real-Time PCR System (Applied Biosystems). The primer pairs used were:（未発表の共同研究内容が含まれるので未掲載） forward, 5'-GCGAATTCTCATCCAGTTTGGCTATGTA-3' and reverse 5'-GCGTCGACTCACTGTCCTTCCATGGCTAA-3' for Yip1A, and forward, 5'-GCCATCAATGACCCCTTCATTGACC-3' and reverse, 5'-CGCCTGCTTCACCACCTTCTTGATG-3' for GAPDH. GAPDH was used as an internal standard.

2.15 未発表の共同研究内容が含まれるので未掲載

2.16 未発表の共同研究内容が含まれるので未掲載

2.17 未発表の共同研究内容が含まれるので未掲載

2.18 Statistical analysis

Differences between individual sets of data were assessed using a Welch's t-test. Differences were considered significant at $p < 0.05$.

3. Results

3.1 Infection of HeLa cells with *Brucella abortus*

3.1.1 *Brucella* infection activates the IRE1 pathway of the UPR

The unfolded protein response (UPR) has been implicated in the pathogenesis of several viral and bacterial infections (Seimon et al, 2010, Baruch et al., 2014, Hassan et al., 2012, Tardif et al., 2004, Su et al., 2002, Pena and Harris, 2011, Medigeshi et al., 2007). Recent studies have suggested that *Brucella* spp. may also induce the UPR during infection (Qin et al., 2008, de Jong et al., 2013, Smith et al., 2013). However, none of these studies have directly shown the activation of the UPR sensors, and the precise role of the UPR in the intracellular life of *Brucella* spp. remains unknown. Here, I have characterized the activation of three UPR sensors IRE1, PERK, and ATF6 during infection of HeLa cells with *B. abortus*. HeLa cells have been widely used for in vitro studies of *Brucella* infection.

First, I monitored the intracellular replication of *B. abortus* in HeLa cells. HeLa cells were infected with *B. abortus* (strain 544), and extracellular bacteria were eliminated by gentamicin treatment. The number of colony forming units (CFUs) was determined at indicated time points after infection (Figure 7A). Consistent with previous reports (Pizarro-Cerda et al., 1998a, Celli et al., 2003), a significant increase in the number of CFUs was observed at 24hr post infection (p.i.). To further confirm the intracellular replication, I detected *B. abortus* within infected cells by using immunofluorescence microscopy with an anti-*B. abortus* antibody (Figure 7B).

Extensive intracellular replication of *B*. *abortus* was identified at 24hr p.i., indicating that the bacteria had already established a safe niche for their replication.

To investigate the induction of the UPR during *Brucella* infection, HeLa cells were infected or not with *B*. *abortus*, and the activation of three UPR sensors (IRE1, PERK, and ATF6) was analyzed by western blotting (Figure 8A and 9A). IRE1 undergoes trans-autophosphorylation when activated (Korennykh et al., 2009, Li et al., 2010). As shown by the increase in phosphorylated IRE1 (pIRE1), *Brucella* infection triggered the activation of IRE1 (Figure 8B). At early time points (4 hr and 8 hr p.i.), and then later (16 hr p.i. onwards), a drastic increase in pIRE1 was observed in *B*. *abortus*-infected cells. Phosphorylated IRE1 removes a short intron from XBP1 mRNA, which results in the production of spliced-XBP1 protein (Cox and Walter, 1996, Yoshida et al., 2001). Spliced-XBP1 increased over time during *Brucella* infection (Figure 8C).

Upon activation, PERK is also trans-autophosphorylated (Harding et al., 1999), while ATF6 is transported from the ER to the Golgi and cleaved proteolytically (Haze et al., 1999, Ye et al., 2000), thus generating cleaved-ATF6. The amount of phosphorylated PERK (pPERK) and cleaved-ATF6 has not changed significantly over time both in control cells and in infected cells (Figure 9B and 9C), which indicates that the PERK and ATF6 pathways were not activated by *Brucella* infection. These results demonstrate that the infection with *B*. *abortus* preferentially activates the IRE1 pathway of the UPR, but not the PERK and ATF6 pathways, in HeLa cells.

3.1.2 *Brucella* infection leads to the upregulation of the COPII vesicle

components Sar1, Sec23, and Sec24D

Spliced-XBP1 translocates into the nucleus and serves as a transcription factor (Cox and Walter, 1996, Yoshida et al., 2001). It upregulates a wide range of downstream target genes (Sriburi et al., 2007, Yoshida et al., 2001, Hetz, 2012). To confirm the activation of the IRE1-XBP1 pathway during infection with *B. abortus*, I examined the expression of several genes that are involved in the early secretory pathway, because *Brucella* trafficking appears to interplay with the early secretory pathway to establish its replicative niche (Celli et al. 2005, Fugier et al., 2009).

HeLa cells were treated as described in the previous section (3.1.1). At 24hr p.i., cell lysates were prepared and analyzed by western blotting (Figure 10A). I found that the expression of Sar1, Sec23, and Sec24D was enhanced significantly in *Brucella*-infected cells compared to uninfected control cells (Figure 10B). These molecules are all involved in the formation of COPII vesicles at ERES (D'Arcangelo et al., 2013). Sar1 controls the organization of ERES, and Sec23/Sec24D complex constitutes the inner coat of COPII vesicles. Thus, infection with *B. abortus* leads to the upregulation of the COPII vesicle components Sar1, Sec23, and Sec24D through the activation of the IRE1 pathway of the UPR.

3.2 Activation of the IRE1 pathway of the UPR under tunicamycin treatment

3.2.1 Yip1A interacts with pIRE1 at ERES

Functional ERES and COPII vesicles have been implicated in the intracellular replication of *B. abortus* (Celli et al., 2005). The upregulation of the COPII vesicle

components Sar1, Sec23, and Sec24D that follows the activation of the IRE1 pathway of the UPR (Figure 10B) suggested that a host factor that links the UPR and COPII vesicle biogenesis may play an important role in the intracellular replication of *B. abortus*. To search for such a host factor, I performed an immunoprecipation (IP) assay using an anti-pIRE1 antibody against HeLa cells that were treated with tunicamycin (Tm), a compound that causes the UPR by inhibiting N-linked glycosylation. The immunoprecipitates were analyzed by western blotting with a panel of antibodies against molecules involved in the ER-Golgi vesicular transport pathways (Figure 11A). Intriguingly, the inner components of the COPII coat (Sec23, Sec24A, Sec24B, Sec24C and Sec24D), Rab1, and Yip1A were found to interact with pIRE1. In contrast, a component of the outer coat (Sec31A), Rab2, Sar1, as well as some ER- (Sec61α, HSP47 and calnexin), ERGIC- (ERGIC53) and *cis*-Golgi- (GM130) resident proteins showed no specific interaction with pIRE1 (Figure 11A).

Among the test panel, Yip1A was included as a candidate interacting partner for pIRE1, because it localizes to ERES, binds to the Sec23/Sec24 complex, and is involved in COPII vesicle biogenesis (Tang et al., 2001). Since Yip1A had not previously been implicated in the UPR or in the intracellular replication of *B. abortus*, I decided to focus on this protein. To further confirm the specificity of the interaction between Yip1A and pIRE1, the IP assay was repeated but with an anti-Yip1A antibody, and pIRE1 was identified to bind to Yip1A (Figure 11B). The interaction of Yip1A with pIRE1 was enhanced upon Tm treatment (Figure 11C), and thus dependent on the induction of the UPR.

To confirm the IP results, I examined the localization of Yip1A and pIRE1 in HeLa cells that were treated with Tm to induce the UPR. Under the UPR condition, IRE1 molecules cluster into oligomers, and undergo trans-autophosphorylation. Accordingly, pIRE1 can be detected as large foci with an anti-pIRE1 antibody by immunofluorescence microscopy (Kimata et al., 2007, Korennykh et al., 2009, Li et al., 2010). HeLa cells were double-stained for pIRE1 and Yip1A after Tm treatment (Figure 12A). Large pIRE1 foci were detected throughout the cytoplasm and co-localized with Yip1A. Yip1A is localized to ERES and the Golgi (Tang et al., 2001), and to the ERGIC (Yoshida et al., 2008, Kano et al., 2009). Given that the large pIRE1 foci were co-stained with Sec31, a marker for ERES (Figure 12B), Yip1A and pIRE1 were located at ERES upon the induction of the UPR.

3.2.2 Yip1A is responsible for the phosphorylation of IRE1 and the upregulation of the COPII components Sar1, Sec23, and Sec24D

I assumed that Yip1A at ERES might be involved in the activation of IRE1. To address this, I knocked down the expression of Yip1A by using small interfering RNA (siRNA) and investigated the effect on the activation of the UPR. First, the depletion of Yip1A was evaluated by western blot analysis (Figure 13A). HeLa cells were transfected with control scramble siRNA or Yip1A siRNA for 24 hr. The expression of Yip1A was reduced by 72.5% (Figure 13A). The knockdown of Yip1A was further confirmed by immunofluorescence microscopy (Figure 13B).

The cells transfected with siRNA were then treated with Tm to induce the UPR.

There was no difference in the total levels of IRE1 between control and Yip1A-knockdown cells throughout the experiment (Figure 14A). Activation of the IRE1 pathway was analyzed by western blotting (Figure 14B). In control cells, the phosphorylation of IRE1 peaked at 5 hr after the addition of Tm, and then began to decrease (Figure 14C). The splicing of XBP1 mRNA correlated with the activation of IRE1 (Figure 14D), which resulted in an increase in spliced-XBP1 protein from 5 hr onwards (Figure 14E). Strikingly, the knockdown of Yip1A suppressed the increase in pIRE1 throughout the course of Tm treatment (Figure 14C). Consistent with this result, the splicing of XBP1 mRNA (Figure 14D) and the amount of spliced-XBP1 protein (Figure 14E) were reduced by the depletion of Yip1A. In contrast, Yip1A knockdown had little effect on the activation of PERK or ATF6 during Tm treatment (Figure 15A and 15B).

During infection with *B. abortus*, the COPII components Sar1, Sec23, and Sec24D were upregulated significantly (Figure 10B). Under tunicamycin treatment, the amounts of these molecules were also increased in control cells (Figure 16A and 16B), whereas Yip1A-knockdown cells showed little upregulation of these COPII components. This indicates that the upregulation of Sar1, Sec23 and Sec24D is triggered by the induction of the UPR, and that it depends on Yip1A. To further confirm the connection between IRE1 pathway of the UPR and the upregulation of the COPII components, I knocked down the expression of IRE1 by using siRNA. The depletion of IRE1 protein was 84.3% (Figure 16C). IRE1-knockdown produced similar results to those of Yip1A-knockdown (Figure 16A and 16B). Collectively, these results strongly suggest

that the upregulation of the COPII components Sar1, Sec23, and Sec24D depends on the activation of IRE1 that is mediated by Yip1A.

3.2.3 Yip1A mediates a high-order assembly of IRE1 molecules

Upon the induction of the UPR, IRE1 molecules oligomerize into higher-order species. This causes the autophosphorylation of IRE1, resulting in the appearance of large pIRE1 foci throughout the cytoplasm (Kimata et al., 2007, Korennykh et al., 2009, Li et al., 2010). I hypothesized that the deficiency in IRE1 phosphorylation observed in Yip1A-knockdown cells may be attributed to the inability of IRE1 molecules to form oligomers. To examine this possibility, the formation of large pIRE1 foci was assessed by immunofluorescence microscopy under Tm treatment (Figure 17A and 17B). HeLa cells were transfected with scramble siRNA or Yip1A siRNA for 24 hr, and then treated with Tm to induce the UPR. The number of pIRE1 foci per cell was counted in these cells. In control cells, time-dependent appearance of pIRE1 foci was observed: the number of foci increased during the first 6 hr of Tm treatment, and then started to decrease (Figure 17A, upper panels, 17B), consistent with the result obtained in the western blot analysis of pIRE1 (Figure 14C). By contrast, in Yip1A knockdown cells, pIRE1 foci were hardly observed throughout the Tm treatment (Figure 17A, lower panels, 17B). These results support the idea that IRE1 molecules fail to assemble into cluster in the absence of Yip1A under Tm treatment.

The above effect of Yip1A-knockdown on the oligomeric state of IRE1 was further demonstrated by native polyacrylamide gel electrophoresis (PAGE), which permits the

separation of multi-protein complexes under native conditions. Phosphorylated IRE1 molecules were resolved as two high-order complexes with apparent molecular weights of approximately 500kDa and 1000kDa (termed pIRE1-I and pIRE1-II, respectively) (Figure 18A). In control cells, the amount of pIRE1-I was increased after 4 hr of Tm treatment and then decreased (Figure 18A, lanes labeled 'S' and 18B), which coincides with the results of the western blot analysis of pIRE1 (Figure 14C) or the formation of pIRE1 foci (Figure 17A and 17B). The amount of pIRE1-II remained constant throughout the Tm treatment. In Yip1A knockdown cells, the amount of both high-order complexes was reduced significantly (Figure 18A, lanes labeled 'Y', and 18B). These data support the idea that Yip1A is responsible for the phosphorylation of IRE1 via the high-order assembly of IRE1 molecules under the UPR condition.

3.2.4 Yip1A-knockdown has little effect on the ER localization of IRE1

Yip1A has been implicated in the maintenance of ER structure (Dykstra et al., 2010). The deficiency in oligomerization or high-order assembly of IRE1 molecules caused by Yip1A-knockdown may be attributed to morphological deformation of the ER membrane where IRE1 localizes. To evaluate this possibility, the localization of total IRE1 was examined by immunofluorescence microscopy. HeLa cells were transfected with scramble siRNA or Yip1A siRNA for 24 hr, and then treated with Tm for 5 hr to induce the UPR. Several large vacuoles were observed in control cells, but not in Yip1A-knockdown cells (Figure 19). Otherwise, IRE1 was stained throughout the cytoplasm in a reticular pattern both in control and in Yip1A-knockdown cells,

indicating its intrinsic localization in the ER. Concentric whorl structures of ER membrane reported by Dykstra et al. (2010) were not observed by the depletion of Yip1A. I therefore concluded that the ER localization of IRE1 was not affected by Yip1A-knockdown.

3.3 Formation of autophagosome-like vacuoles under tunicamycin treatment

3.3.1 Yip1A mediates the formation of large vacuoles through the IRE1 pathway

During Tm treatment, large vacuoles were observed in control cells but not in Yip1A-knockdown cells (Figure 19). To determine whether vacuolization induced by Tm treatment is also dependent on the Yip1A-mediated IRE1 activation, I investigated the effect of Yip1A- or IRE1-knockdown on vacuolization under Tm treatment. HeLa cells were transfected with each siRNA and then treated with Tm to induce the UPR. The ER structure was visualized by immunofluorescence microscopy with an anti-calnexin antibody (Figure 20A). Whereas large vacuoles were formed after Tm treatment in control cell (Figure 20A, left-hand panels, arrows), such vacuolization was not seen in Yip1A-knockdown (Figure 20A, middle panels) or IRE1-knockdown (Figure 20A, right-hand panels) cells. The percentage of cells with vacuoles was significantly lower in Yip1A- or IRE1-knockdown cells than in control cells after Tm treatment (Figure 20B). Thus, there is likely to be a link between Yip1A-mediated activation of IRE1 and the formation of large vacuoles under Tm treatment.

3.3.2 Yip1A mediates the formation of autophagosome-like vacuoles through the

IRE1 pathway.

The activation of the UPR has been implicated in the induction of autophagy (Bernales et al., 2006, Hoyer-Hansen et al., 2007). In addition, the COPII vesicles budding from ERES have been shown to supply membrane for autophagosome formation (Graef et al., 2013, Tan et al., 2013, Wang et al., 2014). Given these recent findings, I assumed that the formation of large vacuoles might be related to ER-derived autophagy that is triggered by the UPR. I characterized the large vacuoles by using LC3 as a marker for autophagosome formation. When autophagy is induced, cytosolic LC3 (LC3-I) becomes lipidated (LC3-II) and translocated onto isolation membranes. These structures can be visualized as dots by fluorescence microscopy. An expression construct for GFP-LC3 was co-transfected with siRNA. In control cells, a number of large GFP-LC3 dots appeared after Tm treatment (Figure 21, left-hand panels), and some were detected along the periphery of large vacuoles (Figure 21, left-hand panel, inset, arrowheads), indicating that these Tm-induced vacuoles have an autophagic nature. Notably, the knockdown of Yip1A or IRE1 significantly reduced the number of GFP-LC3 dots (Figure 21, middle and right-hand panels). Taking together, these findings suggest that Yip1A mediates the formation of large autophagosome-like vacuoles via the activation of IRE1 under Tm treatment.

3.4 Activation of the IRE1 pathway of the UPR during infection with *B. abortus*

3.4.1 Depletion of Yip1A with siRNA.

In the present study, the IRE1 pathway of the UPR was preferentially induced by infection with *B. abortus* (Figure 8) and Yip1A was responsible for the activation of IRE1 under Tm treatment (Figure 14). To determine whether Yip1A has the same function during infection with *B. abortus*, I assessed the effect of Yip1A-knockdown on the activation of the IRE1 pathway during *Brucella* infection. HeLa cells were infected with *B. abortus*, and then transfected with scramble siRNA or Yip1A siRNA at 1 hr p.i. Infection with *B. abortus* preceded the siRNA transfection to eliminate any effects of Yip1A knockdown on the internalization of *B. abortus*. To evaluate the depletion of Yip1A during infection, RT-PCR and western blotting were performed for Yip1A. Yip1A mRNA was reduced by approximately 80% from 12 hr p.i. onwards (Figure 22A). Yip1A protein was reduced by 72.0% at 12 hr p.i., and by more than 80% at16 hr p.i. onwards (Figure 22B and 22C), and this knockdown of Yip1A protein was considered to be sufficient to demonstrate the role of Yip1A on the intracellular replication of *B. abortus* at these later time points. At 4 hr or 8 hr p.i., the knockdown of Yip1A protein was 16.8% or 46.1%, and thus the effects of Yip1A knockdown at these time points were likely to be limited.

3.4.2 Yip1A is responsible for the activation of the IRE1 pathway of the UPR

Then the activation of the UPR sensors IRE1, PERK, and ATF6 was analyzed by western blotting (Figure 23B and 24A). There was little difference in the total levels of IRE1 between control and Yip1A-knockdown cells throughout the experiment (Figure 23A). Control cells (Figure 23C, 24B and 24C) showed activation kinetics for these

molecules similar to those obtained in infected cells (Figure 8B, 9B and 9C). IRE1 was activated at early time points (4 hr and 8hr p.i.) and then at later time points (16 hr p.i. onwards) (Figure 23C), and PERK and ATF6 were not significantly activated during the course of infection (Figure 24B and 24C). In Yip1A-knockdown cells, the increase in pIRE1 at early time points (4 hr and 8 hr p.i.) was partially suppressed (Figure 23C), presumably reflecting insufficient knockdown of Yip1A (Figure 22C), but was abolished completely at 12 hr p.i. onwards (Figure 23C). The splicing of XBP1 appeared to be delayed in these cells (Figure 23D). RT-PCR for spliced-XBP1 mRNA revealed the distinct splicing kinetics between control and Yip1A-knockdown cells more clearly (Figure 23E). In control cells, the levels of spliced-XBP1 mRNA increased along with the increase in pIRE1: first at 4-8 hr p.i., and then at 20 hr p.i (Figure 23E). In Yip1A-knockdown cells, the lack of IRE1 activation at later time points led to complete loss of spliced XBP1 mRNA (Figure 23E). The levels of pPERK and cleaved-ATF6 remained almost the same between control and Yip1A-knockdown cells during infection (Figure 24B and 24C). These results support that Yip1A mediates the activation of IRE1 pathway of the UPR during infection with *B. abortus*.

3.4.3 Yip1A is responsible for the upregulation of Sar1, Sec23, and Sec24D

Next, I investigated the effects of Yip1A-knockdown on the upregulation of the COPII components Sar1, Sec23, and Sec24D. At 24 hr p.i., the levels of Sar1, Sec23, and Sec24D were significantly lower in Yip1A-knockdown cells than in control cells (Figure 25A and 25B). Here again, to further confirm the functional connection between

Yip1A and IRE1 in terms of these results, I knocked down the expression of IRE1 by using siRNA. IRE1 protein was reduced by 73.4% at 12 hr p.i., and by more than 80% at 16 hr p.i. onwards (Figure 26A). Similar to Yip1A-knockdown, IRE1-knockdown suppressed the upregulation of Sar1, Sec23, and Sec24D significantly (Figure 26B and 26C). Collectively, these results indicate that the upregulation of the COPII components Sar1, Sec23, and Sec24D during infection with *B. abortus* depends on the Yip1A-mediaed IRE1 activation.

3.5 Intracellular replication of *B. abortus.*

3.5.1 Depletion of Yip1A or IRE1 with siRNA

Several studies have suggested that *Brucella* infection induces the UPR (Qin et al., 2008, de Jong et al., 2013, Smith et al., 2013), but its functional significance in *Brucella* intracellular life remains unknown. To investigate the role of the IRE1 pathway of the UPR, the effects of Yip1A- or IRE1-knockdown on the intracellular replication of *B. abortus* was examined. HeLa cells were infected with *B. abortus*, and then transfected with scramble siRNA, Yip1A siRNA, or IRE1 siRNA at 1 hr p.i. The knockdown efficiency of Yip1A or IRE1 in infected cells was evaluated by quantifying the intensity of immunofluorescence staining for endogenous Yip1A (Figure 27A) or IRE1 (Figure 27C) at 24 hr p.i. Approximately 80% and 90% of depletion had been achieved for Yip1A (Figure 27B) and IRE1 (Figure 27D), respectively.

3.5.2 Yip1A-knockdown suppresses the intracellular growth of *B. abortus*

First, intracellular bacterial growth was evaluated by counting CFUs over 24 hr following infection. The kinetics of *Brucella* replication in control cells agreed with those obtained in previous studies (Pizarro-Cerda, 1998a, Celli et al., 2003) (Figure 28, solid bars). Robust increase in CFU occurred at 16 hr p.i. onwards, which indicates that *B. abortus* undergoes extensive replication. At 24hr p.i., 51.8-fold increase in CFU was observed. Intriguingly, Yip1A-knockdown inhibited bacterial growth, which resulted in about a 40% reduction in CFUs at 24 hr p.i. (Figure 28, open bars). IRE1-knockdown suppressed the increase in CFU in a similar manner to Yip1A-knockdown, and caused an about 50% reduction in CFU at 24 hr p.i. (Figure 28, solid gray bars).

To confirm further the effect on intracellular replication, the number of *B. abortus* within infected cells was examined by using immunofluorescence microscopy. Fixed cells were stained with an anti-*B. abortus* antibody. Consistent with the results in the CFU counting (Figure 28), only a few bacteria were observed in each siRNA-treated cells at 8hr p.i. (Figure 29A, upper panels). In control cells, the onset of bacterial replication could be seen at 16 hr p.i., and the cytoplasm of an infected cell was filled with robustly replicating bacteria at 24 hr p.i. (Figure 29, left-hand panels; also Figure 27A and 27C, left-hand panels). In contrast, Yip1A-knockdown cells (Figure 29A, middle panels; also and Figure 27A, right-hand panel) or IRE1-knockdown cells (Figure 29A, right-hand panels; also Figure 27C, right-hand panel) contained a considerably small number of *B. abortus* at 24 hr p.i. To assess the replication efficiency, the percentage of infected cells with fewer than ten *B. abortus* was determined. As can be seen in Figure 29B, significantly less bacteria were observed in Yip1A- or

IRE1-knockdown cells. Altogether, these results indicate that the activation of the IRE1 pathway is critical for *B. abortus* to establish a safe replication niche, and that Yip1A is indispensable for this process during infection.

3.6 Maturation of *B. abortus* into ER-derived BCVs.

3.6.1 Ultrastructural analysis of BCVs by electron microscopy

To characterize the deficiency in intracellular replication observed in Yip1A- or IRE1-knockdown cells, an ultrastructural analysis of BCVs by electron microscopy (EM) was performed at 24 hr p.i. (Figure 30A, 30B, and 30C). In control cells, infection with *B. abortus* generated a significant number of replicative BCVs with vacant vacuoles in their vicinity (Figure 30A). These membrane-bound compartments were derived from the ER, because ribosomes lined their surface (Figure 30A, inset, arrowheads). The lumens of the vacuoles were dilated, which resulted in massive ER expansion. As compared with control cells, Yip1A-knockdown cells (Figure 30B) displayed distinct morphological features. Only a few bacteria were observed within the cells, and enlarged vacuoles were rarely seen. Notably, most BCVs were not enclosed in ER-derived membranes (Figure 30B, inset). Similar results were obtained in IRE1-knockdown cells (Figure 30C).

Thus, the EM analysis of infected cells revealed two forms of BCVs, one with an outermost ER-derived membrane (Figure 30A, inset; defined as I), and the other devoid of the ER-derived membrane (Figure 30B, inset; defined as II). The percentage of these two types of BCVs was determined. At 24 hr p.i., about 85% of BCVs in control cells

acquired the ER-derived membrane, whereas approximately 70% of BCVs in Yip1A-knockdown cells were not sequestered into such a membrane (Figure 30D).

3.6.2 Characterization of vacuoles by immunofluorescence microscopy

In Brucella-infected control cells, large autolysosomal vacuoles that contained degraded cellular debris were observed (Figure 30A and 31A, asterisks). Interestingly, these vacuoles were also studded with ribosomes (Figure 31A, arrows), which indicated that fusogenic events had occurred with ER-derived vacuoles. To further confirm the ER feature on these vacuoles, immunofluorescence microscopy was performed. The replicating *B. abortus* were co-stained with Sec61α but not with Lamp2 (Figure 31B, arrows), consistent with the transition from endosomal/lysosomal to ER-derived BCVs. The vacant vacuoles (Figure 31B, arrowheads) and large autolysosomal vacuoles (Figure 31B, asterisks) were stained for both Lamp2 (a marker for endosomes/lysosomes) and Sec61α (a marker for rough ER), attesting to the endosomal/lysosomal as well as ER-derived origin of these compartments. In addition, some of large autolysosomal vacuoles (Figure 32, asterisk) were found to be GFP-LC3-positive (Figure 32, arrows), which indicates that the vacuoles have an autophagosome-like nature. The GFP-LC3 dots were also observed adjacent to *B. abortus* (Figure 32, arrowheads). Taken together, these results strongly suggest that *B. abortus* induces a marked accretion of ER-derived autophagosome-like vacuoles around replicating bacteria to mature into ER-derived replicative BCVs, and that the activation of IRE1, which is mediated by Yip1A, is required for this process.

3.6.3 Lamp2-positive BCVs

In Yip1A-knockdown cells, ER-derived autophagosome-like vacuoles were absent and BCVs were not sequestered into an ER-derived membrane (Figure 30B). This can be attributed to the defect in trafficking of BCVs from endosomal/lysosomal compartments to the ER or to the deficiency in the formation of ER-derived autophagosome-like vacuoles. First, the intracellular trafficking of BCVs in Yip1A-knockdown cells was examined by immunofluorescence microscopy for Lamp2, a marker for late endosomes/lysosomes. Co-localization of BCVs with Lamp2-positive vacuoles was assessed over time (Figure 33A and 33B). In control cells, BCVs left Lamp2-positive compartments in a time-dependent manner, and 92% of BCVs were Lamp2-negative at 24 hr p.i. (Figure 33B). By contrast, about 50% of BCVs were co-localized with Lamp2 in Yip1A-knockdown cells (Figure 33B), suggesting that these BCVs were confined within endosomal/lysosomal compartments. This implies that Yip1A may play an additional role in trafficking from the endosomal/lysosomal compartments to the ER to generate ER-derived BCVs. However, IRE1-knockdown cells showed kinetics similar to those of Yip1A-knockdown cells, and about half of BCVs were still retained in Lamp2-positive compartments at 24 hr i.p. (Figure 33B). Therefore, it is not likely that the absence of the ER-derived membrane around BCVs is due to the trafficking defects caused by Yip1A-knockdown.

3.6.4 Formation of autophagosomes

Next, the formation of autophagosomes was examined by fluorescence microscopy at 24hr p.i. An expression construct for GFP-LC3 was co-transfected with siRNA. In control cells infected with *B*. *abortus*, a number of large GFP-LC3 dots were observed in the vicinity of replicating bacteria (Figure 34A, left-hand panel); by contrast, the fluorescence staining of GFP-LC3 was faint and diffuse throughout the cytoplasm in *Brucella*-infected Yip1A-knockdown cells (Figure 34A, middle panel). A similar result was obtained by the knockdown of IRE1 (Figure 34A, right-hand panel). The number of GFP-LC3 dots was significantly low in Yip1A- or IRE1-knockdown cells (Figure 34B). These results demonstrate that HeLa cells induce autophagosomes during infection with *B*. *abortus*, and that there is a possible link between autophagosome formation and the Yip1A-mediated activation of IRE1. The transition from endosomal/lysosomal to ER-derived BCVs are likely to occur not via trafficking to the ER but via a fusogenic event with ER-derived autophagosome-like vacuoles, and Yip1A-mediated activation of IRE1 is required for the induction of autophagosome formation.

3.7 未発表の共同研究内容が含まれるので未掲載

3.7.1 未発表の共同研究内容が含まれるので未掲載

3.7.2 未発表の共同研究内容が含まれるので未掲載

3.7.3 未発表の共同研究内容が含まれるので未掲載

3.7.4 未発表の共同研究内容が含まれるので未掲載

3.7.5 未発表の共同研究内容が含まれるので未掲載

3.8 Proposed model of how *B. abortus* matures into ER-derived replicative BCVs

On the basis of the findings in the present study, I propose a model for the maturation of *B. abortus* into ER-derived replicative BCVs (Figure 46A). During infection, *B. abortus* triggers the activation of IRE1, presumably by secreting effector molecules（未発表の共同研究内容が含まれるので未掲載）into the cytoplasm of host cells. IRE1 molecules form high-order complexes at ERES with the aid of Yip1A, and are activated by trans-autophosphorylation. The activated IRE1 in turn triggers the biogenesis of ER-derived autophagosome-like vacuoles. These vacuoles then fuse with endolysosomal vesicles. *B. abortus* might intercept this UPR-induced ER-derived autophagy process to acquire ER-derived membranes. Since the bacteria that have reached the ER are located in late endosomal/lysosomal compartments (Starr et al., 2008), they would be able to fuse with these vacuoles. Once they have acquired the ER-derived membrane, BCVs retain functional features of the ER, and replication of *B. abortus* in individual vacuoles might be supported through continual accretion of ER membranes derived from the IRE1-specific UPR. In contrast, the knockdown of Yip1A (Figure 46B) or IRE1 (Figure 46C) prevents the activation of IRE1, and therefore ER-derived membranes are not available for *Brucella* replication. Consequently, BCVs remain in endosomal/lysosomal compartments.

4. Discussion

4.1 Yip1A functions in the activation of the IRE1 pathway of the UPR

In the present study, I identified a novel function of Yip1A in the activation of the IRE1 pathway of the UPR using tunicamycin treatment and infection with *B. abortus*. The activation of the IRE1 pathway leads to the biogenesis of ER-derived autophagosome-like vacuoles, which is required for *B. abortus* to establish its ER-derived replicative niche. The finding of Yip1A as a regulatory protein for the UPR and autophagy was unexpected. Yeast homolog of Yip1A, Yip1p, was first identified as a binding partner for Rab proteins (Yang et al., 1998), and Yip1A has been proposed to be involved in vesicle trafficking. To date, several functions in membrane trafficking have been suggested for Yip1A, including involvement in COPII vesicle budding at ERES (Tang et al., 2001), vesicle tethering to the Golgi membrane (Jin et al., 2005), and COPI-independent retrograde vesicle transport (Kano et al., 2009). However, in mammalian cells, interaction with Rab proteins has not been reported for Yip1A, and its function is still controversial. Recently, Dykstra et al. (2010) reported that ER morphology was affected by the depletion of Yip1A, but I did not observe such whorled ER formation, presumably because the event occurs after long-term treatment with Yip1A siRNA (48-72 hr) in contrast to the shorter-term treatment in this study (24 hr).

The precise mechanism for the involvement of Yip1A in the activation of IRE1 remains to be determined. However, several results in the present study suggest that the role of Yip1A in IRE1 activation is direct. First, the interaction between Yip1A and

pIRE1 is specific (Figure 11A and 11B, Figure 12) and depends on the induction of the UPR (Figure 11C). Second, the formation of large pIRE1 foci under Tm treatment is severely impaired by the depletion of Yip1A (Figure 17), which indicates that IRE1 fails to assemble into cluster under the UPR condition in the absence of Yip1A. Finally, Yip1A-knockdown prevents the formation of high-order complexes of pIRE1 (Figure 18). IRE1 is usually held in its inactive state by binding the ER chaperon protein Bip. Under conditions of ER stress, Bip is released from IRE1. However, the dissociation of Bip is not sufficient to fully activate IRE1 (Pincus et al., 2010), and unfolded proteins are required to promote oligomerization (Kimata et al., 2007). Yip1A may function as an additional regulatory molecule to stabilize high-order oligomeric state of IRE1 by limiting membrane diffusion or some other mechanisms.

4.2 Yip1A may coordinate COPII vesicle transport between the secretory pathway and the autophagy pathway

A model that I proposed for *Brucella* intracellular replication (Figure 46A) is in line with previous studies that demonstrate an intriguing link between the UPR and autophagic vacuole formation (Bernales et al., 2006, Hoyer-Hansen et al., 2008, Ogata et al., 2006, Li et al., 2008). Ogata et al. (2006) demonstrated that the IRE1 signaling pathway is required for the activation of autophagy under the UPR. They showed that the PERK and ATF6 pathways are not needed for the activation of autophagy. Our data also strongly suggest that the IRE1 pathway can regulate autophagic events independently from the other ER sensors.

In the present study, both tunicamycin treatment and infection with *B. abortus* upregulated the COPII vesicle components Sar1, Sec23, and Sec24D. These proteins assemble at ERES and lead to the curvature of the ER membrane. This might enhance the capacity of COPII vesicles to export from ERES by promoting to pinch off vesicles from the ERES. Several recent studies suggest that ER-derived COPII vesicles are destined not only for the early secretory pathway to the Golgi, but also for autophagy (Graef et al., 2013, Tan et al., 2013, Wang et al., 2014). Autophagosomes are formed at ERES, and newly budded COPII vesicles might function as a structural core and/or membrane source for autophagosome formation (Graef et al., 2013, Wang et al., 2014). Tan et al. (2013) indicate that COPII vesicles are rerouted from the secretory pathway to the autophagy pathway under starvation, and might supply membrane for autophagosome formation. They showed that distinct effectors of Ypt1 (the yeast homolog of Rab1) direct COPII vesicles to different pathways.

Brucella spp. might modulate these intracellular trafficking via multiple effectors. Myeni et al. (2013) demonstrated that the *Brucella* effectors BspB and BspF inhibit the host early secretory pathway prior to the biogenesis of replicative BCVs.（未発表の共同研究内容が含まれるので未掲載）These effectors might act coordinately to interrupt the host secretory pathway and to redirect trafficking to the ER-derived autophagy pathway. The upregulation of the COPII components Sar1, Sec23, and Sec24D during *Brucella* infection could facilitate the formation of autophagosomes. Given the dual function of Yip1A in COPII vesicle formation or budding at ERES (Tang et al., 2001) and in regulating the activation of IRE1 pathway of the UPR, which

has been documented in this study, Yip1A might coordinate COPII vesicle transport between the secretory pathway and the autophagy pathway.

4.3 Yip1A may transduce signals through the IRE1-JNK or IRE1-NF-κB pathway

In the present study, the levels of spliced-XBP1 were not reduced as drastically as IRE1 phosphorylation upon knockdown of Yip1A. This might indicate that other downstream pathways of IRE1 are affected by Yip1A-knockdown. Smith et al. (2013) suggest that the IRE1- c-Jun NH_2-terminal kinase (JNK) signaling pathway, rather than the IRE1-XBP1 pathway, supports *Brucella* replication in macrophages. In addition to the splicing of XBP1 mRNA, activated IRE1 also transmits signals through the tumor-necrosis factor receptor associated factor 2 (TRAF2) and JNK pathway. It also modulates the nuclear factor kappa light chain enhancer of activated B cells (NF-κB) and extracellular signal-regulated kinase (ERK) signaling pathways. Bernales et al. (2006) showed that expression of Hac1, the yeast homolog of XBP1, was insufficient to induce autophagosome formation, which suggests that other signaling pathways besides XBP1 are required. Ogata et al. (2006) suggest that activation of autophagy during the UPR is mediated by the IRE1-TRAF2-JNK pathway. I have found that the phosphorylation of JNK and NF-κB was reduced significantly in Yip1A-knockdown cells (unpublished data). Therefore, Yip1A may transduce signals through the IRE1-JNK or IRE1-NF-κB pathways.

4.4 Intracellular replication of *B. abortus*

Brucella spp. replicates within an ER-derived membrane-bound compartment in host cells. However, the molecular mechanisms by which the pathogen establishes the replicative niche remain unclear. In the present study, I demonstrated several lines of evidence that clarify the mechanism by which *B. abortus* acquires the ER-derived membrane. First, during *Brucella* infection, the IRE1 pathway, but not the PERK and ATF6 pathways, of the UPR was activated, and the COPII vesicle components Sar1, Sec23, and Sec24D were upregulated. Second, biogenesis of ER-derived autophagosome-like vacuoles was observed in *Brucella*-infected cells. Third, Yip1A was identified as a novel host factor that is required for the activation of IRE1 and the subsequent formation of ER-derived autophagosome-like vacuoles. In Yip1A-knockdown cells, *B. abortus* failed to be sequestered within an ER-derived membrane, and remained in an endosomal/lysosomal compartment. （未発表の共同研究内容が含まれるので未掲載）On the basis of these findings, I proposed a model for *Brucella* maturation into ER-derived replicative BCVs. (Figure 46).

The proposed model explains many previous findings. For example, *Brucella* exploits the host autophagy machinery to reach its replication compartment (Pizarro-Cerdá et al., 1998b, Celli et al., 2003). Functional ERES, but not the subsequent secretory pathway, are required for the biogenesis of replicative BCVs and Sar1 mediates the fusion event between BCVs and the ER at ERES. COPII complexes are formed in close proximity to BCVs (Celli et al., 2005). These earlier reports did not address the mechanism by which the interaction of BCVs with Sar1/ERES and COPII

complexes enables the bacteria to mature into ER-derived replicative BCVs. The extensive *Brucella* replication is linked to an accretion of the ER (Celli et al., 2005). Mutants of the *Brucella virB* operon, encoding the T4SS, are unable to sustain interaction with the ER, which suggests that the translocation of the *Brucella* VirB effector is involved in this step (Celli et al., 2003). In the present study, I characterized the interplay between the host and pathogen at the molecular level, thereby showing how *B. abortus* subverts the host UPR and autophagy machineries to mature into ER-derived replicative BCVs.

The depletion of Yip1A confined BCVs within Lamp2-positive compartments. This implies that Yip1A may play an additional role in trafficking from the endosomal/lysosomal compartments to the ER to generate ER-derived BCVs. Kano et al. (2009) proposed that Yip1A regulates retrograde trafficking to the ER, which is associated with membrane recruitment of Rab6. Chen and Machner (2013) demonstrated that *L. pneumophila* secretes an effector protein LidA (Lowered viability in the presence of dotA) through its Dot (Defective for organelle trafficking)/Icm (Intracellular multiplication) type IV secretion system to recruit Rab6 on *Legionella*-containing vacuoles (LCVs), which is required for efficient intracellular replication of the pathogen. In the present study, however, the knockdown of IRE1 yielded similar effects to those of Yip1A-knockdown: BCVs were locked in a Lamp2-positive stage devoid of ER-derived membrane, the upregulation of the COPII components was suppressed, and ER-derived autophagosome-like vacuoles were diminished. These results indicate that the transition from endosomal/lysosomal to

ER-derived BCVs occurs not via trafficking to the ER but via a fusogenic event with

ER-derived autophagosome-like vacuoles, and that Yip1A-mediated activation of IRE1

at ERES is required for the induction of the ER-derived autophagy.

4.5 未発表の共同研究内容が含まれるので未掲載

4.6 UPR and autophagy in therapeutic aspects.

In the present study, I provided the first evidence showing that Yip1A plays a

pivotal role in the activation of the IRE1 pathway of the UPR and the subsequent

formation of ER-derived autophagosome-like vacuoles. Functional interaction between

two cellular machineries, the UPR and autophagy, was demonstrated in the context of

infection of HeLa cells with *B*. *abortus* as well as under tunicamycin treatment. The

challenge for the future is to characterize the interaction between Yip1A and IRE1, and

to elucidate the molecular mechanisms of how Yip1A regulates the activation of the

IRE1 pathway of the UPR and transits signals to the autophagy pathway.

Both the UPR and autophagy function to alleviate adverse physiological or

pathological conditions and to restore cellular homeostasis, which determines whether

cells survive or die. Currently, the UPR and autophagy represent promising pathways

for treatment of a number of human diseases including cancers, diabetes, atherosclerosis,

and neurodegenerative diseases (Suh et al., 2012, Cao and Kaufman, 2013). On the

other hand, the UPR and autophagy may play a causative role in a variety of disorders.

For example, cancer cells are constitutively under high oxidative stress and the

activation of the UPR and autophagy has been reported in several cancers. Molecules that modulate the UPR and autophagy can be therapeutic candidates for diverse diseases. The characterization of the function of Yip1A will provide new insights into the molecular mechanisms of these diseases, and contributes to design therapeutic strategies against these diseases.

5. Figures
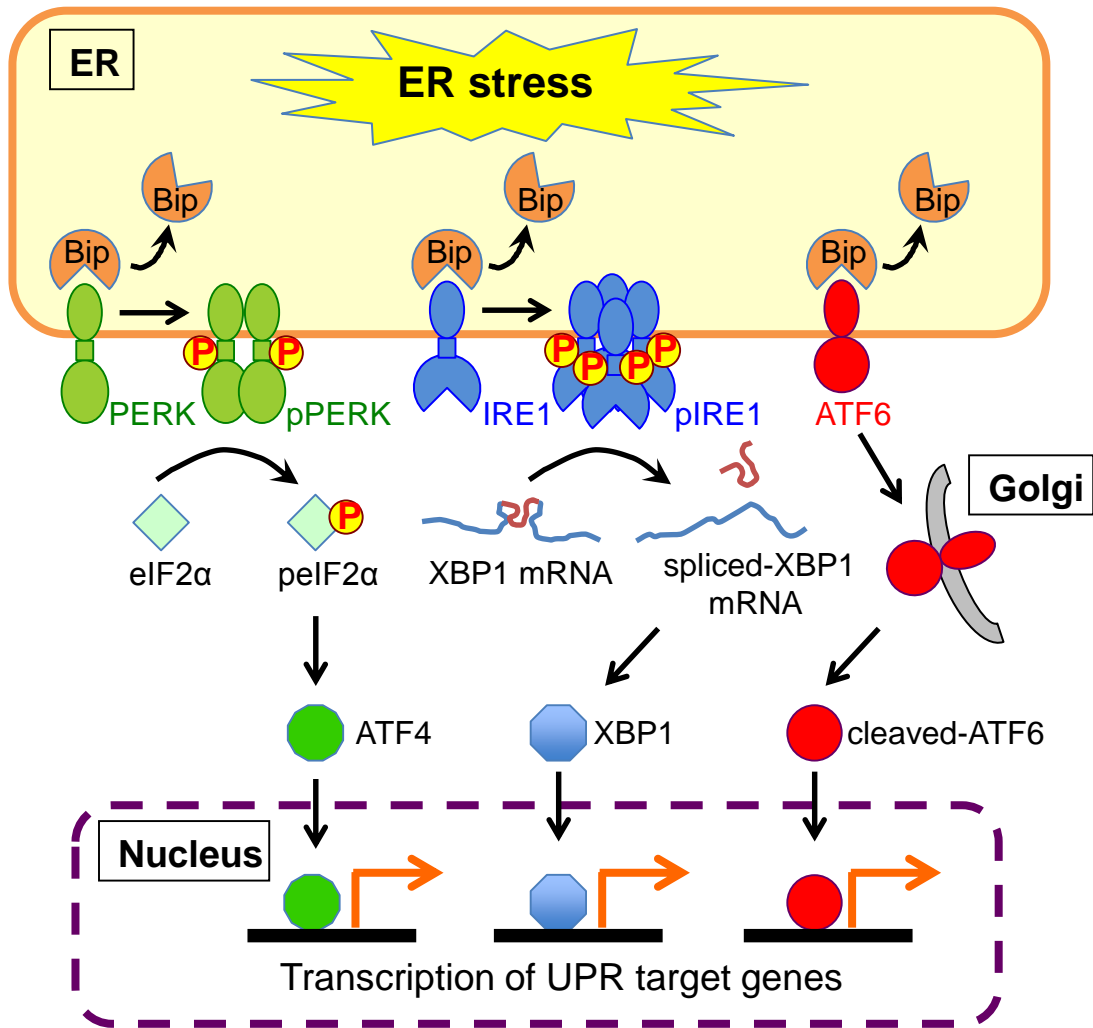
Figure 1. Unfolded protein response in mammalian cells

The accumulation of misfolded or unfolded proteins induces ER stress. To restore homeostasis in the ER, cells trigger intracellular signaling pathway called unfolded protein response (UPR). The UPR is composed of three pathways that are initiated by distinct ER sensors: IRE1, PERK and ATF6. These sensors are usually held in an inactive state by binding the ER chaperon protein Bip. IRE1 oligomerizes upon release of Bip, which drives trans-autophosphorylation. Activated IRE1 splices the XBP1 mRNA to produce an active transcription factor, spliced-XBP1 protein. PERK homodimerizes and undergoes trans-autophosphorylation in response to ER stress. Activated PERK phosphorylates eIF2α, which activates translation of ATF4. ATF6 translocates from the ER to the the Golgi, where it is cleaved proteolytically, producing an active transcription factor, cleaved-ATF6 protein. Spliced-XBP1, ATF4, and cleaved-ATF6 translocate to the nucleus, where they induce the transcription of UPR target genes. These responses alleviate the ER stress by reducing global protein synthesis, by increasing the folding capacity of the ER, and by removing misfolded or unfolded proteins from the ER. When the UPR cannot restore ER stress, apoptotic pathway is initiated to removed the stressed cells.
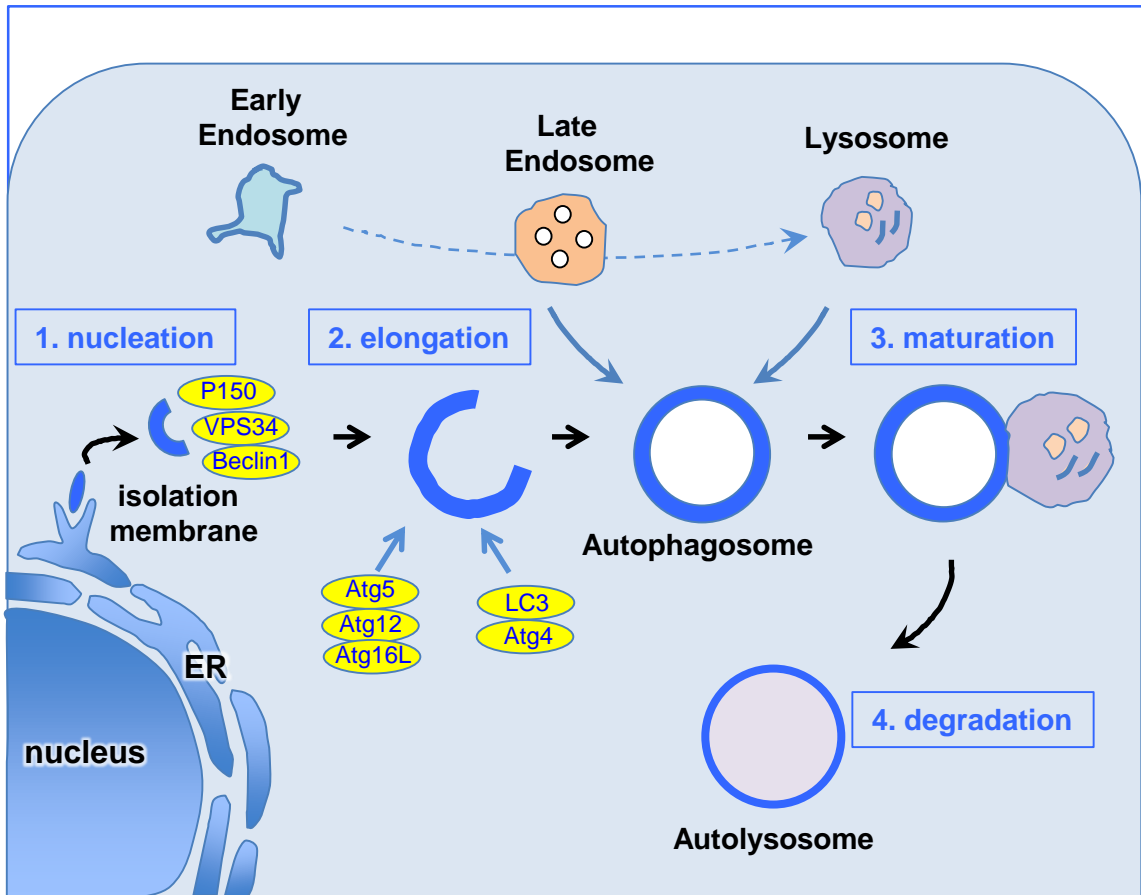
Figure 2. Autophagy pathway

Autophagy consists of four steps: nucleation, elongation, maturation, and degradation. The isolation membrane is formed to initiate autophagy. The P150-VPS34-Beclin1 complex involves in this nucleation step. During elongation step, the Atg5-Atg12-Atg16L complex and the LC3-Atg4 complex are recruited to the isolation membrane. Closed autophagosomes mature into autolysosomes by fusing with endocytic compartments including late endosomes and lysosomes. The inner membrane and contents of autophagosome are degraded by lysosomal proteases.
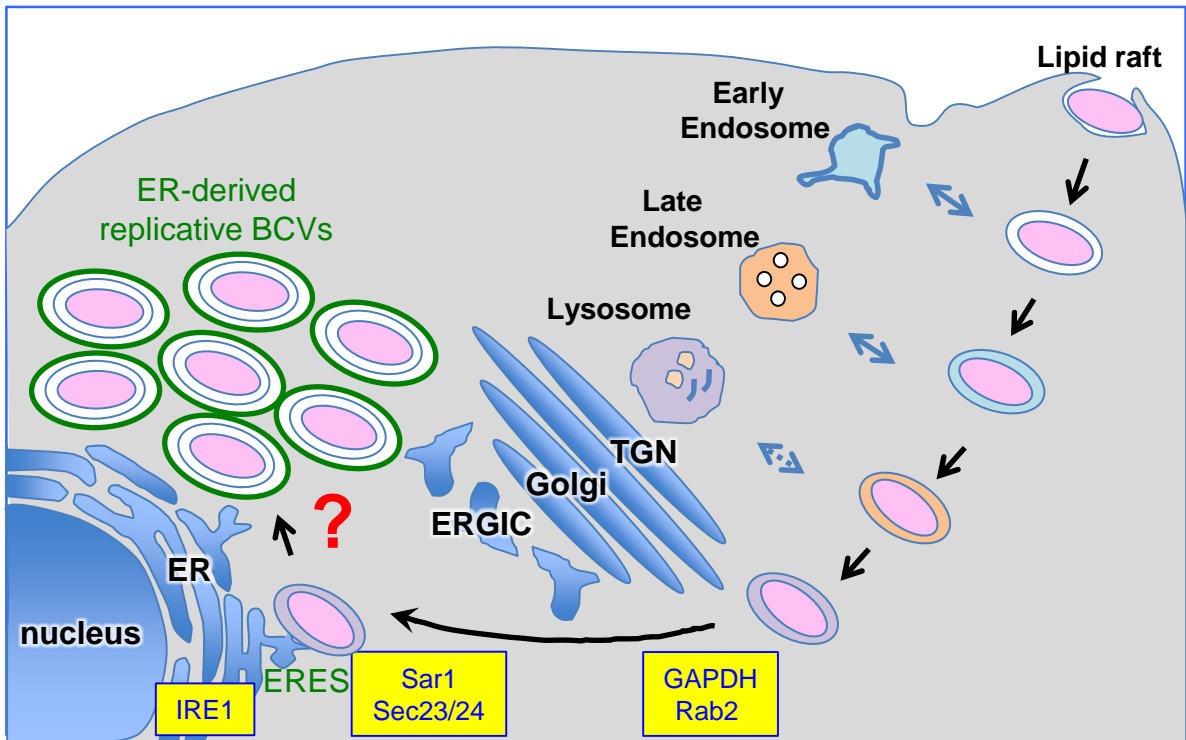
Figure 3. *Brucella* **intracellular trafficking in host cells**

Once inside host cells, *Brucella* resides in a membrane-bound compartment, the *Brucella*-containing vacuole (BCV). BCVs undergo a series of interactions with vesicular trafficking pathways in host cells. They transiently interact early and late endosomes, and then lysosomes in a limited way. Following the interaction with the endocytic compartments, BCVs are targeted to the ER, where they interact with ERES. The interaction leads to fusogenic events between the BCVs and ER membranes, generating ER-derived replicative BCVs. However, the mechanisms by which the bacteria are sequestered into such vacuoles and obtain a continuous membrane supply for their replication remain unknown. Host factors that are necessary for *Brucella* replication are shown.

A.
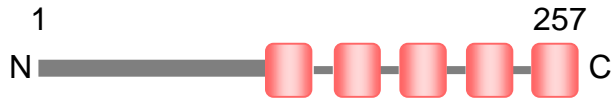
B.

```
  1 MSGFENLNTD FYQTSYSIDD QSQQSYDYGG SGGPYSKQYA

 41 GYDYSQQGRF VPPDMMQPQQ PYTGQIYQPT QAYTPASPQP

 81 FYGNNFEDEP PLLEELGINF DHIWQKTLTV LHPLKVADGS

121 IMNETDLAGP MVFCLAFGAT LLLAGKIQFG YVYGISAIGC

161 LGMFCLLNLM SMTGVSFGCV ASVLGYCLLP MILLSSFAVI

201 FSLQGMVGII LTAGIIGWCS FSASKIFISA LAMEGQQLLV

241 AYPCALLYGV FALISVF
```

Figure 4. Human Yip1A protein

(A) Schematic representation of human Yip1A protein. Yip1A is a 257 amino acids multi-pass transmembrane protein with the hydrophilic N-terminus and the hydrophobic C-terminus. ▬ represents hydrophilic regions, and ▢ shows hydrophobic regions.
(B) The amino acid sequences of human Yip1A. Hydrophobic regions are shaded in red. The region that interacts with Sec23 is underlined (amino acid residues 75-106, Tang et al, 2001).
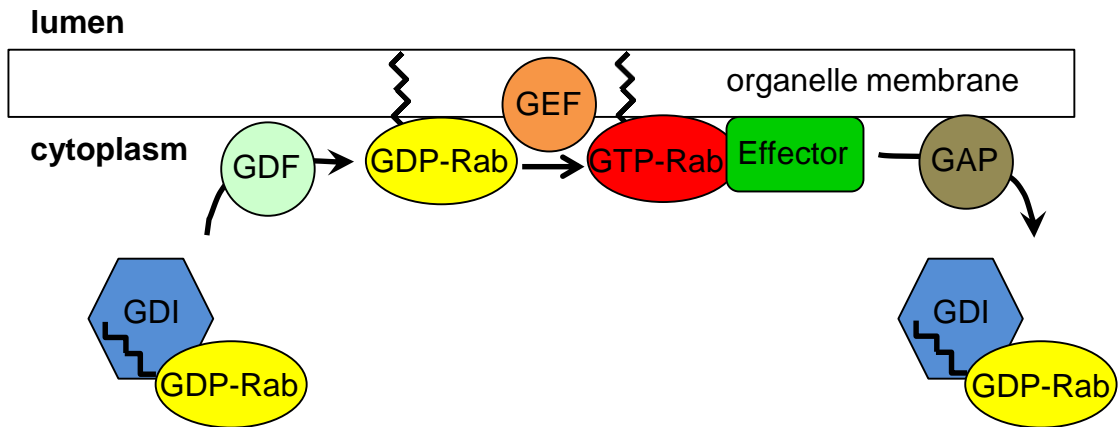
Figure 5. Rab small GTPase
The inactive GDP-bound form of Rab binds a guanine nucleotide dissociation inhibitor (GDI) in the cytoplasm. A GDI displacement factor (GDF) dissociates GDI from the Rab, which leads to insertion of the Rab into the membrane via a prenyl group. The prenylated Rab is activated by a guanine nucleotide exchange factor (GEF) to the GTP-bound form. The GTP-bound Rab interacts with effectors that mediate vesicle trafficking. Finally, a GTPase activating protein (GAP) catalyzes the hydrolysis of GTP to GDP, and the GDP-bound Rab is released from the membrane into the cytoplasm.
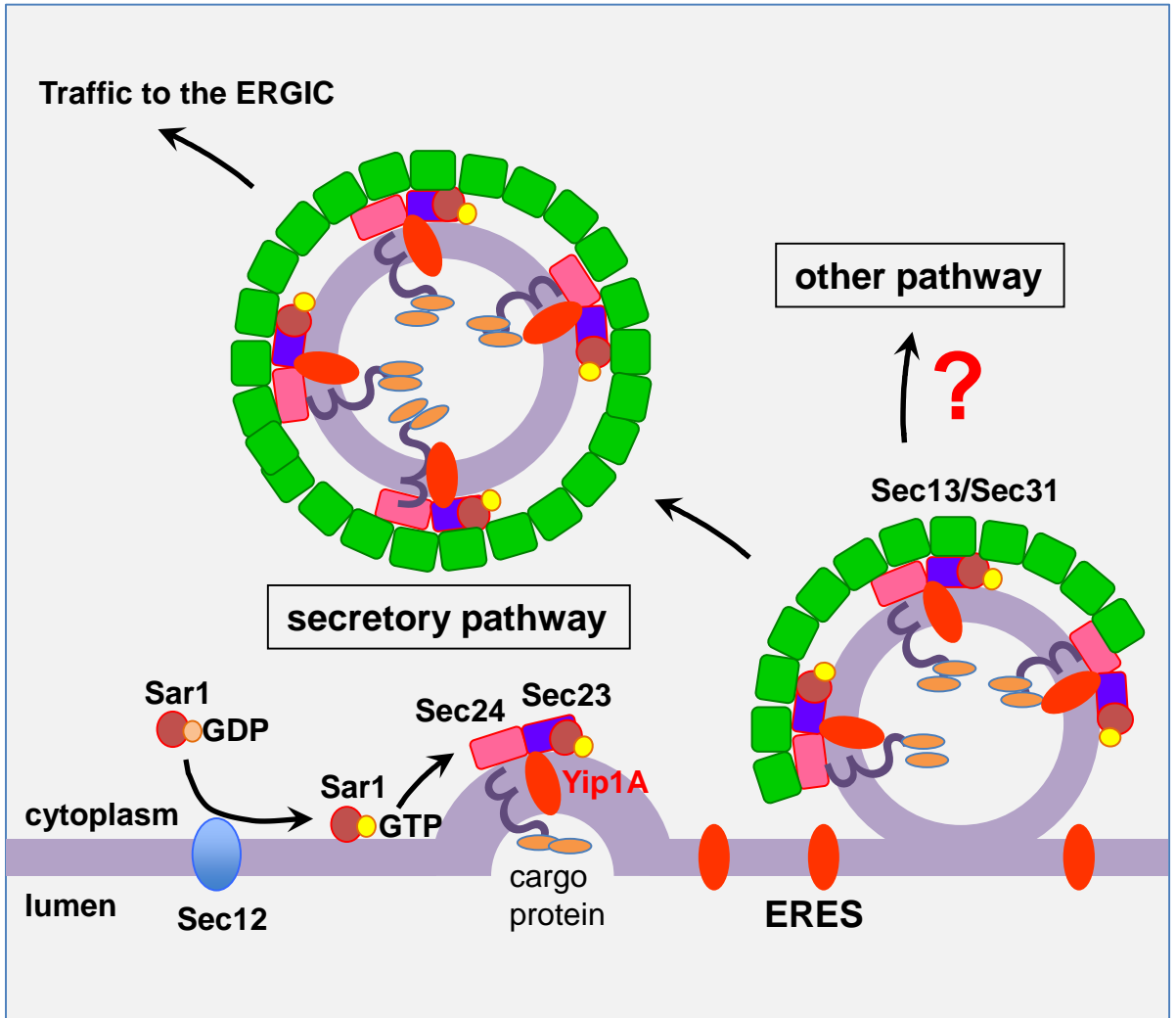
Figure 6. COPII vesicle biogenesis at ERES

The small GTPase Sar1 is recruited on the ER membrane through the membrane bound GEF Sec12 that converts the GDP-bound form of Sar1 into GTP-bound form. Activated Sar1 induces membrane bending, and leads to recruitment of the inner coat components Sec23-Sec24 by directly binding Sec23. Sec24 binds cargo proteins and concentrates them, thus forming a 'pre-budding complex'. Then the outer coat components Sec13-Sec31 polymerize to collect pre-budding complexes and shape the vesicles. Finally, a transport vesicle buds from the ER and delivers cargo proteins to the ERGIC. Yip1A cycles between the ER and the cis-Golgi. At ERES, Yip1A interacts with the Sec23/Sec24 complex. Yip1A might be involved in biogenesis of COPII vesicles that are not destined for the secretory pathway.
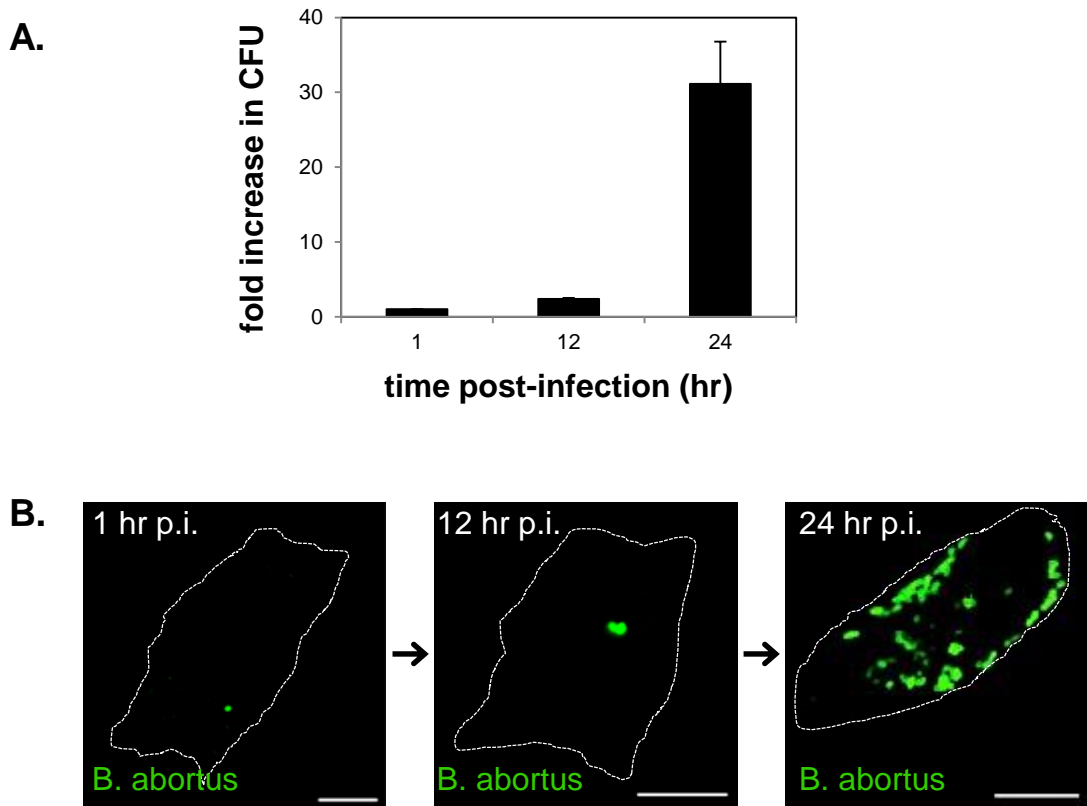
Figure 7. Replication of *B. abortus* within HeLa cells
(A) Intracellular growth of *B. abortus* within HeLa cells. HeLa cells were infected with *B. abortus* and extracellular bacteria were eliminated by treatment with gentamicin for 1 hr. CFUs were determined at 1, 12, and 24 hr p.i. A significant increase in the number of CFUs was observed at 24hr p.i. Data are means ± SD from three independent experiments.
(B) Representative confocal micrograph of HeLa cells infected with *B. abortu*s at 1, 12, and 24 hr p.i. Fixed cells were stained for *B. abortus* (green). Extensive intracellular replication of *B. abortus* was observed at 24hr p.i. The infected cell is outlined with white dashed lines. Scale bar is 10 μm.
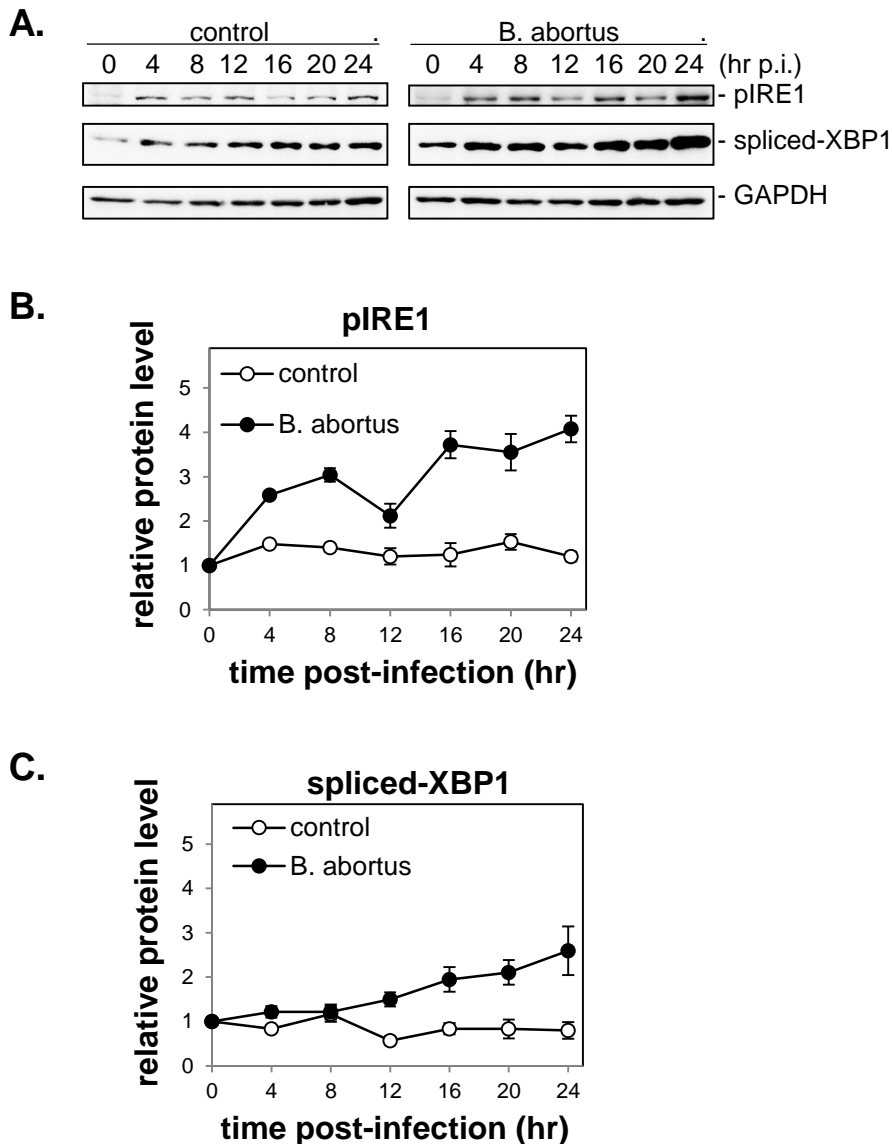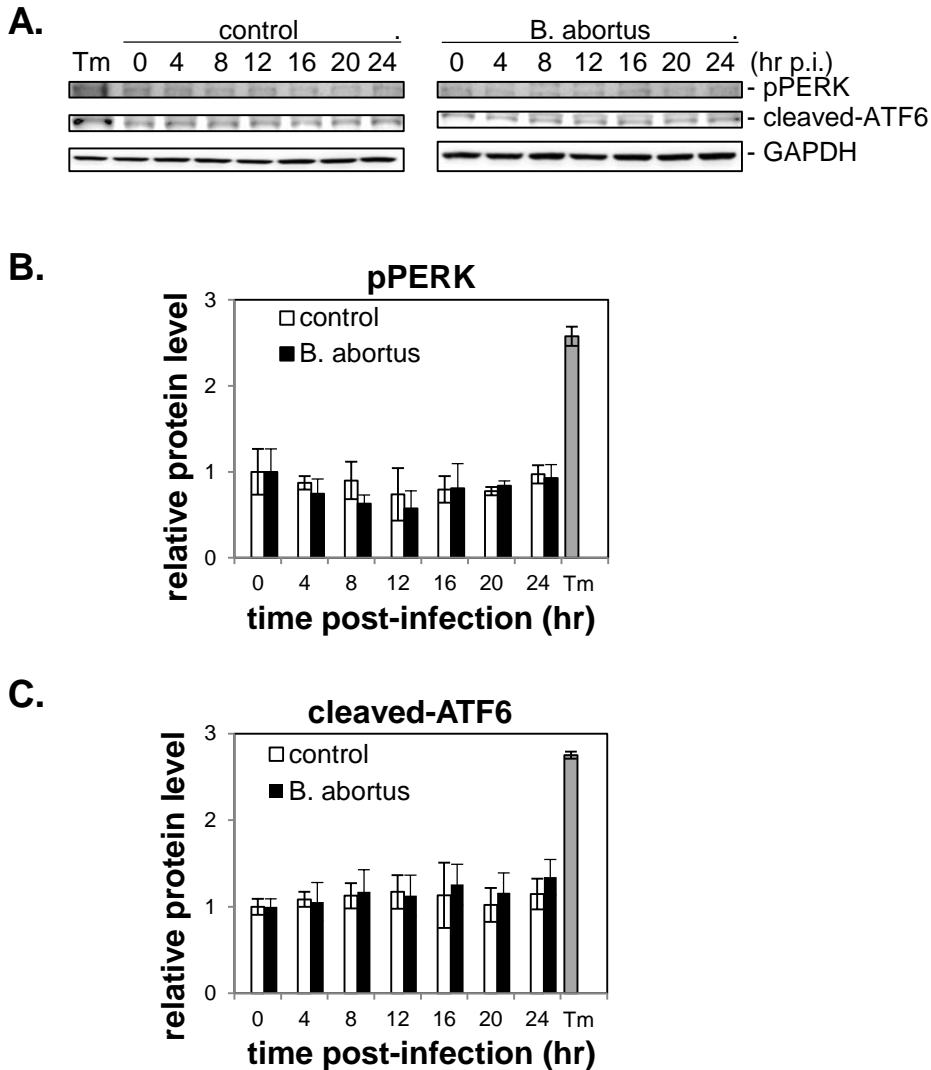
Figure 8. The IRE1 pathway of the UPR was activated by infection with *B. abortus*
HeLa cells were uninfected ('control') or infected with *B. abortus* ('B. abortus'). Cell lysates
were collected at the indicated time points after infection and analyzed by western blotting.
(A) Representative immunoblots for phosphorylated IRE1 (pIRE1), spliced-XBP1, and GAPDH.
GAPDH was used for normalization. The intensity of the bands was quantified using the
MultiGauge software.
(B) Relative protein levels of pIRE1 in uninfected control (open circles) and *Brucella*-infected
(solid circles) cells. The protein levels at time 0 hr were assigned the value 1. A drastic increase
in pIRE1 was observed in *B. abortus*-infected cells at early time points (4 hr and 8 hr p.i.), and
then later (16 hr p.i. onwards). Data are means ± SD from three independent experiments.
(C) Relative protein levels of spliced-XBP1 in uninfected control (open circles) and *Brucella*-
infected (solid circles) cells. The protein levels at time 0 hr were assigned the value 1. Spliced-
XBP1 increased over time in *B. abortus*-infected cells. Data are means ± SD from three
independent experiments.

A.

B.

pPERK

C.

cleaved-ATF6

Figure 9. The PERK and ATF6 pathways of the UPR were not activated by infection with
B. abortus

HeLa cells were uninfected ('control') or infected with *B. abortus* ('B. abortus'). Cell lysates
were collected at the indicated time points after infection and analyzed by western blotting. As a
positive control for the activation of PERK and ATF6, HeLa cells treated with 5 μg/ml of
tunicamycin for 8 hr were included in the analysis ('Tm').

(A) Representative immunoblots for pPERK, cleaved-ATF6, and GAPDH. GAPDH was used
for normalization. The intensity of the bands was quantified using the MultiGauge software.

(B) Relative protein levels of pPERK in control (open bars) and *Brucella*-infected (solid bars)
cells. The protein levels at time 0 hr were assigned the value 1. The levels of phosphorylated
PERK (pPERK) were similar between control and infected cells, and relatively constant during
the course of infection, which indicates that the PERK pathway of the UPR was not activated by
infection with *B. abortus*. Data are means ± SD from three independent experiments.

(C) Relative protein levels of cleaved-ATF6 in control (open bars) and *Brucella*-infected (solid
bars) cells. The protein levels at time 0 hr were assigned the value 1. The levels of cleaved-ATF6
in *Brucella*-infected were comparable to those in control cells, and did not changed significantly,
which indicates that the ATF6 pathway was not activated by infection with *B. abortus*. Data are
means ± SD from three independent experiments.

A.

control B. abortus

- Sar1
- Sec23
- Sec24D
- GAPDH

B.

Sar1 — relative protein level — control B. abortus — **

Sec23 — relative protein level — control B. abortus — **

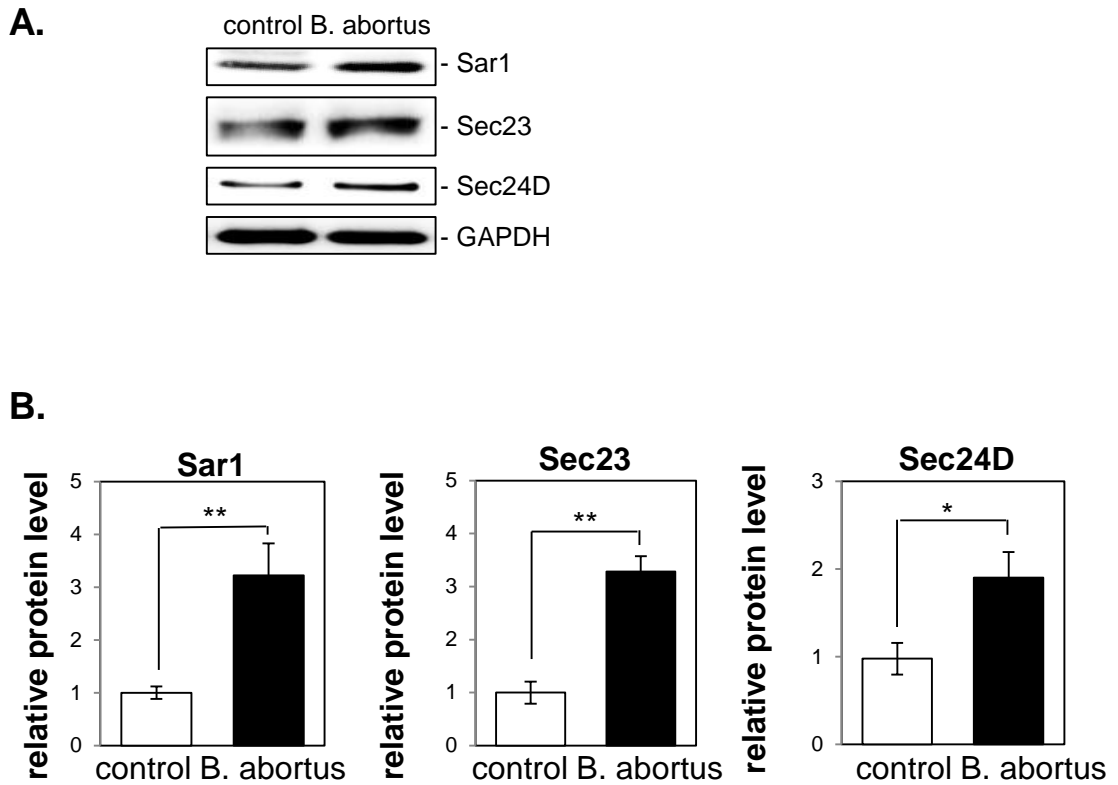Sec24D — relative protein level — control B. abortus — *

Figure 10. The COPII components Sar1, Sec23, and Sec24D were upregulated by infection with *B. abortus*

HeLa cells were uninfected ('control') or infected with *B. abortus* ('B. abortus'). Cell lysates were collected at 24hr p.i. and analyzed by western blotting.

(A) Representative immunoblots for Sar1, Sec23, Sec24D, and GAPDH. GAPDH was used for normalization. The intensity of the bands was quantified using the MultiGauge software.

(B) Relative protein levels of Sar1, Sec23, and Sec24D in uninfected control (open bars) and *Brucella*-infected (solid bars) cells. The protein levels in control cells were assigned the value 1. The expression of Sar1, Sec23, and Sec24D was increased significantly in *Brucella*-infected cells. Data are means ± SD from three independent experiments. *: $p<0.05$**; **: $p<0.01$.
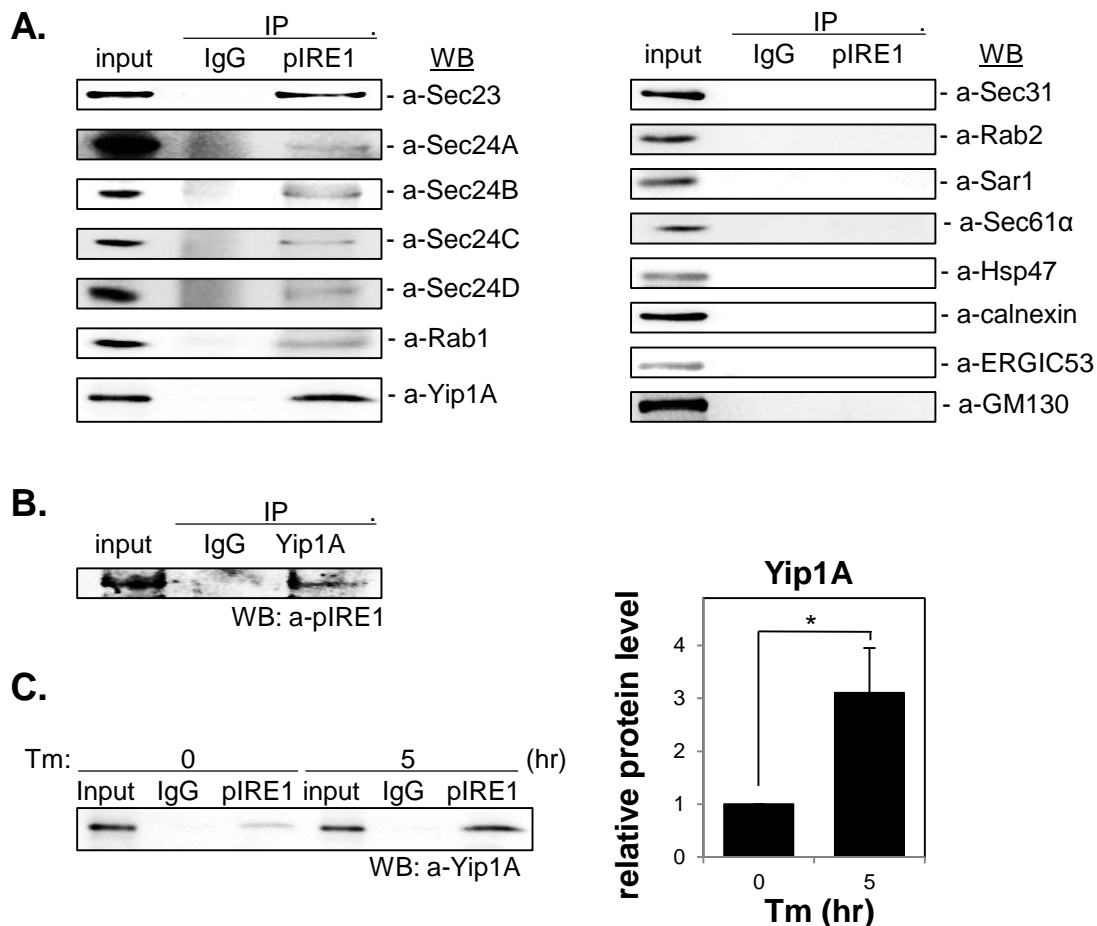
Figure 11. Yip1A specifically interacts with pIRE1

(A) Representative immunoblots showing co-immunoprecipitation with pIRE1. After 5 hr of Tm treatment, immunoprecipitation was performed on HeLa cell lysates with an anti-pIRE1 antibody (lanes labeled 'pIRE1') or control anti-rabbit IgG (lanes labeled 'IgG'), and the immunoprecipitates were analyzed by western blotting for a panel of molecules known to be involved in the ER-Golgi vesicular transport pathways or for ER- (Sec61α, HSP47, and calnexin), ERGIC- (ERGIC53) and *cis*-Golgi- (GM130) resident proteins. Phosphorylated IRE1 interacts with the inner components of the COPII coat (Sec23, Sec24A, Sec24B, Sec24C, and Sec24D), Rab1, and Yip1A, but not with a component of the outer coat (Sec31A), Rab2, Sar1, and some ER- (Sec61α, HSP47 and calnexin), ERGIC- (ERGIC53) and *cis*-Golgi- (GM130) resident proteins.

(B) Representative immunoblot showing the co-immunoprecipitation of pIRE1 with Yip1A. After 5 hr of Tm treatment, immunoprecipitation was performed on HeLa cell lysates with an anti-Yip1A antibody (lane labeled 'Yip1A') or control anti-rabbit IgG (lane labeled 'IgG'), and the immunoprecipitates were analyzed by western blotting with an anti-pIRE1 antibody. Phosphorylated IRE1 was identified to bind to Yip1A.

(C) Representative immunoblot showing the co-immunoprecipitation of Yip1A with pIRE1. After 0 hr or 5 hr of Tm treatment, immunoprecipitation was performed on HeLa cell lysates with an anti-pIRE1 antibody (lane labeled 'pIRE1') or control anti-rabbit IgG (lane labeled 'IgG'), and the immunoprecipitates were analyzed by western blotting with an anti-Yip1A antibody. The intensity of the bands was quantified using the MultiGauge software, and the results are shown in the bar graph. The protein levels at 0 hr of Tm treatment were assigned the value 1. The interaction of Yip1A with pIRE1 was enhanced upon Tm treatment. Data are means ± SD from three independent experiments. *: p<0.05.
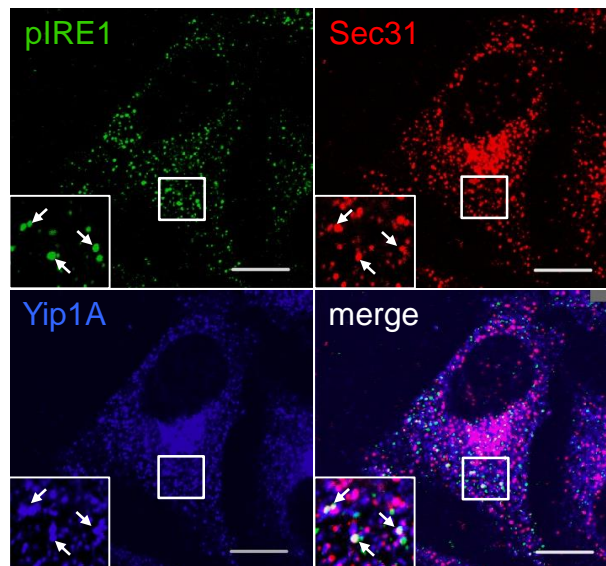
A.
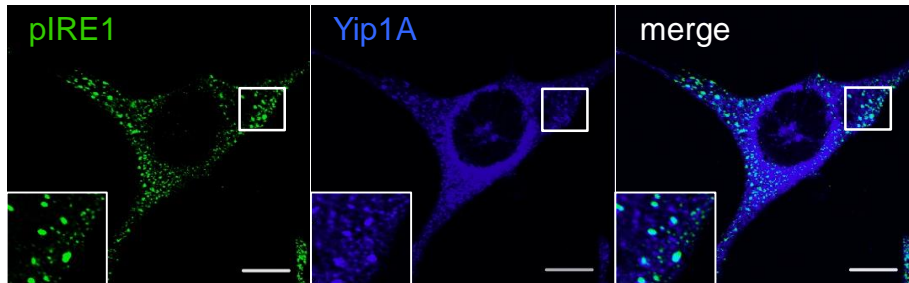
B.

Figure 12. Yip1A co-localizes with pIRE1 at ERES
(A) Representative confocal micrographs of HeLa cells double-stained for pIRE1 (green) and Yip1A (blue) after 5 hr of Tm treatment. Insets are magnifications of the boxed areas on the main image. Large pIRE1 foci co-localized with Yip1A. Scale bars are 10 μm.
(B) Representative confocal micrographs of HeLa cells triple-stained for pIRE1 (green), Sec31 (red), a marker for ERES, and Yip1A (blue) after 5 hr of Tm treatment. Insets are magnifications of the boxed areas on the main image. Co-localized Yip1A, pIRE1 and Sec31 were identified as large, bright foci (arrows). Thus pIRE1 were co-located with Yip1A at ERES upon the induction of the UPR. Scale bars are 10 μm.

A.

B.
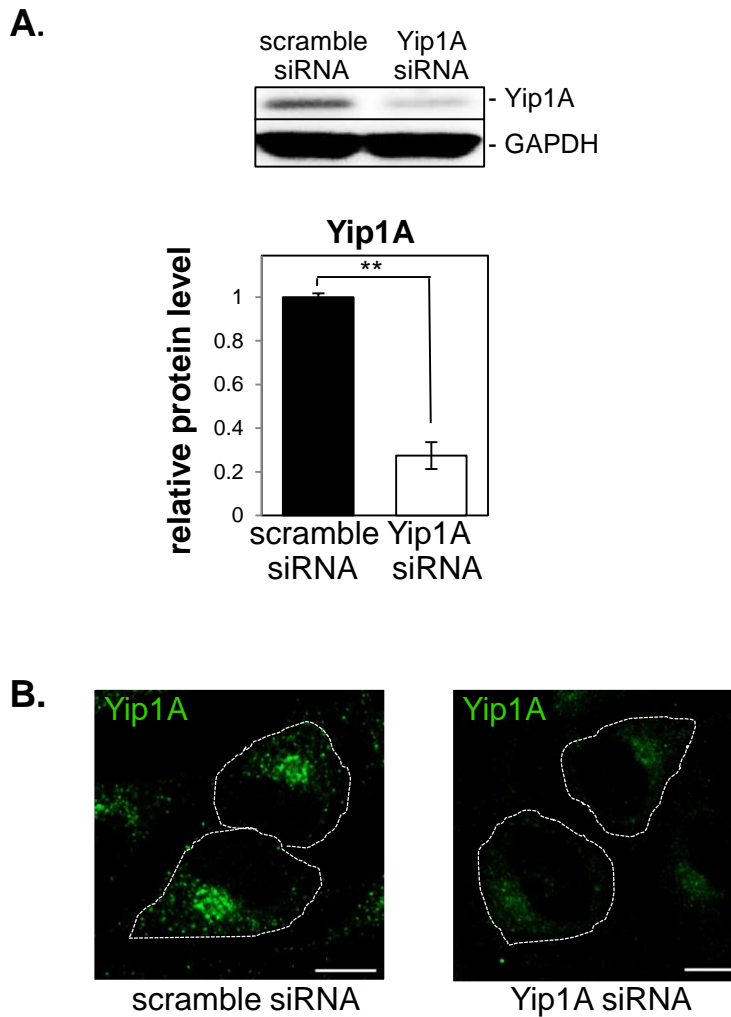
Figure 13. Depletion of Yip1A with siRNA

(A) Representative immunoblots showing the knockdown efficiency of Yip1A in HeLa cells at 24 hr after siRNA transfection. GAPDH was used for normalization. The intensity of the bands was quantified using the MultiGauge software, and the results are shown in the bar graph. The protein levels in control cells were assigned the value 1. The expression of Yip1A was reduced by 72.5%. Data are means ± SD from three independent experiments. **: $p<0.01$.

(B) Representative confocal micrographs of control (left-hand panel) and Yip1A-knockdown (right-hand panel) cells stained for Yip1A, showing the depletion of Yip1A at 24 hr after siRNA transfection. Cells are outlined with white dashed lines. Scale bars are 10 μm.
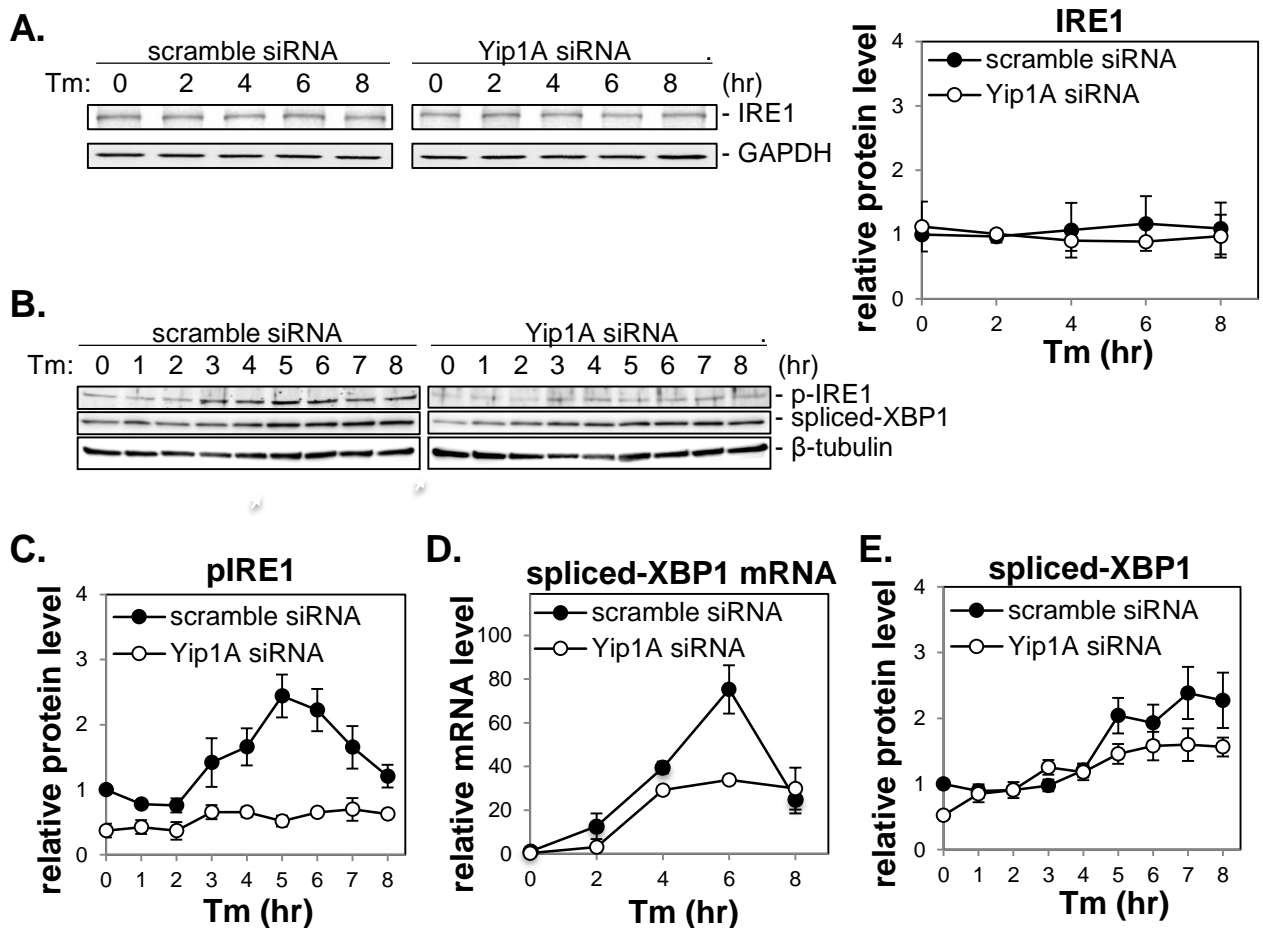
Figure 14. Yip1A is responsible for the activation of the IRE1 pathway of the UPR
HeLa cells were transfected with control scramble siRNA or Yip1A siRNA for 24 hr, and then treated with Tm to induce the UPR. Cell lysates were prepared at the indicated time points and analyzed by western blotting.

(A) Representative immunoblots for IRE1 and GAPDH. GAPDH was used for normalization. The intensity of the bands was quantified using the MultiGauge software. Relative protein levels of IRE1 in control (solid circles) and Yip1A-knockdown (open circles) cells during Tm treatment are shown in the line graph. The protein levels in control cells at the beginning of the Tm treatment were assigned the value 1. There was no difference in the total levels of IRE1 between control and Yip1A-knockdown cells throughout the experiment. Data are means ± SD from three independent experiments.

(B) Representative immunoblots for pIRE1, spliced-XBP1, and β-tubulin. β-tubulin was used for normalization. The intensity of the bands was quantified using the MultiGauge software.

(C-E) Relative protein levels of pIRE1 (C), relative mRNA levels of spliced-XBP1 (D), and relative protein levels of spliced-XBP1 (E) in control (solid circles) and Yip1A-knockdown (open circles) cells. The protein or mRNA levels in control cells at the beginning of the Tm treatment were assigned the value 1. The phosphorylation of IRE1 peaked at 5 hr after the addition of Tm, and then began to decrease (C). The splicing of XBP1 mRNA correlated with the activation of IRE1 (D), which resulted in an increase in spliced-XBP1 protein from 5 hr onwards (E). Knockdown of Yip1A diminished the increase in pIRE1 during Tm treatment (C). The splicing of XBP1 mRNA (D) and the amount of spliced-XBP1 protein (E) were reduced by the depletion of Yip1A. Data are means ± SD from three independent experiments.
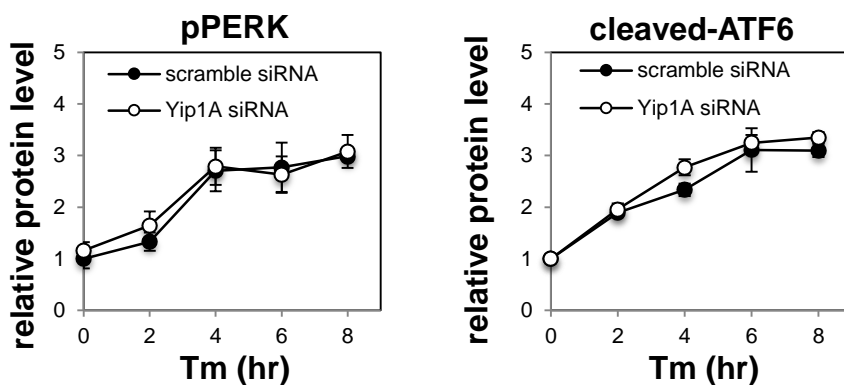
A.
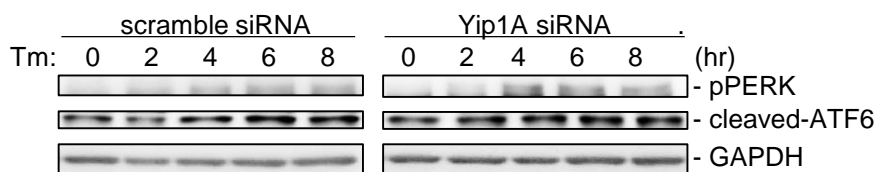
B.

Figure 15. Yip1A knockdown had no effect on the activation of PERK or ATF6
HeLa cells were transfected with control scramble siRNA or Yip1A siRNA for 24 hr, and then treated with Tm to induce the UPR. Cell lysates were prepared at the indicated time points and analyzed by western blotting.
(A) Representative immunoblots for pPERK, cleaved-ATF6 and GAPDH. GAPDH was used for normalization. The intensity of the bands was quantified using the MultiGauge software.
(B) Relative protein levels of pPERK and cleaved-ATF6 in control (solid circles) and Yip1A-knockdown (open circles) cells during Tm treatment. The protein levels in control cells at the beginning of the Tm treatment were assigned the value 1. There is no significant difference between control and Yip1A-knockdown cells in the activation of PERK or ATF6. Data are means $\pm$ SD from three independent experiments.

A.

B.

C.
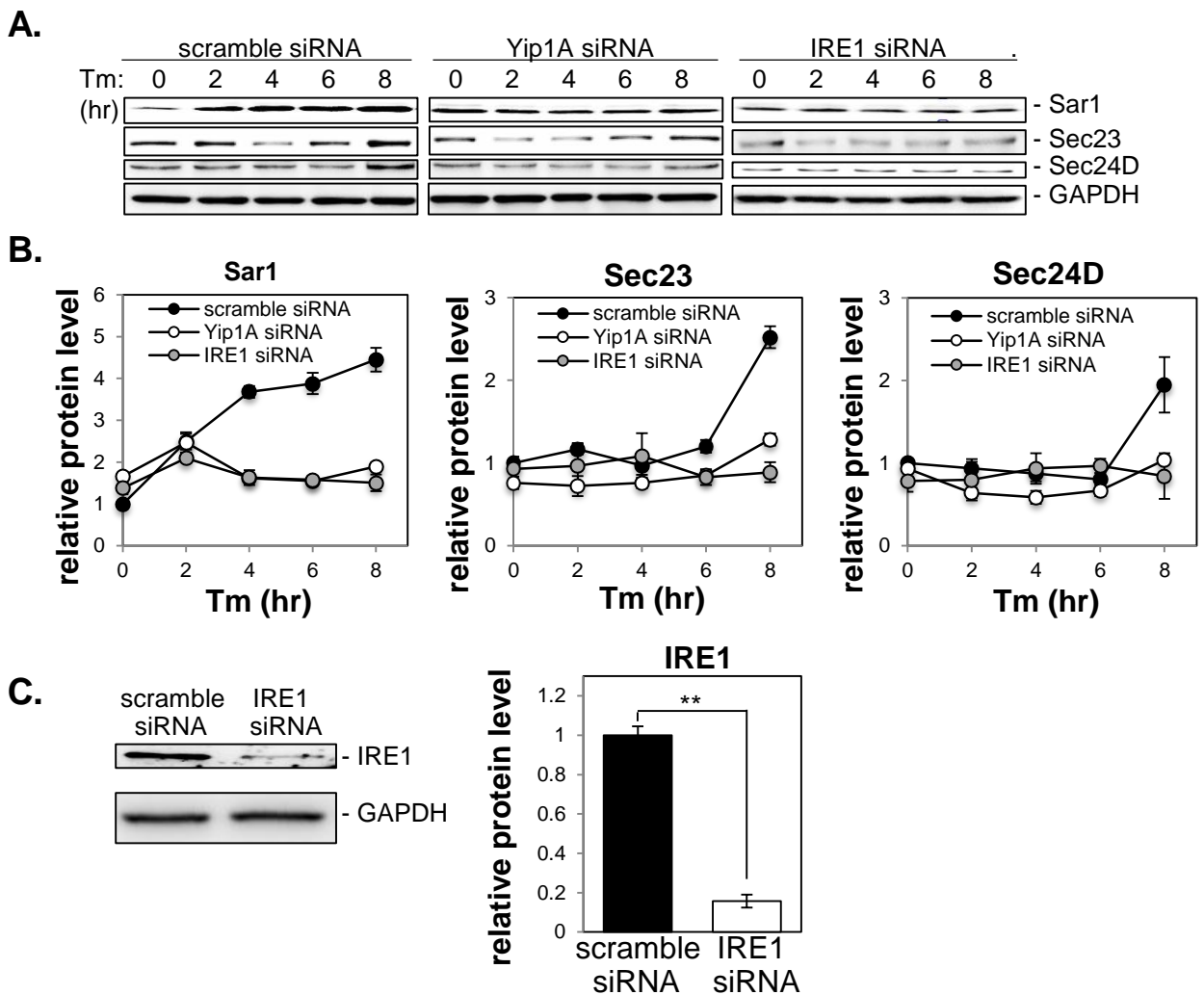
Figure 16. The upregulation of Sar1, Sec23, and Sec24D was triggered during Tm treatment through the IRE1 pathway

HeLa cells were transfected with control scramble siRNA or Yip1A siRNA for 24 hr, and then treated with Tm to induce the UPR. Cell lysates were prepared at the indicated time points and analyzed by western blotting.

(A) Representative immunoblots for Sar1, Sec23, Sec24D, and GAPDH. GAPDH was used for normalization. The intensity of the bands was quantified using the MultiGauge software.

(B) Relative protein levels of Sar1, Sec23, and Sec24D in control (solid circles), Yip1A-knockdown (open circles), and IRE1-knockdown (solid gray circles) cells. The protein levels in control cells at the beginning of the Tm treatment were assigned the value 1. Tm treatment induced the upregulation of Sar1, Sec23, and Sec24D. Yip1A- or IRE1-knockdown suppressed the upregulation of these molecules, suggesting that the upregulation of these COPII components under Tm treatment depends on the activation of IRE1 that is mediated by Yip1A. Data are means ± SD from three independent experiments.

(C) Representative immunoblot showing the depletion of IRE1 in HeLa cells at 24 hr after siRNA transfection. GAPDH was used for normalization. The intensity of the bands was quantified using the MultiGauge software, and the results are shown in the bar graph. The protein levels in control cells were assigned the value 1. The depletion of IRE1 protein was 84.3%. Data are means ± SD from three independent experiments. **: $p<0.01$.
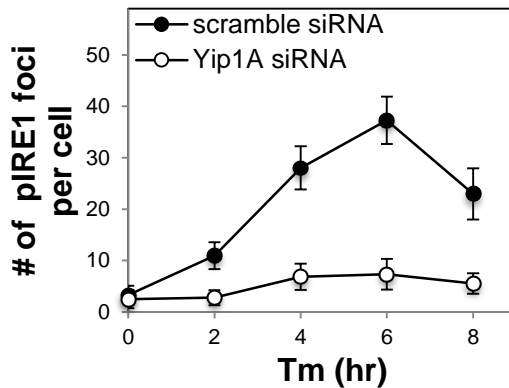
A.
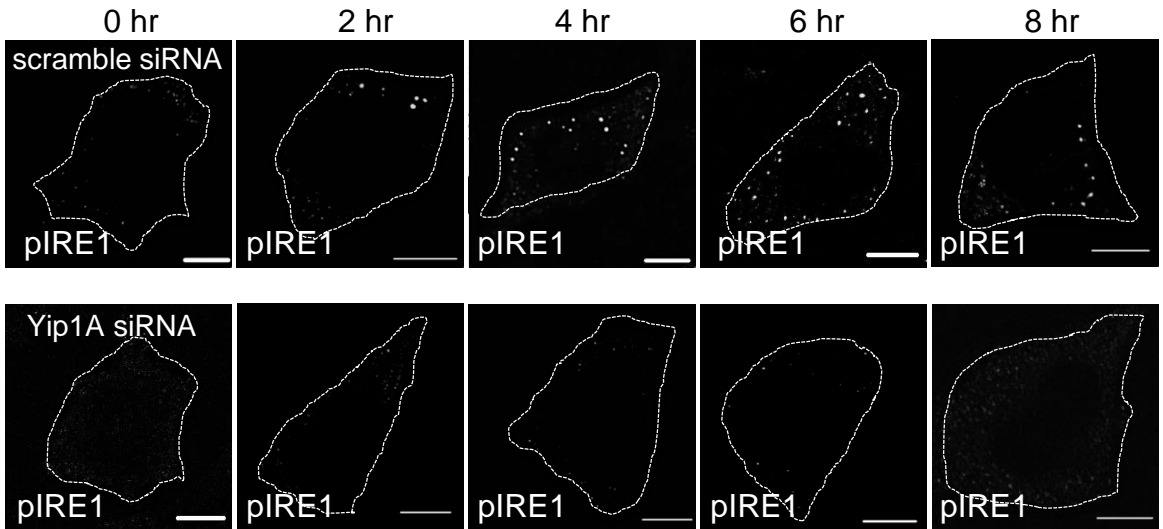
B.

Figure 17. Yip1A mediates the oligomerization of IRE1 molecules under Tm treatment
(A) Representative confocal micrographs of control (upper panels) or Yip1A-knockdown (lower panels) cells during the Tm treatment. Fixed cells at the indicated time points were stained for pIRE1. Cells are outlined with white dashed lines. In control cells, the number of foci increased during the first 6 hr of Tm treatment, and then started to decrease. In Yip1A knockdown cells, pIRE1 foci were hardly observed throughout the Tm treatment. Scale bars are 10 μm.
(B) The numbers of pIRE1 foci per cell were counted, and are shown in the line graph. Data are means ± SD (N=30).

A.

Tm: 0 4 8 (hr)
S Y S Y S Y

1048kDa - — - pIRE1-I
720kDa -
480kDa - — - pIRE1-II
242kDa -

WB: a-pIRE1

B.

pIRE1-I

■ scramble siRNA
□ Yip1A siRNA

pIRE1-II

■ scramble siRNA
□ Yip1A siRNA
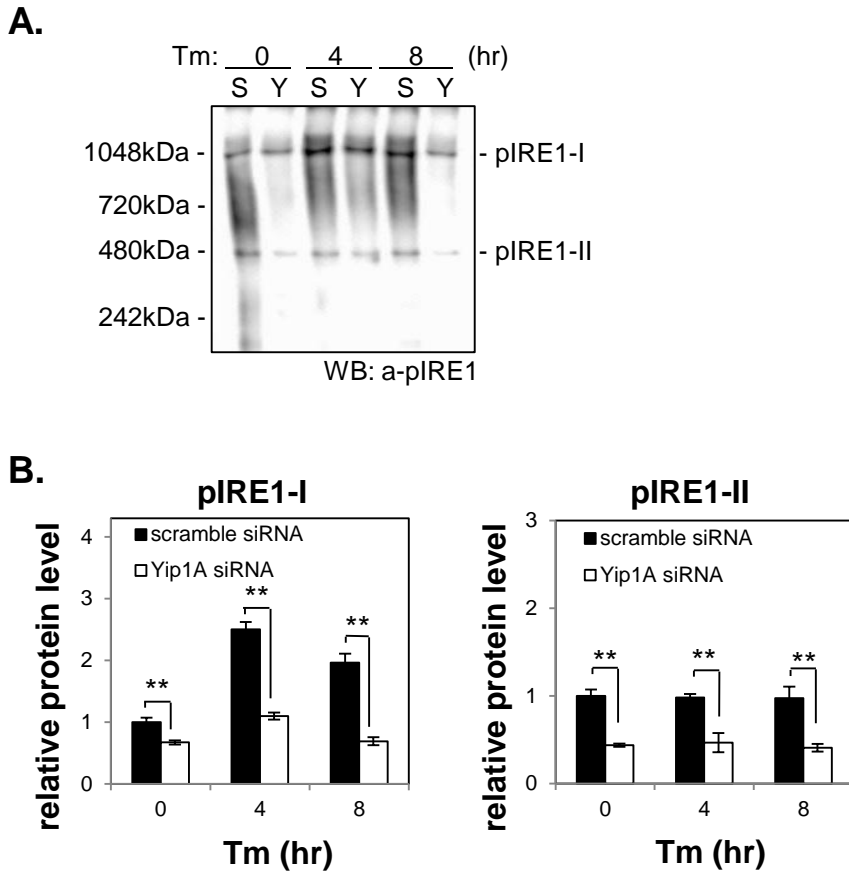
Figure 18. Yip1A mediates the formation of high-order species of IRE1 molecules under Tm treatment

(A) Representative immunoblot for pIRE1 after native PAGE, showing two high-order complexes of pIRE1 (termed pIRE1-I and pIRE1-II). Lane 'S' represents lysate from HeLa cells transfected with control scramble siRNA, and lane 'Y' represents lysate from HeLa cells transfected with Yip1A siRNA. Numbers on the left-hand side correspond to the standard molecular weight. The intensity of the bands was quantified by using the MultiGauge software. (B) Relative protein levels of pIRE1-1 and pIRE1-II in control (solid bars) and Yip1A-knockdown (open bars) cells during Tm treatment. Protein levels in control cells at the beginning of the Tm treatment were assigned the value 1. In control cells, the amount of pIRE1-I was increased after 4 hr of Tm treatment and then decreased. The amount of pIRE1-II remained constant throughout the Tm treatment. In Yip1A knockdown cells, the amount of both high-order complexes was reduced significantly. Data are means ± SD from three independent experiments. **: p<0.01.
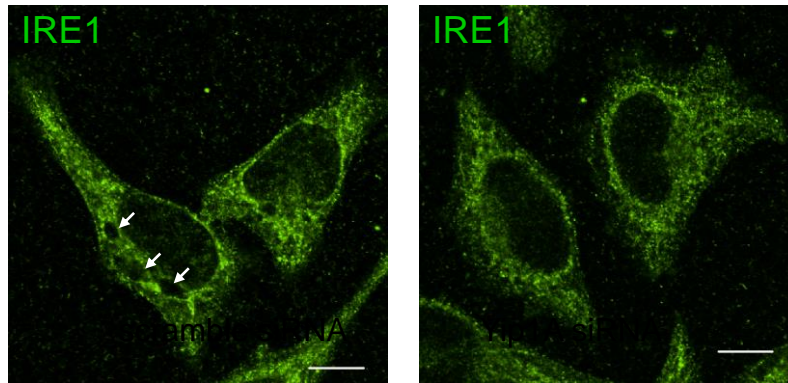
Figure 19. The ER localization of IRE1 was not affected by Yip1A-knockdown
Representative confocal micrographs showing the localization of total IRE1 in control (left-hand panel) or Yip1A-knockdown (right-hand panel) cells. HeLa cells were transfected with each siRNA for 24 hr, and then treated with Tm for 5 hr to induce the UPR. Fixed cells were stained for IRE1 (green). Several large vacuoles were observed in control cells (arrows), but not in Yip1A-knockdown cells. Otherwise, IRE1 was stained throughout the cytoplasm in a reticular pattern both in control and in Yip1A-knockdown cells, indicating its intrinsic localization in the ER. Scale bars are 10 μm.

A.

scramble siRNA   Yip1A siRNA   IRE1 siRNA   <u>Tm</u>

calnexin   calnexin   calnexin   0 hr

calnexin   calnexin   calnexin   5 hr

B.
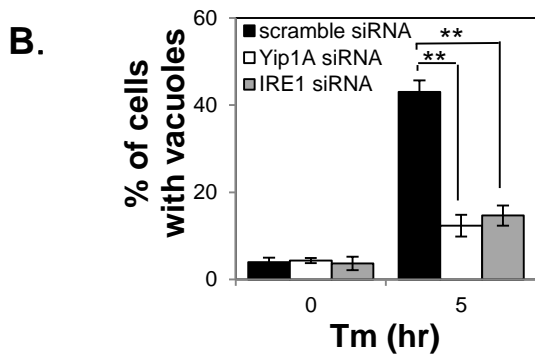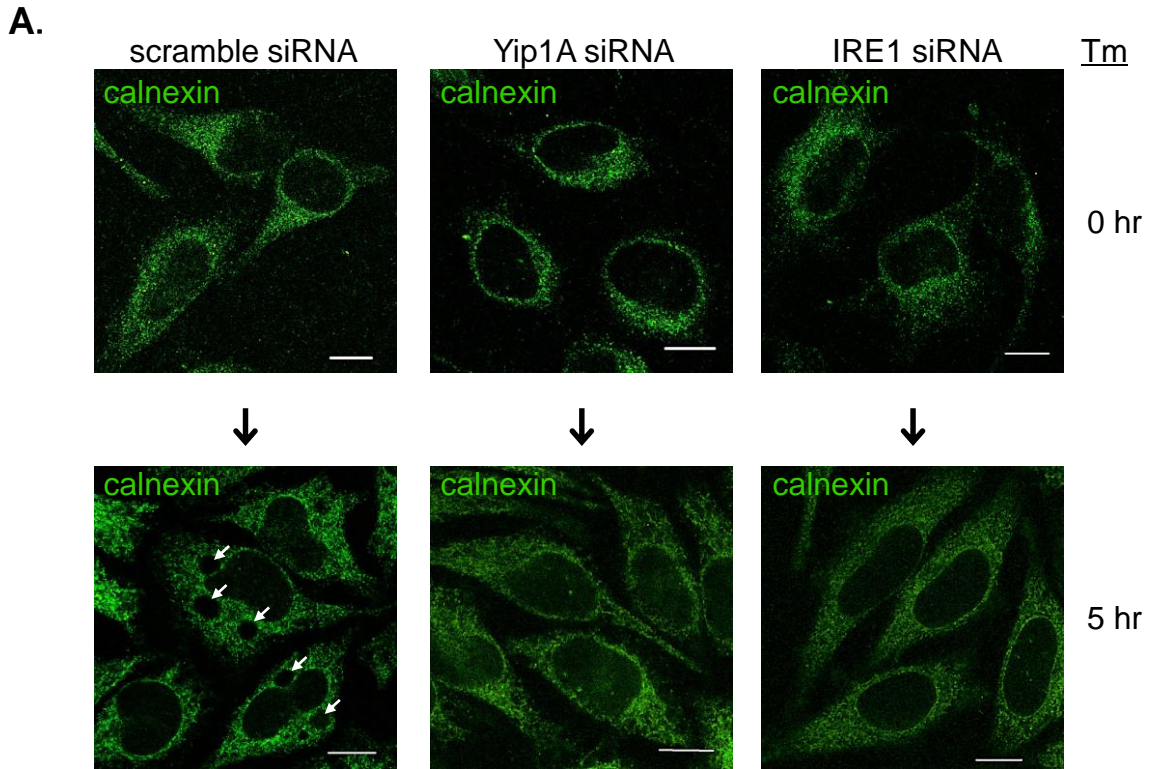
Figure 20. Yip1A mediates the formation of large vacuoles through the IRE1 pathway under Tm treatment

HeLa cells were transfected with scramble siRNA, Yip1A siRNA or IRE1 siRNA for 24 hr, and then treated with Tm for 5 hr to induce the UPR.

(A) Representative confocal micrographs of control (left-hand panels), Yip1A-knockdown (middle panels), and IRE1-knockdown (right-had panels) cells after 0 hr or 5 hr of Tm treatment. The ER structure was visualized with an anti-calnexin antibody. Large vacuoles were observed in control cells (arrows), but not in Yip1A- or IRE1-knockdown cells. Scale bars are 10 μm.

(B) The percentage of cells with vacuoles was counted, and is shown in the bar graph. The percentage of cells with vacuoles was significantly lower in Yip1A- or IRE1-knockdown cells than in control cells after Tm treatment. Data are means ± SD from three independent experiments (N=100). **: $p < 0.01$.

66
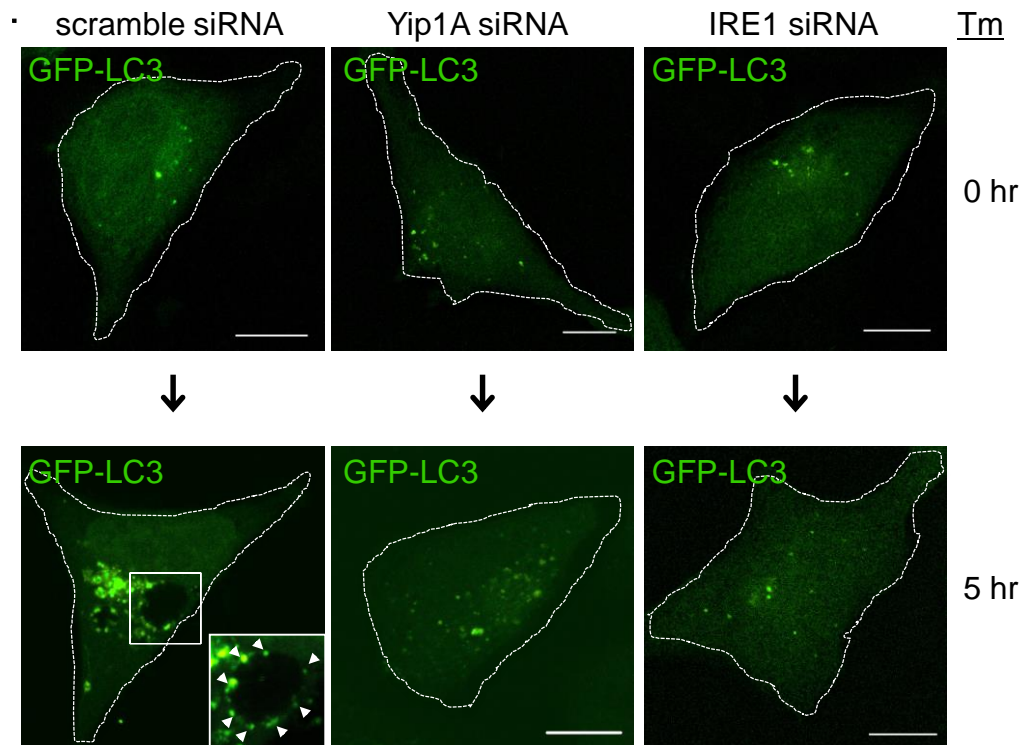
Figure 21. Yip1A mediates the formation of autophagosome-like vacuoles through the IRE1 pathway under Tm treatment

Representative confocal micrographs of control (left-hand panels; magnification of the boxed area is shown in inset), Yip1A-knockdown (middle panels), and IRE1-knockdown (right-hand panels) cells after 0 hr or 5 hr of Tm treatment. An expression construct for GFP-LC3 was co-transfected with siRNA. Cells are outlined with white dashed lines. In control cells, a number of large GFP-LC3 dots appeared after Tm treatment, and some were detected along the periphery of large vacuoles (arrowheads), indicating that these Tm-induced vacuoles have an autophagic nature. Scale bars are 10 μm.

A.

B.

C.
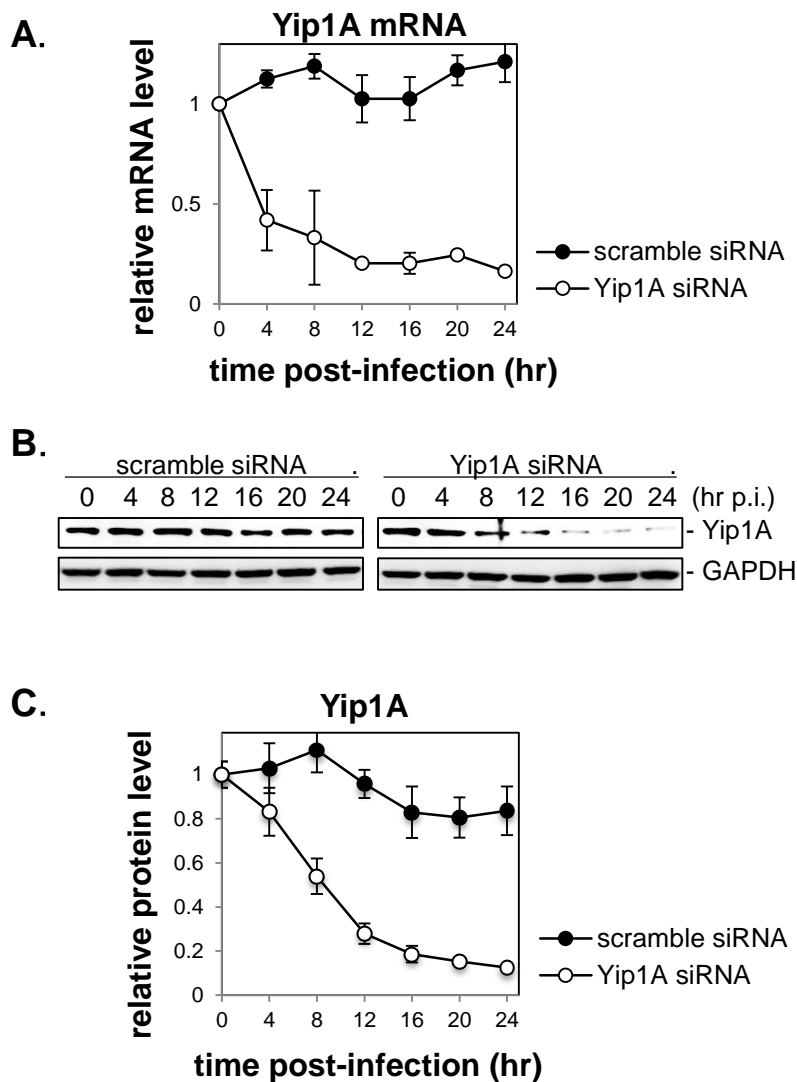
Figure 22. Depletion of Yip1A with siRNA during infection with *B. abortus*
HeLa cells were infected with *B. abortus,* and then transfected with scramble siRNA or Yip1A siRNA at 1 hr p.i.

(A) Relative mRNA levels of Yip1A in control (solid circles) and Yip1A-knockdown (open circles) cells during infection with *B. abortus*. Total RNA was extracted at the indicated time points and RT-PCR was carried out as described in Materials and Methods. The mRNA levels at time 0 hr were assigned the value 1. Yip1A mRNA was reduced by approximately 80% from 12 hr p.i. onwards. Data are means ± SD from three independent experiments.

(B) Representative immunoblots for Yip1A and GAPDH. Cell lysates were collected at the indicated time points, and analyzed by western blotting. GAPDH was used for normalization. The intensity of the bands was quantified using the MultiGauge software.

(C) Relative protein levels of Yip1A in control (solid circles) and Yip1A-knockdown (open circles) cells during infection with *B. abortus*. The protein levels at time 0 hr were assigned the value 1. Yip1A protein was reduced by 72.0% at 12 hr p.i., and by more than 80% at16 hr p.i. onwards. Data are means ± SD from three independent experiments.
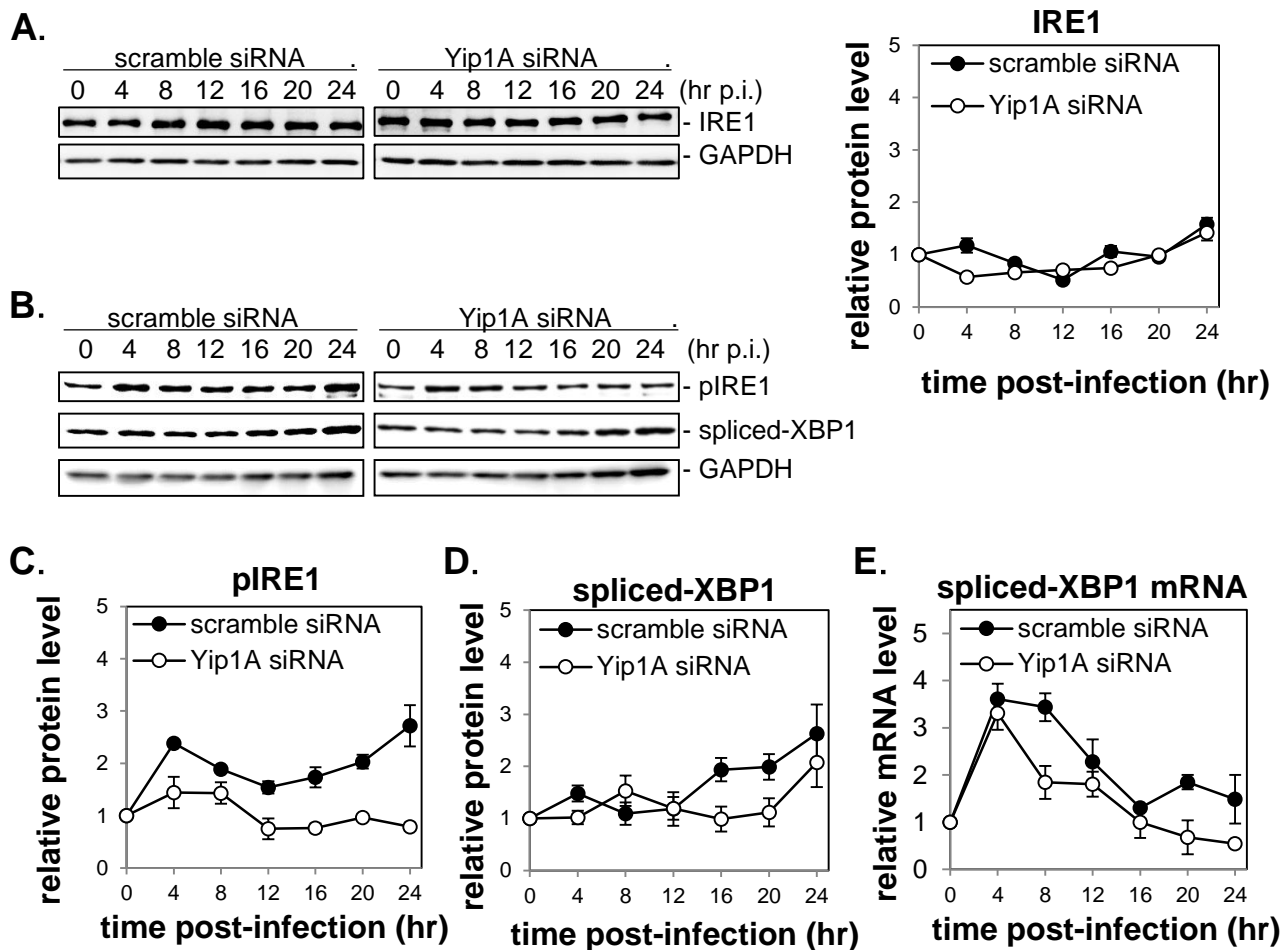
Figure 23. Yip1A mediates the activation of the IRE1 pathway of the UPR during infection with *B. abortus*

HeLa cells were infected with *B. abortus*, and then transfected with scramble siRNA or Yip1A siRNA at 1 hr p.i. Cell lysates were collected at the indicated time points, and analyzed by western blotting.

(A) Representative immunoblots for IRE1 and GAPDH. GAPDH was used for normalization. The intensity of the bands was quantified using the MultiGauge software. Relative protein levels of IRE1 in control (solid circles) and Yip1A-knockdown (open circles) cells during during *Brucella* infection are shown in the line graph. The protein levels at time 0 hr were assigned the value 1. There was little difference in the total levels of IRE1 between control and Yip1A-knockdown cells throughout the experiment. Data are means ± SD from three independent experiments.

(B) Representative immunoblots for pIRE1, spliced-XBP1, and GAPDH. GAPDH was used for normalization. The intensity of the bands was quantified using the MultiGauge software.

(C-E) Relative protein levels of pIRE1 (C) and spliced-XBP1 (D), and relative mRNA levels of spliced-XBP1 (E) in control (solid circles) and Yip1A-knockdown (open circles) cells. The protein or mRNA levels in control cells at time 0hr were assigned the value 1. In Yip1A-knockdown cells, the increase in pIRE1 was abolished completely at 12 hr p.i. onwards (C). The splicing of XBP1 appeared to be delayed in these cells (D). The distinct splicing kinetics was observed between control and Yip1A-knockdown cells (E). The lack of IRE1 activation at later time points led to complete loss of spliced XBP1 mRNA. Data are means ± SD from three independent experiments.
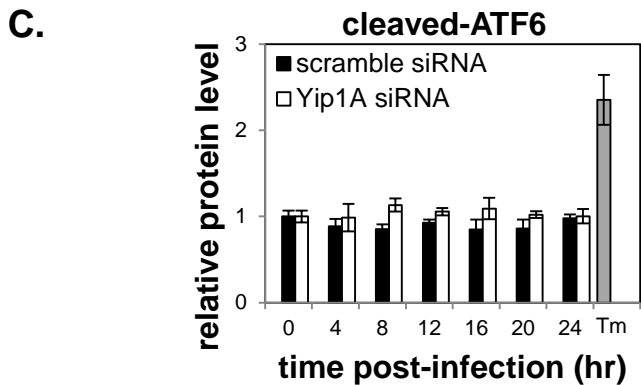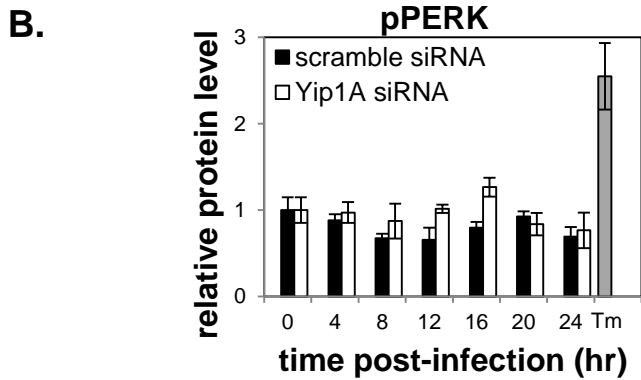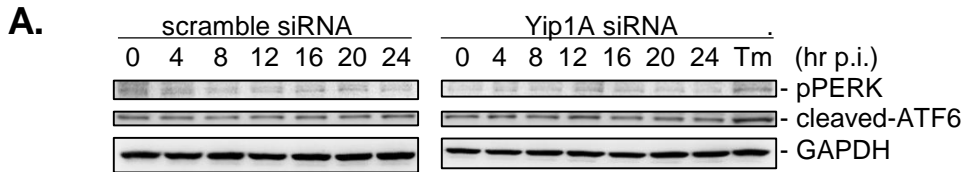
A.

B.

C.

Figure 24. The PERK and ATF6 pathways were not affected byYip1A-knockdown during infection with *B. abortus*

HeLa cells were infected with *B. abortus*, and then transfected with scramble siRNA or Yip1A siRNA at 1 hr p.i. Cell lysates were collected at the indicated time points, and analyzed by western blotting. As a positive control for the activation of PERK and ATF6, HeLa cells treated with 5 μg/ml of tunicamycin for 8 hr were included in the analysis ('Tm').

(A) Representative immunoblots for pPERK, cleaved-ATF6, and GAPDH. GAPDH was used for normalization. The intensity of the bands was quantified using the MultiGauge software.

(B) Relative protein levels of pPERK in control (solid bars) and Yip1A-knockdown (open bars) cells during infection with *B. abortus*. The protein levels at time 0 hr were assigned the value 1. The levels of pPERK were similar between control and Yip1A-knockdown cells during the course of infection, which indicates that the PERK pathway was not affected by Yip1A-knockdown. Data are means ± SD from three independent experiments.

(C) Relative protein levels of cleaved-ATF6 in control (solid bars) and Yip1A-knockdown (open bars) cells during infection with *B. abortus*. The protein levels at time 0 hr were assigned the value 1. The levels of cleaved-ATF6 were similar between control and Yip1A-knockdown cells during the course of infection, which indicates that the ATF6 pathway was not affected by Yip1A-knockdown.
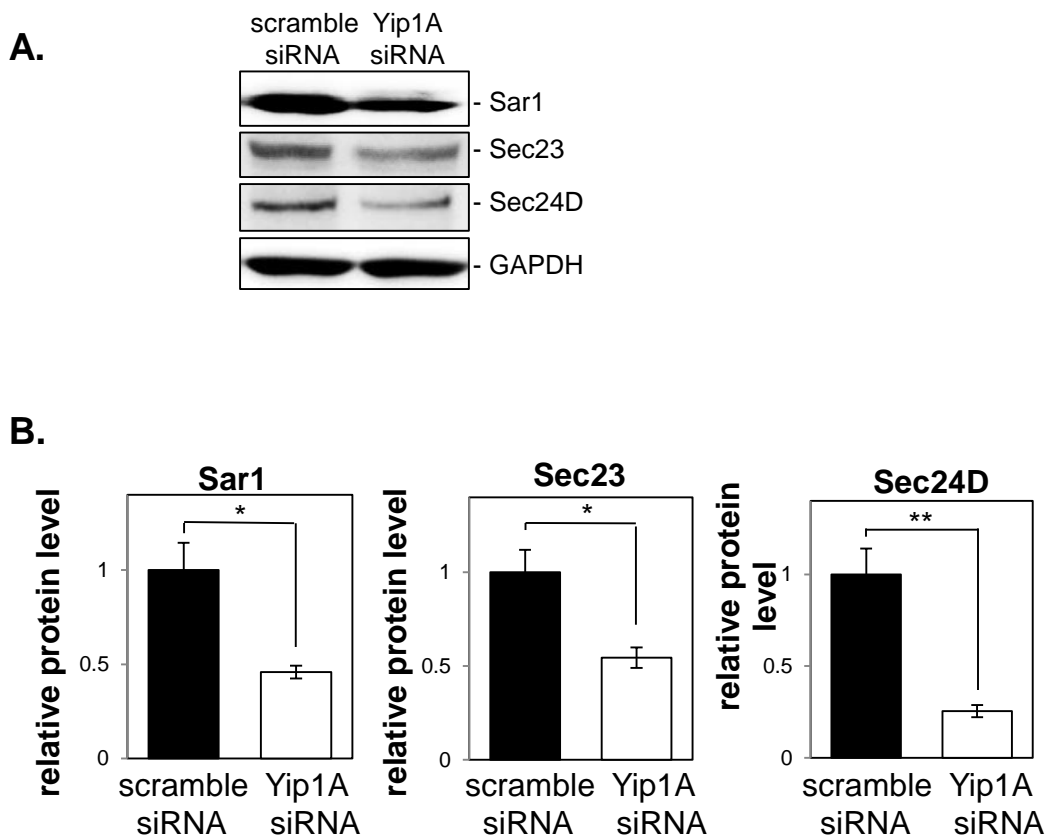
A.

B.

Figure 25. The upregulation of COPII components Sar1, Sec23, and Sec24D was suppressed by Yip1A-knockdown during infection with *B. abortus*

HeLa cells were infected with *B. abortus*, and then transfected with scramble siRNA or Yip1A siRNA at 1 hr p.i. Cell lysates were collected at 24hr p.i., and analyzed by western blotting.

(A) Representative immunoblots for Sar1, Sec23, Sec24D, and GAPDH. GAPDH was used for normalization. The intensity of the bands was quantified using the MultiGauge software.

(B) Relative protein levels of Sar1, Sec23, and Sec24D in control (solid bars) and Yip1A-knockdown (open bars) cells at 24 hr p.i. The protein levels in control cells were assigned the value 1. The upregulation of Sar1, Sec23, and Sec24D was suppressed significantly by Yip1A-knockdown. Data are means $\pm$ SD from three independent experiments. *: $p<0.05$; **: $p<0.01$.
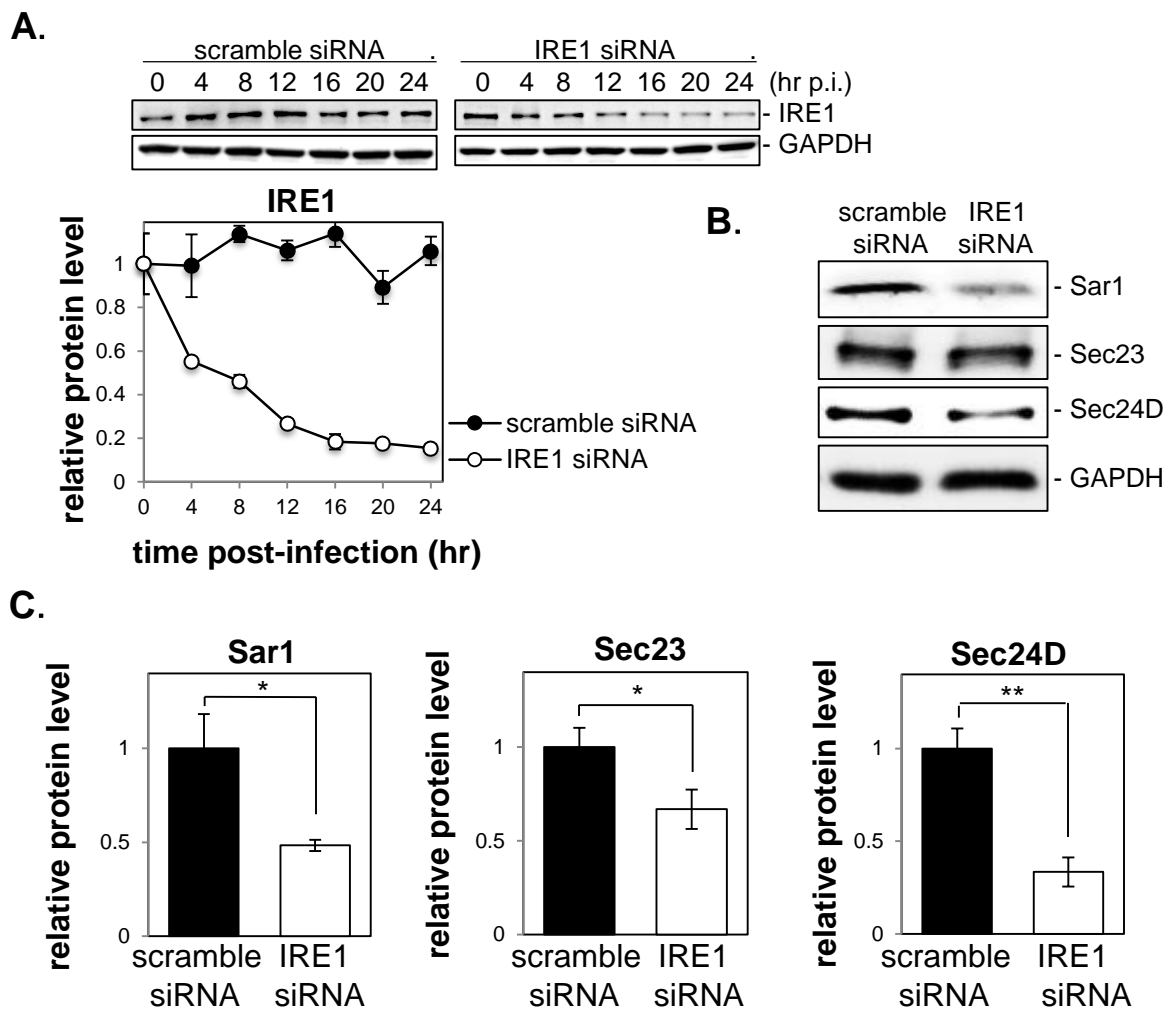
71

Figure 26. The upregulation of COPII components Sar1, Sec23, and Sec24D was suppressed by IRE1-knockdown during infection with *B. abortus*

HeLa cells were infected with *B. abortus*, and then transfected with scramble siRNA or IRE1 siRNA at 1 hr p.i. Cell lysates were collected at 24hr p.i., and analyzed by western blotting.

(A) Representative immunoblots for IRE1 and GAPDH, showing the depletion of IRE1 in HeLa cells during infection with *B. abortus*. GAPDH was used for normalization. The intensity of the bands was quantified using the MultiGauge software. Relative protein levels of IRE1 in control (solid circles) and IRE1-knockdown (open circles) cells are shown in the line graph. The protein levels at time 0 hr were assigned the value 1. IRE1 protein was reduced by 73.4% at 12 hr p.i., and by more than 80% at16 hr p.i. onwards. Data are means ± SD from three independent experiments.

(B) Representative immunoblot for Sar1, Sec23, Sec24D, and GAPDH. GAPDH was used for normalization. The intensity of the bands was quantified using the MultiGauge software.

(C) Relative protein levels of Sar1, Sec23, and Sec24D in control (solid bars) and IRE1-knockdown (open bars) cells at 24 hr p.i. The protein levels in control cells were assigned the value 1. The upregulation of Sar1, Sec23, and Sec24D was suppressed significantly by IRE1-knockdown. Data are means ± SD from three independent experiments. *: $p<0.05$; **: $p<0.01$.
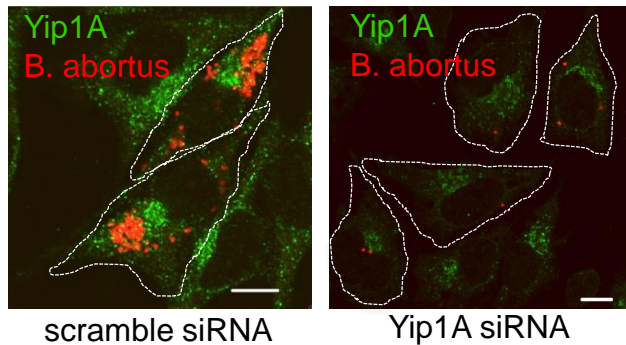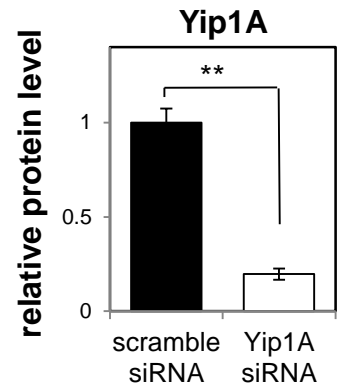
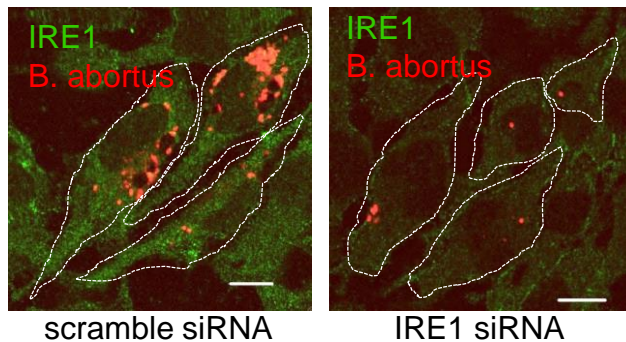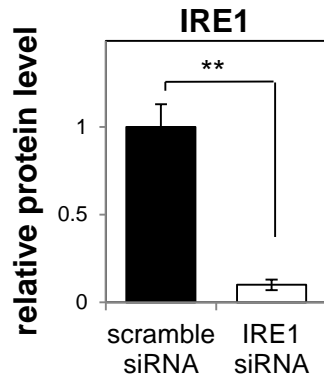**Figure 27. Depletion of Yip1A or IRE1 with siRNA in HeLa cells infected with *B. abortus***
(A) Representative confocal micrographs of control (left-hand panel) and Yip1A-knockdown(right-hand panel) cells at 24 hr p.i. Fixed cells were double-stained for Yip1A (green) and *B. abortus* (red). The infected cells are outlined with white dashed lines. Scale bars are 10 μm.
(B) The knockdown efficiency of Yip1A in infected cells was evaluated by quantifying the intensity of immunofluorescence staining for Yip1A, and the result is shown in the bar graph. Approximately 80% of depletion had been achieved for Yip1A. Data are means $\pm$ SD (N=30). **: $p<0.01$.
(C) Representative confocal micrographs of control (left-hand panel) and IRE1-knockdown(right-hand panel) cells at 24 hr p.i. Fixed cells were double-stained for IRE1 (green) and *B. abortus* (red). The infected cells are outlined with white dashed lines. Scale bars are 10 μm.
(D) The knockdown efficiency of IRE1 in infected cells was evaluated by quantifying the intensity of immunofluorescence staining for IRE1, and the result is shown in the bar graph. Approximately 90% of depletion had been achieved for IRE1. Data are means $\pm$ SD (N=30). **: $p<0.01$.
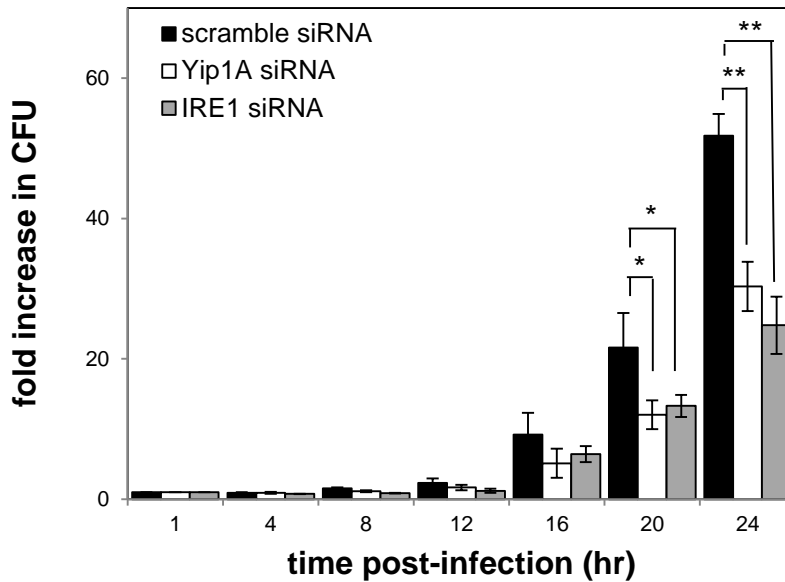
Figure 28. Yip1A-knockdown suppresses the intracellular growth *of B. abortus*
HeLa cells were infected with *B. abortus*, and then transfected with scramble siRNA (solid bars), Yip1A siRNA (open bars) or IRE1 siRNA (solid gray bars) at 1 hr p.i. CFUs were enumerated at the indicated time points. In control cells, robust increase in CFU occurred at 16 hr p.i. onwards, which indicates that *B. abortus* undergoes extensive replication (solid bars). At 24hr p.i., 51.8-fold increase in CFU was observed. Yip1A-knockdown inhibited bacterial growth, which resulted in about a 40% reduction in CFUs at 24 hr p.i. (open bars). IRE1-knockdown suppressed the increase in CFU similar to Yip1A-knockdown, and caused about a 50% reduction in CFU at 24 hr p.i. (solid gray bars). Data are means ± SD from three independent experiments. *: $p<0.05$; **: $p<0.01$.
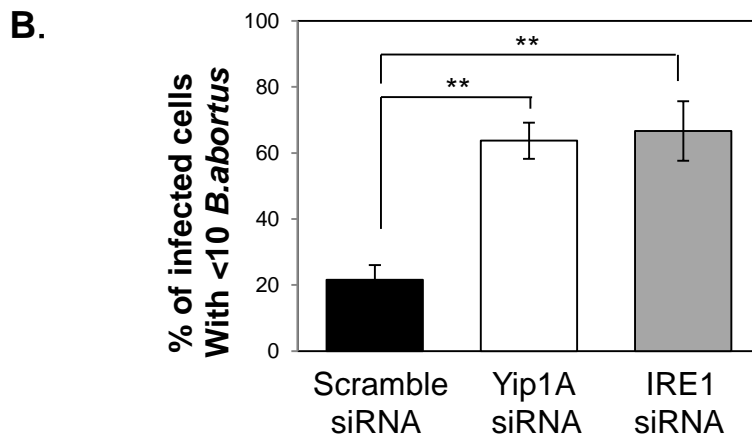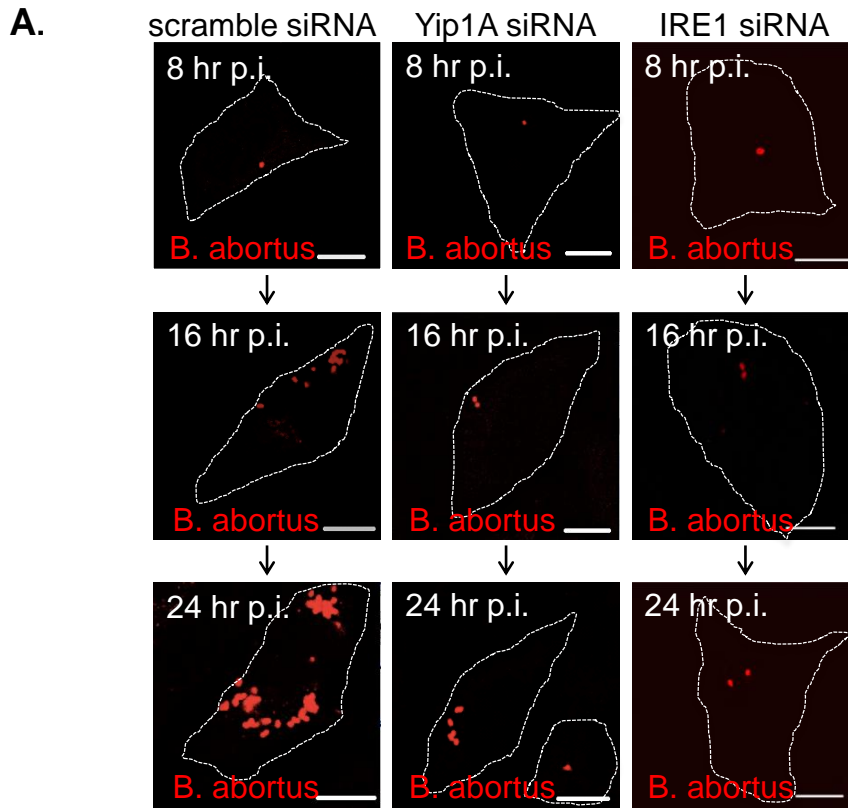
Figure 29. Yip1A-knockdown suppresses the intracellular replication of *B. abortus*
(A) Representative confocal micrographs of control (left-hand panels), Yip1A-knockdown (middle panels), and IRE1-knockdown (right-hand panels) cells at 8 hr, 16 hr, and 24 hr p.i. Fixed cells were stained for *B. abortus*. The infected cells are outlined with white dashed lines. In control cells, the onset of bacterial replication could be seen at 16 hr p.i., and the cytoplasm of an infected cell was filled with robustly replicating bacteria at 24 hr p.i. In contrast, Yip1A- or IRE1-knockdown cells contained a considerably small number of *B. abortus* at 24 hr p.i. Scale bars are 10 μm.
(B) The percentage of infected cells with fewer than ten *B. abortus* was determined, and the result is shown in the bar graph. Yip1A- or IRE1-knockdown significantly suppressed the intracellular replication of *B. abortus*.
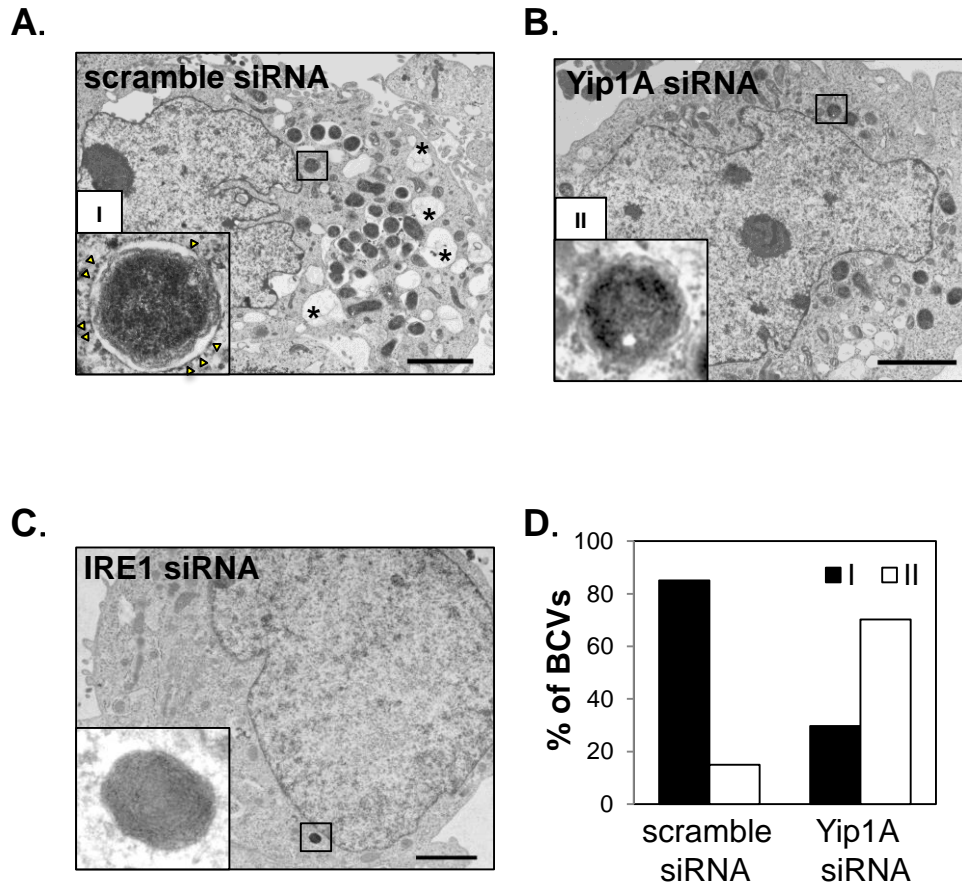
Figure 30. Yip1A is required for maturation of *B. abortus* into ER-derived replicative BCVs

(A-C) Representative electron micrographs of *Brucella*-infected control (A), Yip1A-knockdown (B), and IRE1-knockdown (C) cells at 24 hr p.i. Insets are magnifications of the boxed areas on the main image, showing the typical forms of BCVs. In control cells, a significant number of replicative BCVs can be observed with vacant vacuoles in their vicinity. These BCVs are in the form of ER-derived membrane-bound compartments (inset in (A), defined as 'I'). Note the presence of ribosomes on the membrane (arrowheads). Large autolysosome-like vacuoles that contained degraded cellular debris were also observed (asterisks). In Yip1A-knockdown cells, the bacteria were not sequestered into such compartments (inset in (B), defined as 'II'). Similar results were obtained in IRE1-knockdown cells (C). Scale bars are 2 μm.

(D) The percentages of the two forms of BCVs (I and II) present in control or Yip1A-knockdown cells at 24 hr p.i. In control cells, 85% of BCVs had acquired the ER-derived membrane, whereas 70% of BCVs were not sequestered into such a membrane in Yip1A-knockdown cells. The total numbers of BCVs analyzed were 67 for control cells and 37 for Yip1A-knockdown cells.
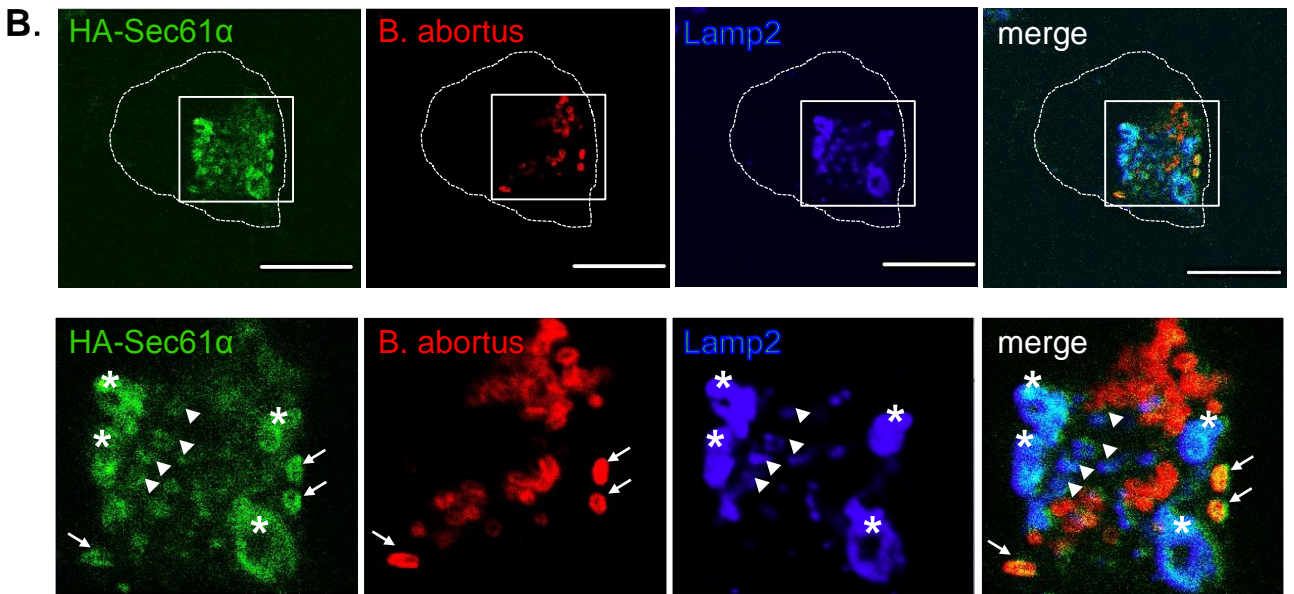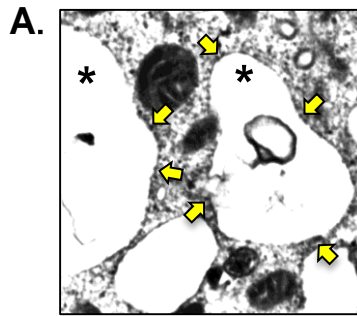
Figure 31. Vacuoles adjacent to replicative BCVs originate from the ER and the endosomes/lysosomes

(A) Representative electron micrograph of *Brucella*-infected control cells at 24 hr p.i., showing large autolysosomal vacuoles that contain degraded cellular debris (asterisks). The vacuoles are studded locally with ribosomes (arrows).

(B) Representative confocal micrographs of *Brucella*-infected control cells at 24 hr p.i. triple-stained for HA-Sec61α (a marker for rough ER; green), *B. abortus* (red), and Lamp2 (a marker for endosomes/lysosomes; blue). An expression construct for HA-Sec61α was co-transfected with scramble siRNA. The infected cells are outlined with white dashed lines. Magnifications of the boxed areas are shown below the main images. *B. abortus* (arrows) was co-stained with Sec61α but not with Lamp2, consistent with the transition from endosomal/lysosomal to ER-derived BCVs. Large autolysosomal vacuoles (asterisks) and the vacuoles adjacent to replicating bacteria (arrowheads) were stained for both Sec61α and Lamp2, indicating both the endosomal/lysosomal and ER-derived origin of these compartments. Scale bars are 10 μm.
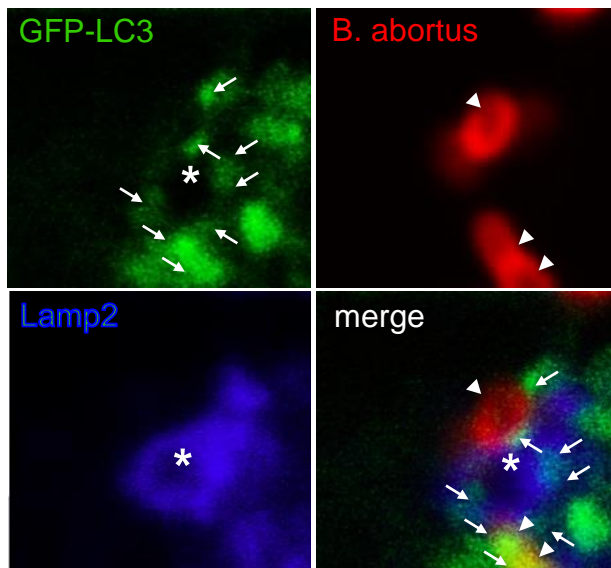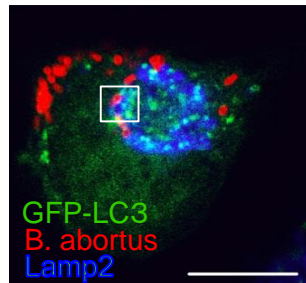
Figure 32. Large vacuoles have an autophagosome-like nature
Representative confocal micrographs of *Brucella*-infected control cells at 24 hr p.i., triple-stained for GFP-LC3 (a marker for autophagosomes; green), *B. abortus* (red), and Lamp2 (blue). An expression construct for GFP-LC3 was co-transfected with scramble siRNA. Magnifications of the boxed areas are shown below the main images. Some of the large autolysosomal vacuoles (asterisk) and replicating B. *abortus* (arrowheads) were co-stained with GFP-LC3 dots (arrows). Scale bar is 10 μm.
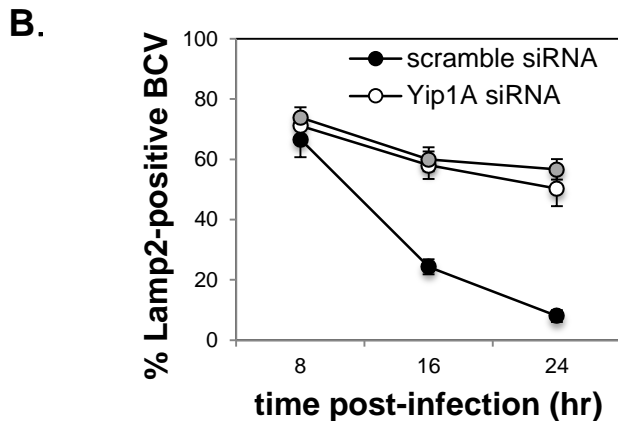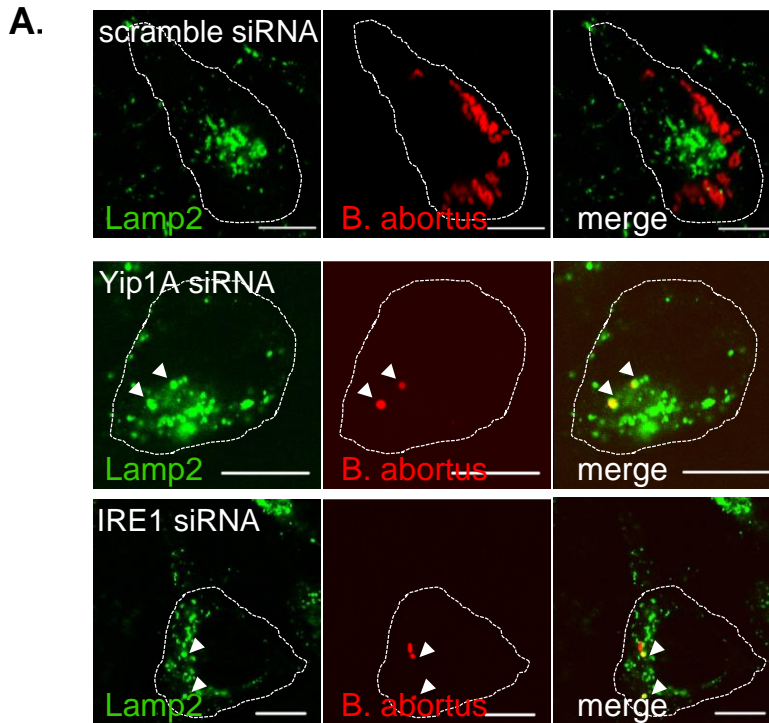
Figure 33. Yip1A-knockdown confined BCVs within Lamp2-positive compartments
(A) Representative confocal micrographs of control (upper panels), Yip1A-knockdown (middle panels), and IRE1-knockdown (lower panels) cells double-stained for Lamp2 (a marker for late endosomes/lysosomes; green) and *B. abortus* (red) at 24 hr p.i. BCVs co-localized with Lamp2 are indicated by arrowheads. The infected cells are outlined with white dashed lines. Scale bars are 10 μm.
(B) The percentage of Lamp2-positive BCVs was determined, and is shown in the line graph. In control cells, BCVs left Lamp2-positive compartments in a time-dependent manner, and 92% of BCVs were Lamp2-negative at 24 hr p.i. By contrast, about 50% of BCVs were co-localized with Lamp2 in Yip1A-knockdown cells. IRE1-knockdown cells showed kinetics similar to those of Yip1A-knockdown cells.
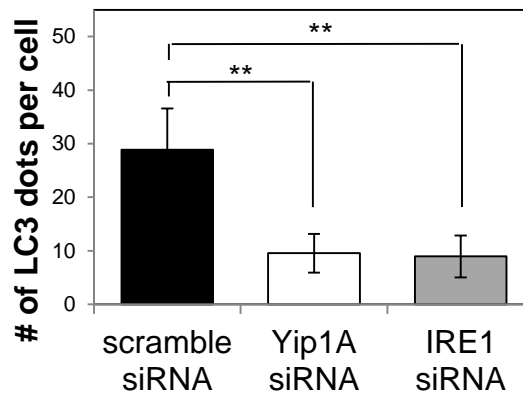
A.
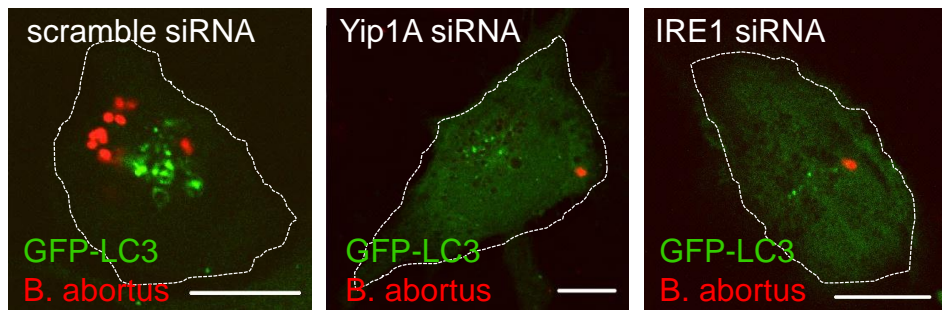
B.

Figure 34. Yip1A-knockdown prevents the formation of autophagosomes

(A) Representative confocal micrographs of control (left-hand panel), Yip1A-knockdown (middle panel), and IRE1-knockdown (right-hand panel) cells double-stained for GFP-LC3 (a marker for autophagosomes; green) and *B. abortus* (red) at 24 hr p.i. An expression construct for GFP-LC3 was co-transfected with each siRNA. The infected cells are outlined with white dashed lines. In control cells infected with *B. abortus*, a number of large GFP-LC3 dots were observed in the vicinity of replicating bacteria. By contrast, the fluorescence staining of GFP-LC3 was faint and diffuse throughout the cytoplasm in *Brucella*-infected Yip1A- or IRE1-knockdown cells. Scale bars are 10 μm.

(B) The numbers of GFP-LC3 dots per cell were counted, and are shown in the bar graph. The number of GFP-LC3 dots was significantly low in Yip1A- or IRE1-knockdown cells. Data are means $\pm$ SD (N=30). **: $p<0.01$.

Figure 35.（未発表の共同研究内容が含まれるので未掲載）

Figure 36.（未発表の共同研究内容が含まれるので未掲載）

Figure 37.（未発表の共同研究内容が含まれるので未掲載）

Figure 38.（未発表の共同研究内容が含まれるので未掲載）

Figure 39.（未発表の共同研究内容が含まれるので未掲載）

Figure 40.（未発表の共同研究内容が含まれるので未掲載）

Figure 41.（未発表の共同研究内容が含まれるので未掲載）

Figure 42.（未発表の共同研究内容が含まれるので未掲載）

Figure 43.（未発表の共同研究内容が含まれるので未掲載）

Figure 44.（未発表の共同研究内容が含まれるので未掲載）
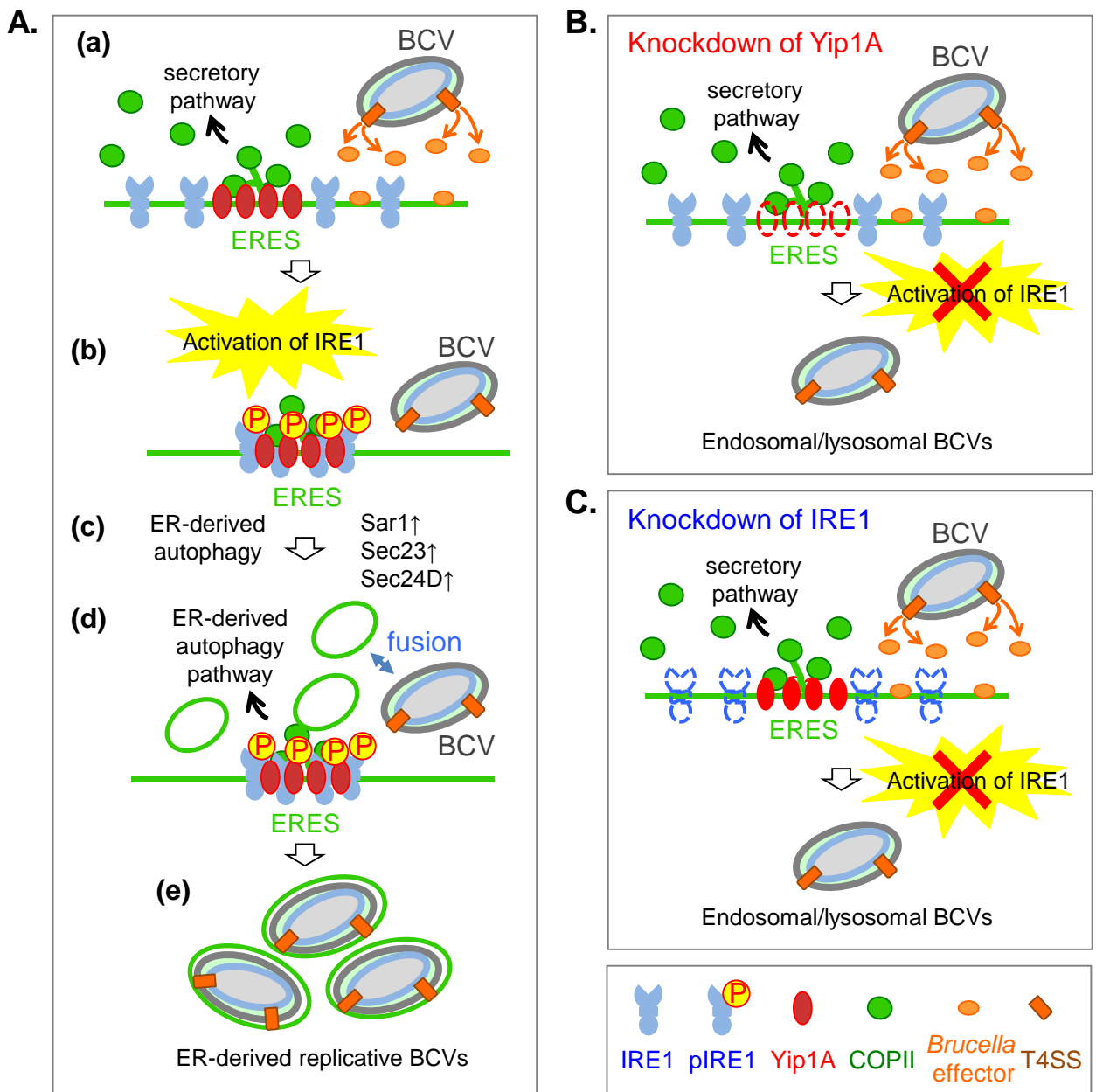
Figure 45.（未発表の共同研究内容が含まれるので未掲載）

Figure 46. Proposed model of how *B. abortus* matures into ER-derived replicative BCVs

(A) (a) During infection, *B. abortus* triggers the activation of IRE1, presumably by secreting effector molecules into the cytoplasm of host cells. (b) IRE1 molecules form high-order complexes at ERES with the aid of Yip1A, and are activated by trans-autophosphorylation. (c) The activated IRE1 in turn triggers the biogenesis of ER-derived autophagosome-like vacuoles. The COPII vesicle components Sar1, Sec23, and Sec24D are upregulated, which might enhance the capacity of COPII vesicles to export from ERES. (d) The ER-derived autophagosome-like vacuoles then fuse with endolysosomal vesicles. Since *B. abortus* that have reached the ER are located in late endosomal/lysosomal compartments, they should be able to fuse with these vacuoles. (e) Once they have acquired the ER-derived membrane, BCVs retain functional features of the ER, and replication of *B. abortus* in individual vacuoles might be supported through continual accretion of ER membranes derived from the IRE1-specific UPR.

(B,C) Knockdown of Yip1A (B) or IRE1 (C) prevents the activation of IRE1. Consequently, ER-derived membranes are not generated for bacterial replication and *B. abortus* remains in endosomal/lysosomal compartments.

6. References

Amer AO, Swanson MS (2005) Autophagy is an immediate macrophage response to *Legionella pneumophila*. Cell Microbiol 7: 765–778

Arenas GN, Staskevich AS, Aballay A, Mayorga LS (2000) Intracellular trafficking of *Brucella abortus* in J774 macrophages. Infect Immun 68: 4255–4263

Axe EL, Walker SA, Manifava M, Chandra P, Roderick HL, Habermann A, Griffiths G, Ktistakis NT (2008) Autophagosome formation from membrane compartments enriched in phosphatidylinositol 3-phosphate and dynamically connected to the endoplasmic reticulum. J Cell Biol 182: 685- 701.

Baruch M, Belotserkovsky I, Hertzog BB, Ravins M, Dov E, McIver KS, Le Breton YS, Zhou Y, Cheng CY, Hanski E (2014) An extracellular bacterial pathogen modulates host metabolism to regulate its own sensing and proliferation. Cell 156: 97-108

Baumann O, Walz B (2001) Endoplasmic reticulum of animal cells and its organization into structural and functional domains. Int Rev Cytol 205: 149-214

Bernales S, McDonald KL, Walter P (2006) Autophagy counterbalances endoplasmic reticulum expansion during the unfolded protein response. PLoS Biol 4: e423

Bi X, Corpina RA, Goldberg J (2002) Structure of the Sec23/24-Sar1 pre-budding complex of the COPII vesicle coat. Nature 419: 271-277

Calero M, Winand NJ, Collins RN (2002) FEBS Lett 515: 89–98

Calero M, Chen CZ, Zhu W, Winand N, Havas KA, Gilbert PM, Burd CG, Collins RN (2003) Dual prenylation is required for Rab protein localization and function. Mol Biol Cell 14: 1852–1867

Cao SS, Kaufman RJ (2013) Targeting endoplasmic reticulum stress in metabolic disease. Expert Opin Ther Targets 17: 437-448

Celli J, de Chastellier C, Franchini DM, Pizarro-Cerda J, Moreno E, Gorvel JP (2003) *Brucella* evades macrophage killing via VirB-dependent sustained interactions with the endoplasmic reticulum. J Exp Med 198: 545–556

Celli J, Salcedo SP, Gorvel JP (2005) *Brucella* coopts the small GTPase Sar1 for intracellular replication. Proc Natl Acad Sci USA 102: 1673–1678

Chen CZ, Calero M, DeRegis CJ, Heidtman M, Barlowe C, Collins RN (2004) Genetic analysis of yeast Yip1p function reveals a requirement for Golgi-localized rab proteins and rab-Guanine nucleotide dissociation inhibitor. Genetics 168: 1827–1841

Chen Y, Machner MP (2013) Targeting of the small GTPase Rab6A' by the *Legionella pneumophila* effector LidA. Infect Immun 81: 2226-2235

Comerci DJ, Martnez-Lorenzo MJ, Sieira R, Gorvel JP, Ugalde RA (2001) Essential role of the VirB machinery in the maturation of the *Brucella abortus*-containing vacuole. Cell Microbiol 3: 159-168

Cox JS, Walter P (1996) A novel mechanism for regulating activity of a transcription factor that controls the unfolded protein response. Cell 87: 391-404

D'Arcangelo JG, Stahmer KR, Miller EA (2013) Vesicle-mediated export from the ER: COPII coat function and regulation. Biochim Biophys Acta 1833: 2464–2472

de Barsy M, Jamet A, Filopon D, Nicolas C, Laloux G, Rual JF, Muller A, Twizere JC, Nkengfac B, Vandenhaute J, Hill DE, Salcedo SP, Gorvel JP, Letesson JJ, De Bolle X (2011) Identification of a *Brucella* spp. secreted effector specifically interacting with human small GTPase Rab2. Cell Microbiol 13: 1044–1058

de Barsy M, Mirabella A, Letesson JJ, De Bolle X (2012) A *Brucella abortus* cstA mutant is defective for association with endoplasmic reticulum exit sites and displays altered trafficking in HeLa cells. Microbiology 158: 2610-2618

de Jong MF, Sun YH, den Hartigh AB, van Dijl JM, Tsolis RM (2008) Identification of VceA and VceC, two members of the VjbR regulon that are translocated into macrophages by the *Brucella* type IV secretion system. Mol Microbiol 70: 1378–1396

de Jong MF, Starr T, Winter MG, den Hartigh AB, Child R, Knodler LA, van Dijl JM, Celli J, Tsolis RM (2013) Sensing of Bacterial Type IV Secretion via the Unfolded Protein Response. mBio 4: e00418

Dreux M, Chisari FV (2010) Viruses and the autophagy machinery. Cell Cycle 9: 1295–1307

Dreux M, Chisari FV (2011) Impact of the autophagy machinery on hepatitis C virus infection. Viruses 3: 1342-1357

Dykstra KM, Pokusa JE, Suhan J, Lee TH (2010) Yip1A structures the mammalian endoplasmic reticulum. Mol Biol Cell 21: 1556–1568

Franco IS, Shuman HA, Charpentier X (2009) The perplexing functions and surprising origins of *Legionella pneumophila* type IV secretion effectors. Cell Microbiol 11: 1435–1443

Fugier E, Salcedo SP, de Chastellier C, Pophillat M, Muller A, Arce-Gorvel V,

Fourquet P, Gorvel JP (2009) The glyceraldehyde-3-phosphate dehydrogenase and the small GTPase Rab 2 are crucial for *Brucella* replication. PLoS Pathog 5: e1000487

Ge L, Melville D, Zhang M, Schekman R (2013) The ER–Golgi intermediate compartment is a key membrane source for the LC3 lipidation step of autophagosome biogenesis. Elife 2: e00947

Graef M, Friedman JR, Graham C, Babu M, Nunnari J (2013) ER exit sites are physical and functional core autophagosome biogenesis components. Mol Biol Cell 24: 2918–2931

Guo F, Zhang H, Chen C, Hu S, Wang Y, Qiao J, Ren Y, Zhang K, Wang Y, Du G (2012) Autophagy favors *Brucella melitensis* survival in infected macrophages. Cell Mol Biol Lett 17: 249-257

Gutierrez MG, Vázquez CL, Munafó DB, Zoppino FC, Berón W, Rabinovitch M, Colombo MI (2005) Autophagy induction favours the generation and maturation of the *Coxiella*-replicative vacuoles. Cell Microbiol 7: 981–993

Hailey DW, Rambold AS, Satpute-Krishnan P, Mitra K, Sougrat R, Kim PK, Lippincott-Schwartz J (2010) Mitochondria supply membranes for autophagosome biogenesis during starvation. Cell 141: 656–667

Harding HP, Zhang Y, Ron D (1999) Protein translation and folding are coupled by an endoplasmic-reticulum-resident kinase. Nature 397: 271-274

Harding HP, Zhang Y, Bertolotti A, Zeng H, Ron D (2000) Perk is essential for translational regulation and cell survival during the unfolded protein response. Mol Cell 5: 897-904

Hassan IH, Zhang MS, Powers LS, Shao JQ, Baltrusaitis J, Rutkowski DT, Legge K, Monick MM (2012) Influenza A viral replication is blocked by inhibition of the inositol-requiring enzyme 1 (IRE1) stress pathway. J Biol Chem 287: 4679–4689

Hayashi-Nishino M, Fujita N, Noda T, Yamaguchi A, Yoshimori T, Yamamoto A (2009) A subdomain of the endoplasmic reticulum forms a cradle for autophagosome formation. Nat Cell Biol 11: 1433-1437

Haze K, Yoshida H, Yanagi H, Yura T, Mori K (1999) Mammalian transcription factor ATF6 is synthesized as a transmembrane protein and activated by proteolysis in response to endoplasmic reticulum stress. Mol Biol Cell 10: 3787-3799

Hetz C (2012) The unfolded protein response: controlling cell fate decisions under ER stress and beyond. Nature Rev Mol Cell Biol 13: 89–102

Hoyer-Hansen M and Jaattela M (2007) Connecting endoplasmic reticulum stress to autophagy by unfolded protein response and calcium. Cell Death Differ 14: 1576– 1582

Ito T, Chiba T, Ozawa R, Yoshida M, Hattori M, Sakaki Y (2001) A comprehensive two-hybrid analysis to explore the yeast protein interactome. Proc Natl Acad Sci USA 98: 4569–4574

Jackson WT, Giddings TH Jr, Taylor MP, Mulinyawe S, Rabinovitch M, Kopito RR, Kirkegaard K (2005) Subversion of cellular autophagosomal machinery by RNA viruses. PLoS Biol 3: e156

Jin C, Zhang Y, Zhu H, Ahmed K, Fu C, Yao X (2005) Human Yip1A specifies the localization of Yif1 to the Golgi apparatus. Biochem Biophys Res Commun 334: 16-22

Jin R, Zhu W, Cao S, Chen R, Jin H, Liu Y, Wang S, Wang W, Xiao G (2013) Japanese encephalitis virus activates autophagy as a viral immune evasion strategy. PLoS One 8: e52909

Kano F, Yamauchi S, Yoshida Y, Watanabe-Takahashi M, Nishikawa K, Nakamura N, Murata M (2009) Yip1A regulates the COPI-independent retrograde transport from the Golgi complex to the ER. J Cell Sci 122: 2218–2227

Kano F, Nakatsu D, Noguchi Y, Yamamoto A, Murata M (2012) A resealed-cell system for analyzing pathogenic intracellular events: Perturbation of endocytic pathways under diabetic conditions. PLoS One 7: e44127

Khakpoor A, Panyasrivanit M, Wikan N, Smith DR (2009) A role for autophagolysosomes in dengue virus 3 production in HepG2 cells. J Gen Virol 90: 1093-1103.

Kimata Y, Ishiwata-Kimata Y, Ito T, Hirata A, Suzuki T, Oikawa D, Takeuchi M, Kohno K (2007) Two regulatory steps of ER-stress sensor Ire1 involving its cluster formation and interaction with unfolded proteins. J Cell Biol 179: 75-86

Korennykh AV, Egea PF, Korostelev AA, Finer-Moore J, Zhang C, Shokat KM, Stroud RM, Walter P (2009) The unfolded protein response signals through high-order assembly of Ire1. Nature 457: 687–693

Kouroku Y, Fujita E, Tanida I, Ueno T, Isoai A, Kumagai H, Ogawa S, Kaufman RJ, Kominami E, Momoi T (2007) ER stress (PERK/eIF2alpha phosphorylation) mediates the polyglutamine-induced LC3 conversion, an essential step for autophagy formation. Cell Death Differ 14: 230–239

Lamb CA, Yoshimori T, Tooze SA (2013) The autophagosome: origins unknown,

biogenesis complex. Nat Rev Mol Cell Biol 14: 759-774

Lee MC, Miller EA, Goldberg J, Orci L, Schekman R (2004) Bi-directional protein transport between the ER and golgi. Annu Rev Cell Dev Biol 20: 87-123

Lee MC, Miller EA (2007) Molecular mechanisms of COPII vesicle formation. Semin Cell Dev Biol 18: 424-434

Li H, Korennykh AV, Behrman SL, Walter P (2010) Mammalian endoplasmic reticulum stress sensor IRE1 signals by dynamic clustering. Proc Natl Acad Sci USA 107: 16113-16118

Li J, Ni M, Lee B, Barron E, Hinton DR, Lee AS (2008) The unfolded protein response regulator GRP78/BiP is required for endoplasmic reticulum integrity and stress-induced autophagy in mammalian cells. Cell Death Differ 15: 1460–1471

Liu CY, Kaufman RJ (2003) The unfolded protein response. J Cell Sci 116: 1861-1862

Longatti A, Lamb CA, Razi M, Yoshimura S, Barr FA, Tooze SA (2012) TBC1D14 regulates autophagosome formation via Rab11 and recycling endosomes. J Cell Biol 197: 659–675

Marchesini MI, Herrmann CK, Salcedo SP, Gorvel JP, Comerci DJ (2011) In search of *Brucella abortus* type IV secretion substrates: screening and identification of four proteins translocated into host cells through VirB system. Cell Microbiol 13: 1261-1274

Medigeshi GR, Lancaster AM, Hirsch AJ, Briese T, Lipkin WL, Defilippis V, Früh K, Mason PW, Nikolich-Zugich J, Nelson JA (2007) West Nile virus infection activates the unfolded protein response, leading to CHOP induction and apoptosis. J Virol 81: 10849-10860

Miller E, Antonny B, Mamamoto S, Schekman R (2002) Cargo selection into COPII vesicles is driven by the Sec24p subunit. EMBO J 21: 6105-6113

Mizushima N, Yoshimori T, Ohsumi Y (2011) The role of Atg proteins in autophagosome formation. Annu Rev Cell Dev Biol 27: 107-132

Myeni S, Child R, Ng TW, Kupko JJ 3rd, Wehrly TD, Porcella SF, Knodler LA, Celli J (2013) *Brucella* modulates secretory trafficking via multiple type IV secretion effector proteins. PLoS Pathog 9: e1003556

Ogata M, Hino S, Saito A, Morikawa K, Kondo S, Kanemoto S, Murakami T, Taniguchi M, Tanii I, Yoshinaga K, Shiosaka S, Hammarback JA, Urano F, Imaizumi K (2006) Autophagy is activated for cell survival after endoplasmic reticulum stress.

Mol Cell Biol 26: 9220-9231

Ohashi, Y, Munro S (2010) Membrane delivery to the yeast autophagosome from the Golgi–endosomal system. Mol Biol Cell 21: 3998–4008

Panyasrivanit M, Khakpoor A, Wikan N, Smith DR (2009) Co-localization of constituents of the dengue virus translation and replication machinery with amphisomes. J Gen Virol 90: 448-56

Pappas G, Akritidis N, Bosilkovski M, Tsianos E (2005) Brucellosis. N Engl J Med 352: 2325–2336

Pena J, Harris E (2011) Dengue virus modulates the unfolded protein response in a time-dependent manner. J Biol Chem 286: 14226-14236

Pincus D, Chevalier MW, Aragón T, van Anken E, Vidal SE, El-Samad H, Walter P (2010) Bip binding to the ER-stress sensor IRE1 tune the homeostatic behavior of the unfolded protein response. PLoS Biol 8: e1000415

Pizarro-Cerda J, Meresse S, Parton RG, van der Goot G, Sola-Landa A, Lopez-Goñi I, Moreno E, Gorvel JP (1998a) *Brucella abortus* transits through the autophagic pathway

and replicates in the endoplasmic reticulum of nonprofessional phagocytes. Infect Immun 66: 5711–5724

Pizarro-Cerdá J, Moreno E, Sanguedolce V, Mége J-L, Gorvel JP (1998b) Virulent *Brucella abortus* avoids lysosome fusion and distributes within autophagosome-like compartments. Infect Immun 66: 2387–2392

Qin QM, Pei J, Ancona V, Shaw BD, Ficht TA, de Figueiredo P (2008) RNAi screen of endoplasmic reticulum-associated host factors reveals a role for IRE1alpha in supporting *Brucella* replication. PLoS Pathog 4: e1000110

Ravikumar B, Moreau K, Jahreiss L, Puri C, Rubinsztein DC (2010) Plasma membrane contributes to the formation of pre-autophagosomal structures. Nature Cell Biol 12: 747–757

Romano PS, Gutierrez MG, Beron W, Rabinovitch M, Colombo MI (2007) The autophagic pathway is actively modulated by phase II *Coxiella burnetii* to efficiently replicate in the host cell. Cell Microbiol 9: 891–909

Ron D, Walter P (2007) Signal integration in the endoplasmic reticulum unfolded protein response. Nat Rev Mol Cell Biol 8: 519–529.

Schnaith A, Kashkar H, Leggio SA, Addicks K, Krönke M, Krut O (2007) *Staphylococcus aureus* subvert autophagy for induction of caspase-independent host cell death. J Biol Chem 282: 2695–2706

Schröder M, Kaufman RJ (2005) The mammalian unfolded protein response. Annu Rev Biochem 74: 739–789

Seimon TA, Kim MJ, Blumenthal A, Koo J, Ehrt S, Wainwright H (2010) Induction of ER stress in macrophages of *tuberculosis* granulomas. PLoS One 5: e12772.

Shakoori A, Fujii G, Yoshimura S, Kitamura M, Nakayama K, Ito T, Ohno H, Nakamura N (2003) Identification of a five-pass transmembrane protein family localizing in the Golgi apparatus and the ER. Biochem Biophys Res Commun 312: 850–857

Shinohara Y, Imajo K, Yoneda M, Tomeno W, Ogawa Y, Kirikoshi H, Funakoshi K, Ikeda M, Kato N, Nakajima A, Saito S (2013) Unfolded protein response pathways regulate Hepatitis C Virus replication via modulation of autophagy. Biochem Biophys Res Commun 432: 326-332

Simonsen A, Stenmark H (2008) Self-eating from an ER-associated cup. J Cell Biol 182: 621-622.

Smith JA, Khan M, Magnani DD, Harms JS, Durward M, Radhakrishnan GK, Liu YP, Splitter GA (2013) *Brucella* induces an unfolded protein response via TcpB that supports intracellular replication in macrophages. PLoS Pathog 9: e1003785

Sriburi R, Bommiasamy H, Buldak GL, Robbins GR, Frank M, Jackowski S, Brewer JW (2007) Coordinate regulation of phospholipid biosynthesis and secretory pathway gene expression in XBP-1(S)-induced endoplasmic reticulum biogenesis. J Biol Chem 282: 7024–704

Starr T, Ng TW, Wehrly TD, Knodler LA, Celli J (2008) *Brucella* intracellular replication requires trafficking through the late endosomal/lysosomal compartment. Traffic 9: 678–694

Stenmark H (2009) Rab GTPases as coordinators of vesicle traffic. Nat Rev Mol Cell Biol 10: 513–525

Su HL, Liao CL, Lin YL (2002) Japanese encephalitis virus infection initiates endoplasmic reticulum stress and an unfolded protein response. J Virol 76: 4162–4171

Suh DH, Kim Mi-K, Kim HS, Chung HH, Song YS (2012) Unfolded protein response to autophagy as a promising druggable target for anticancer therapy. Ann NY Acad Sci 1271: 20-32

Tan D, Cai Y, Wang J, Zhang J, Menon S, Chou H-T, Ferro-Novick S, Reinisch KM, Walz T (2013) The EM structure of the TRAPPIII complex leads to the identification of a requirement for COPII vesicles on the macroautophagy pathway. Proc Natl Acad Sci USA 110: 19432–19437

Tang BL, Ong YS, Huang B, Wei S, Wong ET, Qi R, Horstmann H, Hong W (2001) A membrane protein enriched in endoplasmic reticulum exit sites interacts with COPII. J Biol Chem 276: 40008-40017

Tardif KD, Mori K, Kaufman RJ, Siddiqui A (2004) Hepatitis C virus suppresses the IRE1-XBP1 pathway of the unfolded protein response. J Biol Chem 279: 17158–17164

van der Vaart A, Griffith J, Reggiori F (2010) Exit from the Golgi is required for the expansion of the autophagosomal phagophore in yeast *Saccharomyces cerevisiae*. Mol Biol Cell 21: 2270–2284

Walter P, Ron D (2011) The unfolded protein response: From stress pathway to homeostatic regulation. Science 334: 1081-1086

Wang J, Tan D, Cai Y, Reinisch KM, Walz T, Ferro-Novick S (2014) A requirement for ER-derived COPII vesicles in phagophore initiation. Autophagy 10: 708-709

Yang X, Matern HT, Gallwitz D (1998) Specific binding to a novel and essential Golgi membrane protein (Yip1p) functionally links the transport GTPases Ypt1p and Ypt31p. EMBO J 17:4954-4963

Ye J, Rawson RB, Komuro R, Chen X, Davé UP, Prywes R, Brown MS, Goldstein JL (2000) ER stress induces cleavage of membrane-bound ATF6 by the same proteases that process SREBPs. Mol Cell 6: 1355–1364

Yla-Anttila P, Vihinen H, Jokitalo E, Eskelinen EL (2009) 3D tomography reveals connections between the phagophore and endoplasmic reticulum. Autophagy 5: 1180-1185

Yorimitsu T, Nair U, Yang Z, Klionsky DJ (2006) Endoplasmic reticulum stress triggers autophagy. J Biol Chem 281: 30299-30304

Yoshida H, Haze K, Yanagi H, Yura T, Mori K (1998) Identification of the *cis*-acting endoplasmic reticulum stress response element responsible for transcriptional induction of mammalian glucose-regulated proteins – Involvement of basic leucine zipper transcription factors. J Biol Chem 273: 33741-33749

Yoshida H, Matsui T, Yamamoto A, Okada T, Mori K (2001) XBP1 mRNA is induced

by ATF6 and spliced by IRE1 in response to ER stress to produce a highly active transcription factor. Cell 107: 881–891

Yoshida Y, Suzuki K, Yamamoto A, Sakai N, Bando M, Tanimoto K, Yamaguchi Y, Sakaguchi T, Akhter H, Fujii G, Yoshimura S, Ogata S, Sohda M, Misumi Y, Nakamura N (2008) YIPF5 and YIF1A recycle between the ER and the Golgi apparatus and are involved in the maintenance of the Golgi structure. Exp Cell Res 314: 3427–3443

Zoppino FC, Militello RD, Slavin I, Alvarez C, Colombo MI (2010) Autophagosome formation depends on the small GTPase Rab1 and functional ER exit sites. Traffic 11: 1246–1261

Acknowledgments